State of Global Water Resources 2025

Report



WEATHER CLIMATE WATER

WORLD METEOROLOGICAL ORGANIZATION

WMO-No. 1402

WMO-No. 1402

© World Meteorological Organization, 2026

The right of publication in print, electronic and any other form and in any language is reserved by WMO. Short extracts from WMO publications may be reproduced without authorization, provided that the complete source is clearly indicated. Editorial correspondence and requests to publish, reproduce or translate this publication in part or in whole should be addressed to:

Chair, Publications Board
World Meteorological Organization (WMO)
7 bis, avenue de la Paix
P.O. Box 2300
CH-1211 Geneva 2, Switzerland

Email: publications@wmo.int

ISBN 978-92-63-11402-01

https://doi.org/10.59327/WMO/WATER/2025

Cover photo: Ramazan Cirakoglu, WMO 2020 Calendar Competition.

NOTE

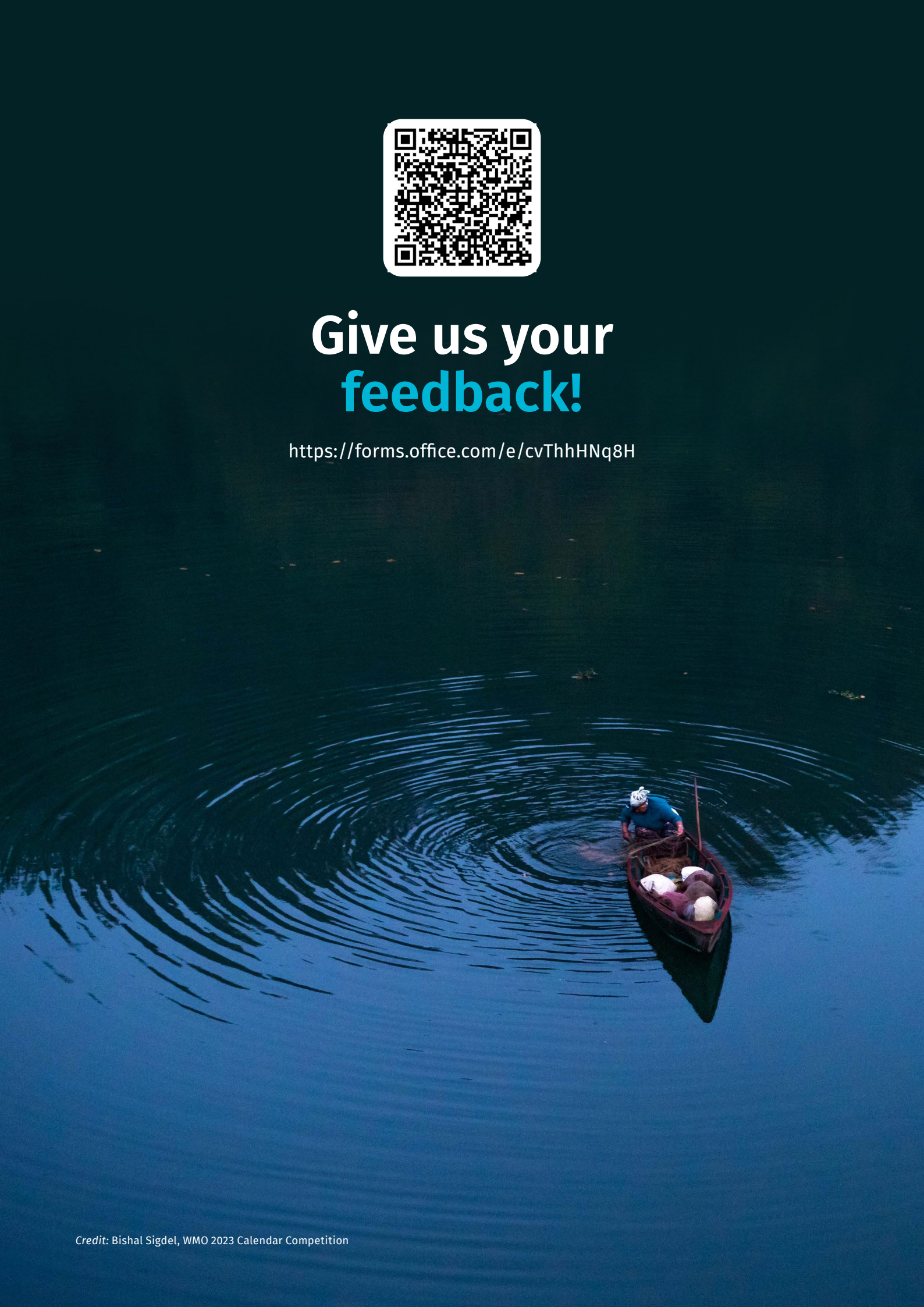
The designations employed and the presentation of material herein do not imply the expression of any opinion whatsoever on the part of the Secretariats of WMO or the United Nations concerning the legal status of any country, area or territory, or of its authorities, or concerning the delimitation of its borders. The depiction and use of boundaries, geographic names and related data on maps and in lists, tables, documents and databases herein are not warranted to be error-free and do not imply official endorsement or acceptance by WMO or the United Nations.

The mention of specific companies or products does not imply that they are endorsed or recommended by WMO in preference to others of a similar nature which are not mentioned or advertised.

The findings, interpretations and conclusions expressed in WMO publications with named authors are those of the authors alone and do not necessarily reflect those of WMO or its Members.

Give us your feedback!

https://forms.office.com/e/cvThhHNq8H



Credit: Bishal Sigdel, WMO 2023 Calendar Competition

Contents

Scope . . . ii
Foreword . . . iii
Acknowledgements . . . iv
List of abbreviations . . . vii
Executive summary . . . viii
Introduction . . . 1
Data sources . . . 3
Anomaly calculation . . . 4
Semi-decadal statement . . . 6
Report background and developments . . . 7
Semi-decadal status . . . 8
Perspective . . . 11
Overview of climatic conditions in 2025 . . . 13
Precipitation . . . 14
Extreme precipitation . . . 16
River discharge . . . 17
Reservoirs . . . 22
Inflow into selected reservoirs . . . 22
Reservoir storage . . . 23
Lakes . . . 25
Lake levels . . . 26
Lake water temperature . . . 27
Ice cover duration . . . 28
Groundwater levels . . . 29
Soil moisture . . . 32
Evapotranspiration . . . 35
Terrestrial water storage . . . 37
Snow cover and glaciers . . . 39
Snow water equivalent and peak snow mass . . . 39
Glaciers . . . 41
Water quality . . . 44
Observed water quality . . . 44
Observed water temperature . . . 44
Modelled river temperature . . . 46
High-impact hydrological events . . . 48
Floods in the Democratic Republic of the Congo . . . 50
Drought in the Greater Horn of Africa . . . 50
Floods in Nigeria . . . 50
Floods in southern Africa . . . 50
Floods in Pakistan . . . 51
Floods in Sri Lanka . . . 51
Floods in Indonesia, Thailand and Malaysia . . . 51
Floods in Viet Nam . . . 51
Floods in the Philippines . . . 51
Drought in Armenia, Türkiye, the Islamic Republic of Iran, the Syrian Arab Republic and Jordan . . . 51
Floods in Jamaica, Cuba, Haiti and the Dominican Republic . . . 52
Floods in northern Australia . . . 52
Floods in the United States . . . 52
Drought in Argentina and Chile . . . 53
Drought in Europe . . . 53
Floods in France . . . 53
Outlook . . . 54
References . . . 56
Annex. Technical annex . . . 61

Scope

About the report:

The State of Global Water Resources report, published annually by WMO, provides a comprehensive quantitative overview of global water resources, with a focus on hydrological variability and trends. It supports countries, decision makers and stakeholders in understanding the current state of water resources, identifying areas with significant anomalies and supporting effective water management strategies. The report is based on data contributed by WMO Members, as well as information from global hydrological modelling systems and satellite observations provided by various partners.

What the report contains:

- An assessment of global freshwater availability, including river discharge, lakes, groundwater, soil moisture, snow and ice, and combined terrestrial water storage.
- A map of key hydrological extreme events throughout the year such as floods and droughts.
- A case study highlighting regional and national water resource conditions.
- Global maps with easy-to-understand colour-coded indicators.
- Comparative analysis of the current state with long-term hydrological normals, and an evaluation of the impact of climate variability and change on water resources and the hydrological cycle.

What the report does not contain::

- Detailed national or subnational, or regional or trans-boundary water management strategies.
- Projections or future scenario modelling (the focus is retrospective, not predictive).
- Policy recommendations – it is a scientific and technical report that can be used as a basis for future strategy, policies and investment decisions.
- Full raw datasets – only indicators and highlights are included.

Who the report is for:

- Government agencies, policymakers and investors working on water resources and climate adaptation.
- Hydrologists, climatologists and environmental scientists, as well as members of the media and the general public interested in global water resource trends and climate impacts and seeking authoritative and recent global data.
- International organizations involved in water security, development and disaster risk reduction.

How to cite the report:

World Meteorological Organization (WMO). *State of Global Water Resources 2025* (WMO-No. 1402); Geneva, 2026.

Foreword



The rhythms of the water year – when rains arrive, rivers rise, monsoons begin and snow starts to melt – have shaped communities and ways of life for generations. Understanding the extent and underlying causes of changes to these patterns is fundamental to managing water sustainably, reducing the impacts of drought, flooding and cryosphere loss, and safeguarding lives, livelihoods and ecosystems.

These risks are not abstract. The early months of 2026 saw severe flooding in southern Africa, extreme heat across Australia and South Asia, heat and drought in Europe and landslides and destructive floods in Nepal. At the same time, a strengthening El Niño increases risk of drought in some areas, and further flooding in others. Such conditions demonstrate why hydrological information must support preparedness as well as assessment. The WMO State of Global Water Resources report provides that foundation.

Now in its fifth edition, the report offers a global overview of water resources across major basins, drawing on observations and model results, and comparing with long-term normals. Alongside the assessment of 2025, this edition presents a semi-decadal synthesis of 2021–2025.

Data sharing by WMO Members continues to grow, strengthening the reach and credibility of this assessment. Yet important gaps in data sharing remain across several regions and variables, and the economic losses associated with water-related disasters continue to be critically underreported. Sustained investment in open and timely data exchange is essential: without shared data, we cannot see the full picture or act effectively. Within WMO's integrated water data systems, the WMO Hydrological Observing System (WHOS) supports the exchange of observations, the Global Hydrological Status and Outlook System (HydroSOS) provides status and outlook products, and the State of Global Water Resources report brings these together in a global assessment. Their effectiveness depends on open and timely data sharing under the WMO Unified Data Policy.

This report would not have been possible without the contributions of National Meteorological and Hydrological Services, data centres, researchers and partner institutions. I am deeply grateful for their in situ observations, model outputs and space-based data, which together strengthen our understanding of an increasingly complex water cycle.

WMO will continue to work with its Members and partners to strengthen this report series and advance our shared ambition: ensuring that every country and community has access to timely, reliable water information to protect lives, livelihoods and ecosystems.



Prof. Celeste Saulo
Secretary-General

Acknowledgements

WMO is grateful to the following contributors.

WMO MEMBER STATES AND TERRITORIES THROUGH HYDROLOGICAL ADVISERS AND ASSIGNED FOCAL POINTS FOR THE STATE OF THE GLOBAL WATER RESOURCES REPORT

Australia, Austria, Belgium, Belize, Benin, Brazil, Bosnia and Herzegovina, Canada, Chile, Colombia, Costa Rica, Croatia, Cuba, Cyprus, Czechia, Denmark, Dominican Republic, Ecuador, El Salvador, Estonia, Finland, France, Gambia, Georgia, Germany, Greece, Guatemala, Haiti, Hungary, Iceland, India, Iraq, Ireland, Israel, Italy, Jamaica, Jordan, Kazakhstan, Kenya, Latvia, Lesotho, Lithuania, Luxembourg, Malawi, Malaysia, Mexico, Myanmar, Namibia, Netherlands (Kingdom of the), New Zealand, Niger, Nigeria, Norway, Panama, Paraguay, Peru, Poland, Portugal, Qatar, Republic of Korea, Republic of Moldova, Romania, Russian Federation, Rwanda, Senegal, Serbia, Slovakia, Slovenia, Somalia, South Africa, Sweden, Switzerland, Syrian Arab Republic, Thailand, United Arab Emirates, United Kingdom of Great Britain and Northern Ireland, United States of America, Uruguay.

Hydrological Advisers and focal points contributed to and supported the preparation of the present report by providing observational data, information about major hydrological events that occurred in 2025 and other relevant information and participated in the review and validation of the report.

STEERING COMMITTEE MEMBERS

Lucy Barker (United Kingdom, WMO HydroSOS Technical Team Co-Lead); Jan Danhelka (Czechia, Vice-President of WMO INFCOM); Harry Dixon (United Kingdom); Katie Facer-Childs (United Kingdom, WMO HydroSOS Technical Team Co-Lead); Albert Martis (Curaçao and Sint Maarten, Chair of WMO Hydrological Coordination Panel); Michel Jean (Canada, President WMO INFCOM); Harry Lins (United States); Ian Lisk (United Kingdom, President WMO SERCOM); Ilias Pechlivanidis (Sweden, Vice-Chair of the WMO Research Board); Marcelo Uriburu Quirno (Argentina, Vice-Chair of the WMO Standing Committee on Hydrological Services); Yuri Simonov (Russian Federation, Chair of the WMO Standing Committee on Hydrological Services); Narendra Tuteja (Australia, Chair of the WMO Expert Team on Operational Hydrological Prediction Systems); Andy Wood (United States, WMO Expert Team on Operational Hydrological Prediction Systems).

REGIONAL HYDROLOGICAL ADVISERS

Iuma Bani (WMO Regional Association V), Peter Clarke (WMO Regional Association IV), Mohamed Housseini Ibrahim (WMO Regional Association I), Waldo Lavado-Casimiro (WMO Regional Association III), Irakli Megrelidze (WMO Regional Association VI), and Mamoru Miyamoto (WMO Regional Association II), who contributed to the preparation and review of the report.

WMO EXPERTS

Experts from the Standing Committee on Hydrological Services, Standing Committee on Services for Agriculture, Task Team on WIS2 for Hydrology and Subgroup on WIGOS Tools for Hydrology, who participated in the preparation and review of the report.

MEMBERS OF THE GLOBAL HYDROLOGICAL MODELLING COMMUNITY

Diani Nimanthika Abeyrathne (University of Tokyo), Clement Mathieu Jacques Albergel (European Space Agency (ESA)), Alice Andral (CLS Group), Berit Arheimer (Swedish Meteorological and Hydrological Institute (SMHI)), Eva Boergens (German Research Centre for Geosciences (GFZ)

Potsdam), Beatriz Calmettes (CLS Group), Laura Carrea (University of Reading), Elyssa Collins (National Aeronautics and Space Administration (NASA)), Bram Droppers (Utrecht University), Omid Elmi (University of Stuttgart), Mohamed Elshamy (University of Saskatchewan), David Fairbairn (European Organisation for the Exploitation of Meteorological Satellites (EUMETSAT) Satellite Application Facility on Support to Operational Hydrology and Water Management (H SAF)), Huilin Gao (Texas A&M University (TAMU)), Augusto Getirana (NASA), Claudia Giardino (Institute for Electromagnetic Sensing of the Environment of the National Research Council of Italy (CNR-IREA), Riley Hales (Brigham Young University (BYU)), Shaun Harrigan (Maynooth University), Rachel Huber Magoffin (Aquaveo), Yeshewatesfa Hundecha (SMHI), Ruben Imhoff (Deltares), Kristina Isberg (SMHI), Wayne Jenkinson (Environment and Climate Change Canada (ECCC)), Edward Jones (Utrecht University), Jeffrey Karn (ECCC), Frank Kaspar (EUMETSAT), Matthias Kelbling (Helmholtz Centre for Environmental Research – UFZ), Rohini Kumar (Helmholtz Centre for Environmental Research – UFZ), Sujay Kumar (NASA), Jakob Luchner (DHI), Simon Valentin Lüdke (Helmholtz Centre for Environmental Research – UFZ), Henrik Madsen (DHI), Cinzia Mazzetti (ECMWF), Simon A. Mischel (Federal Institute of Hydrology (BfG)), Lawrence Mudryk (ECCC), Sebastian Müller (Helmholtz Centre for Environmental Research – UFZ), Justin Murfitt (University of Waterloo), Alexandra Murray (DHI), Jim Nelson (BYU), Albert Nkwasa (International Institute for Applied Systems Analysis (IIASA), Emmanuel Nyenah (Goethe University Frankfurt), Christel Prudhomme (ECMWF), Oldrich Rakovec (Czech University of Life Sciences Prague), Robert Reinecke (Johannes Gutenberg University Mainz), Jörgen Rosberg (SMHI), Peyman Saemian (University of Stuttgart), Luis Samaniego (Helmholtz Centre for Environmental Research – UFZ), Marc Schröder (EUMETSAT Satellite Application Facility on Climate Monitoring (CM SAF)), Pallav Kumar Shrestha (Helmholtz Centre for Environmental Research – UFZ), Nico Sneeuw (University of Stuttgart), Edwin H. Sutanudjaja (Utrecht University), Maliko Tanguy (ECMWF), Jose Pablo Teran Orsini (Vrije Universiteit Brussel (VUB)), Mohammad J. Tourian (University of Stuttgart), Athanasios Tsiokanos (Deltares), Ann van Griensven (VUB), Michelle van Vliet (Utrecht University), Niko Wanders (Utrecht University), Albrecht Weerts (Deltares), Michel Wortmann (ECMWF), Richard Alpfjord Wylde (SMHI), Wenpeng Xie (University of Tokyo), Anshul Yadav (TAMU), Kosuke Yamamoto (Japan Aerospace Exploration Agency (JAXA)), Kei Yoshimura (University of Tokyo), Xing Yuan (Institute of Atmospheric Physics (IAP), Chinese Academy of Sciences), Yongqiang Zhang (Institute of Geographic Sciences and Natural Resources Research (IGSNRR), China), Markus Ziese (Global Precipitation Climatology Centre (GPCC)) and Ervin Zsoter (ECMWF), who contributed to the initial discussions, report preparation, global modelling and space-based observational data, feedback and review.

GLOBAL HYDROLOGICAL DATA COLLECTION CENTRES AND EXTERNAL EXPERTS

Feifei Cao (International Groundwater Resources Assessment Centre (IGRAC)), Stephan Dietrich (International Center for Water Resources and Global Change (ICWRGC)/Federal Institute of Hydrology (BfG)), David Fairbairn (EUMETSAT H SAF), Jay Famiglietti (Arizona State University (ASU)), Elie Gerges (IGRAC), Claudia Giardino (CNR-IREA), Frank Kaspar (EUMETSAT), Elisabeth Lictevout (IGRAC), Dmytro Lisniak (Global Environment Monitoring System for Freshwater (GEMS/Water)), Simon A. Mischel (Global Runoff Data Centre (GRDC)), Henning Plessow (GRDC), Philipp Saile (GEMS/Water), Marc Schröder (EUMETSAT CM SAF), Markus Ziese (Global Precipitation Climatology Centre (GPCC)) and Matthias Zink (International Soil Moisture Network (ISMN)), who supported the preparation of the report.

We thank Jan Polcher and Aaron A. Boone (Global Energy and Water Exchanges (GEWEX)) for contributing to the preparatory workshop for this report. We also thank the research group of Nico Sneeuw (University of Stuttgart) for datasets for the extension of in situ river discharge data through satellite observations.

CONTRIBUTORS AND CO-AUTHORS FOR SPECIFIC CHAPTERS

Groundwater levels: Feifei Cao (IGRAC), Elie Gerges (IGRAC), Elisabeth Lictevout (IGRAC), who led the preparation of the chapter and developed the methodology.

Soil moisture: Matthias Zink (ISMN), who contributed to the soil moisture chapter with in situ data and supported the drafting of the related section.

Terrestrial water storage: Eva Boergens and Andreas Güntner (GFZ), who provided the terrestrial water storage data which form an important part of the present report; and Jay Famiglietti (ASU) who contributed to drafting the section.

Snow cover and glaciers: Lawrence Mudryk (ECCC) and Albin Wells, Ethan Welty and Michael Zemp (World Glacier Monitoring Service (WGMS), University of Zurich) who provided results on glacier mass changes and snow cover.

Water quality section in the annex: Moritz Heinle, Dmytrow Lisniak and Philipp Saile (GEMS/Water Data Centre), who provided results and drafted the text for the water quality analysis.

WMO SECRETARIAT LEAD AUTHORS

Anastasia Lobanova (Scientific Officer), Sulagna Mishra (Scientific Officer) and Robert Wayne Jenkinson (Director, Hydrology and Cryosphere), who were also supported by colleagues within the Secretariat in producing and reviewing the report.

INDEPENDENT CONSULTANTS

Iulii Didovets, who carried out the scientific analysis of the raw data to produce the results for the chapters on river discharge, reservoirs, lakes, soil moisture, evapotranspiration, snow cover and glaciers, and high-impact hydrological events and contributed to the writing of the report together with the authors mentioned above. Nilay Dogulu created infographics for the publication.

and many more

List of abbreviations

AET	Actual evapotranspiration
DJF	December–January–February
ENSO	El Niño–Southern Oscillation
ESA	European Space Agency
EUMETSAT	European Organisation for the Exploitation of Meteorological Satellites
GHMS	Global hydrological modelling system
GIRAFE	Global Interpolated RAinFall Estimation
GPCC	Global Precipitation Climatology Centre
GRACE	Gravity Recovery and Climate Experiment
GRDC	Global Runoff Data Centre
GTN-G	Global Terrestrial Network for Glaciers
HydroSOS	Hydrological Status and Outlook System
ICWRGC	International Center for Water Resources and Global Change
IGRAC	International Groundwater Resources Assessment Centre
ISMN	International Soil Moisture Network
JJA	June–July–August
MAM	March–April–May
NMHSs	National Meteorological and Hydrological Services
SAF	Satellite Application Facility
SON	September–October–November
SWE	Snow water equivalent
SWOT	Surface Water and Ocean Topography
TWS	Terrestrial water storage
WGMS	World Glacier Monitoring Service
WHOS	WMO Global Hydrological Observing System

Executive summary

Semi-decadal statement

- In five years, the State of Global Water Resources report has expanded from 3 to 15 hydrological variables, while country coverage increased more than sevenfold for river discharge and more than fivefold for groundwater. However, Asia and Africa are still among the least represented regions in terms of hydrological observations in the report.

- The share of global basin area experiencing normal discharge conditions has remained below the historical mean in each of the past seven years (34%–38%, against a 1991–2020 mean of 46%). Terrestrial water storage (TWS) shows a persistent decline since 2014–2016, with increasing area under below-normal conditions.

- Across the five reporting years, recurring below-normal river discharge was observed in major parts of the Amazon and La Plata basins, North America, Central and East Africa, Central Asia and the Middle East.

- Between 2021 and 2025, below-normal TWS repeatedly affected the south-western United States, Patagonia and the subtropical Andes, the Ganges–Indus headwaters, northern Africa, the Middle East, Central Asia and eastern China, while persistent positive anomalies occurred in parts of sub-Saharan Africa, the Sahel and the Tibetan Plateau.

- Between 2023 and 2025, glaciers lost mass in each reporting year, with cumulative global glacier mass loss at 1 400 Gt of water. The year 2025 marked the fourth consecutive year where all major glaciated regions experienced glacier mass loss. Some small-glacier regions (the European Alps, Scandinavia, the Caucasus and others) may already have passed "peak water".[1]

- Persistent groundwater deficits were observed during 2022–2025 in parts of the Americas, Europe, the Middle East, India, southern Africa and Australia, with over-abstraction identified as an important driver in several regions.

- The La Plata and Amazon basins, the Middle East and the Greater Horn of Africa experienced persistent multi-year drought conditions, while severe floods repeatedly affected West and Central Africa and South-East Asia.

- Over the past five years, Asia and Africa together accounted for nearly half of all recorded water-related extreme events and more than 80% of reported associated deaths.[2] Assessing the economic losses from these disasters remains challenging because losses are not reported systematically, particularly in countries with limited insurance coverage and disaster-loss accounting capacity.

---

1 Peak water refers to the threshold where the glacier reaches its maximum runoff due to melting.

2 As reported in EM-DAT. (Events like floods, droughts, glacial lake outbursts, landslides (wet), heavy rainfall events leading to floods, and tropical cyclones were selected. Also, events defined as Storm, Severe weather and Extra-tropical cyclone were included if their primary associated hazard was defined as flooding).

Hydrological conditions and high-impact events in 2025

- **Climatic conditions**: The year 2025 was one of the warmest years on record, at 1.43 °C (±0.13 °C) above the 1850–1900 pre-industrial baseline. Significant warm anomalies affected many regions, including Greenland, northern Canada, Western Europe, Fennoscandia,[3] the Mediterranean, and parts of Asia, Africa, Australia and South America. In terms of the El Niño–Southern Oscillation (ENSO), neutral conditions prevailed for most of 2025, though a weak La Niña re-emerged toward year end. At the same time, a predominantly negative Indian Ocean Dipole favoured reduced rainfall over East Africa and increased rainfall over Indonesia, Australia and the south-western Arabian Peninsula. Annual precipitation was near normal across many major basins, including much of the Amazon, Paraná, Mackenzie, Nelson, St. Lawrence and Fraser basins, although with some seasonal and sub-basin variability. Much-above-normal precipitation affected several regions, including the upstream Mississippi basin, the Limpopo and Orange basins, parts of the Niger and Lake Chad basins, the Volga, Ob, Ural and Yenisei basins, and major basins in India and South-East Asia. Precipitation was below to much below normal in the September–October–November (SON) period across northern Africa, the Mediterranean coast and the Greater Horn of Africa. The Middle East experienced persistent dry conditions, with below- to much-below-normal precipitation throughout the year and drought developing during March–April–May (MAM) and June–July–August (JJA). Extreme precipitation events were observed in southern Africa and Asia, particularly across the Zambezi, Limpopo and Orange basins, and in the headwaters of the Indus basin.

- **River discharge:** Observed daily river discharge data were available for 3 611 stations in total: 3 115 stations provided in situ observations, while discharge records for 496 stations were infilled using space-based observations. Most of these stations are located in Europe (36.9%); North America, Central America and the Caribbean (27.2%); the South-West Pacific (19.2%); and South America (9.6%). The smallest proportion of stations with available data for the report are found in Africa and Asia (7.1% in total). In 2025, approximately 36% of the global catchment area experienced drier-than-normal conditions, 36% was within the normal range, and 21% was wetter than normal.[4] Overall, 2025 was a dry year for river discharge worldwide, and one of the driest in 35 years (1991–2025). Annual river discharge in 2025 was above to much above normal across South, East and South-East Asia, parts of northern South America, and selected African and north-eastern and eastern Australian basins. Below- to much-below-normal river discharge affected several major regions, including much of North America, the La Plata and São Francisco basins of South America, Eastern European basins, the Middle East and Central Asia. Africa showed contrasting river discharge conditions, with above-normal flows in the Senegal, Niger, Lake Chad, Orange and Limpopo basins, but much-below-normal discharge in the Nile, Congo and Zambezi basins.

- **Reservoirs:** Reservoir inflows in 2025 were below to much below normal across the Middle East, Eastern Europe, Central Asia, and parts of North America and South America (across Patagonia, as well as the La Plata and São Francisco basins). In contrast, South and

---

[3] The Fennoscandian Peninsula encompasses Norway, Sweden, Finland and north-western parts of the Russian Federation.

[4] Based on results of simulations performed using global hydrological modelling systems (GHMSs). Note: The normal range is defined as the 25th–75th percentile. Under stationary conditions, the share of area under normal conditions averages around 50% in the long term, though the share in any individual year may fluctuate around this value. In addition, around 7% of the global catchment area is not modelled because of model-resolution limitations.

South-East Asia recorded above- to much-above-normal inflows. Reservoir storage was below to much below normal across Eastern Europe, Central Asia, the Middle East and parts of the United States, broadly reflecting inflow deficits. Above-normal storage was observed in parts of Central America and West Africa (the Niger and Senegal basins). Reservoirs in the Orange River basin (Africa) and across parts of South and South-East Asia (India, Myanmar and Thailand) showed normal to below-normal storage despite above-normal inflow anomalies (likely due to reservoir operations, withdrawals, and the timing of inflow events).

- **Lakes:** African lakes and reservoirs showed widespread much-above-normal water levels in 2025, including Lakes Malawi, Chad, Victoria, Tanganyika, Rukwa and Turkana, as well as Volta and Nasser reservoirs. Kariba reservoir remained much below normal. In Europe, water levels in Lakes Peipus and Ladoga remained near normal, while water levels in Lake Beyşehir in Türkiye and Lake Urmia in the Islamic Republic of Iran were below to much below normal. Across Canada, lake levels were generally below to much below normal. Lake surface water temperature in July 2025 was above normal in Lake Michigan and Lake Erie and across selected African lakes, normal in Lakes Victoria, Ladoga, Peipus, Superior, Huron and Ontario and much below normal in Lakes Chad and Malawi. In January 2025, Lakes Tanganyika, Nasser and Malawi in Africa, together with selected lakes in South America, recorded above- to much-above-normal surface water temperatures, while in Lake Victoria it remained normal. Lake ice cover duration was generally below to much below normal across the assessed Eurasian and North American lakes, with some exceptions, including normal conditions in Lakes Peipus and Michigan and much-above-normal duration in Lakes Huron and Erie.

- **Groundwater levels:** In 2025, 65% of groundwater observation stations recorded annual mean levels outside the normal range, with below- to much-below-normal levels observed at 34% of stations (25% in 2024), and above- to much-above-normal levels at 31% (37% in 2024). The percentages are derived from regions with available groundwater monitoring data, and indicate a shift towards more widespread below-normal groundwater conditions compared to 2024. Persistent and widespread below- to much-below-normal groundwater levels were observed across Central and Eastern Europe, the central United States, parts of Mexico, northern and central Chile, north-eastern and central-western Brazil, northern South Africa, north-western India and parts of southern Australia, pointing to a cumulative depletion with a multi-year drying trend (Jasechko et al., 2024; Cao et al., 2026). Several regions shifted from below normal in 2024 to normal or above normal in 2025, including parts of the Caribbean (Cuba, Jamaica), central to northern Brazil, and northern New Zealand. Additional areas with above- to much-above-normal conditions include parts of France, much of Northern Europe, the south-eastern United States, large parts of South Africa, South-East Asia and eastern Australia.

- **Soil moisture:** Soil moisture was below normal across much of South America and the Middle East during December–January–February (DJF) and JJA, while northern Africa shifted from much-below-normal conditions in DJF to much-above-normal conditions in JJA. Above-normal conditions prevailed in India during both seasons and in southern Africa during JJA. In Europe, below-normal soil moisture conditions developed during JJA. In North America, large areas experienced much-above-normal soil moisture during DJF, followed by widespread much-below-normal conditions during JJA. In the United States, after a mostly dry spring and summer, soil moisture started recovering in September and continued to improve over the subsequent months. In the current edition, the number of stations providing observed soil moisture data has increased, however the geographical coverage has decreased; for this

report only data from the United States were available (183 stations and 119 stations, depending on the depth of measurement).

- **Evapotranspiration:** Persistent negative actual evapotranspiration (AET) anomalies affected several regions, including the Middle East, Central Asia, south-eastern Europe and the Greater Horn of Africa, with below- to much-below-normal conditions continuing through JJA and SON. South America experienced below-normal AET in DJF and JJA, particularly across the Paraná and São Francisco basins. In North America, AET shifted from above-normal conditions in MAM to much-below-normal conditions in several basins during JJA. Much-above-normal AET persisted across large parts of Asia, affecting China, India and major South and South-East Asian basins from MAM into JJA and, in some areas, SON.

- **Terrestrial water storage:** Below-normal terrestrial water storage (TWS) persisted across several major regions in 2025, including northern and south-western North America, Patagonia, Eastern Europe, the Middle East, Central Asia, eastern Brazil, northern India, parts of Northern Europe, the Russian Federation, China and northern Africa, continuing the pattern of the year 2024. South America showed signs of partial TWS recovery, with the area affected by below- to much-below-normal TWS in the La Plata basin decreasing and conditions mostly returning to normal. Much-above-normal TWS in Central and southern Africa continued from 2024 into 2025.

- **Snow cover:** Snow conditions were below normal across Europe, with Eastern European basins, including the Danube, Dnieper, Don and Volga, as well as those in Western and Northern Europe, recording below- to much-below-normal seasonal peak snow mass and March snow water equivalent (SWE). Snow cover in the Russian Federation showed strong regional contrasts in March SWE, with deficits in the upstream Yenisei and Ob basins, but above- to much-above-normal values in the Amur basin and downstream parts of the Ob and Yenisei basins; seasonal peak snow mass was generally near normal. North America had mostly near-normal seasonal peak snow mass, but mixed March SWE, with deficits in parts of the Mississippi and St. Lawrence basins and surpluses in portions of the Nelson, Mackenzie, Churchill and Yukon basins. Seasonal peak snow mass was much below normal in the Colorado basin as well as the Fraser basin and the surrounding Pacific seaboard along the western coast of Canada.

- **Glaciers:** In the hydrological year 2025,[5] glaciers lost 408 ± 132 Gt of mass, equivalent to 1.1 ± 0.4 mm of sea-level rise, marking the fourth consecutive year in which every major glaciated region recorded a net loss. In 2025, the Central Asia, South Asia West, Russian Arctic, Iceland, and Western Canada and USA Global Terrestrial Network for Glaciers (GTN-G) regions (see Figure 24 in the Glaciers chapter) all recorded annual mass balances that ranked among the three most negative years on record for those regions. Some regions dominated by smaller glaciers, such as the Caucasus, Western Canada and USA, and Central Europe regions, experienced little or no increase, or even a decrease, in the 2025 summer balance despite greater annual mass loss compared with 1991–2020.[6] This indicates that these regions may already have reached peak water conditions.[7]

---

[5] The hydrological year used in glacier analysis ran from October 2024 to September 2025.

[6] Summer balance is a minimum approximation of summer runoff.

[7] Peak water refers to the threshold where the glacier reaches its maximum runoff due to melting.

- **Water quality:**[8] January 2025 was characterized by widespread above- to much-above-normal river temperatures, particularly across Africa, Eastern Europe, Eurasia, Australia and parts of South America. In July 2025, the warm river-temperature anomalies persisted across Asia and the Middle East, affecting major basins including the Yangtze, Tarim, Brahmaputra and Amur. Several regions showed near-normal river temperatures in July, including much of South America and the Congo, Zambezi, Limpopo and Orange basins in Africa. In terms of the annual observed water temperature, in the United States, Switzerland, the United Kingdom and the Republic of Korea, most stations for which data were available recorded above- to much-above-normal river temperatures. The east coast of the United States was a notable exception.

- **Significant events:** Asia and Africa were the regions most affected by extreme hydrometeorological events in 2025, with several African countries experiencing major flooding for two consecutive years (as in the case of Nigeria) or even three consecutive years (as in the Democratic Republic of the Congo). South and South-East Asia were hit by the compounded effects of tropical cyclones and intense monsoon rainfall, leading to more than 3 600 deaths across the affected countries – Sri Lanka, Pakistan, Viet Nam, Indonesia, Thailand, Malaysia and the Philippines. In the United States, catastrophic flash flooding hit the Texas Hill Country on 4 July 2025, when the Guadalupe River rose rapidly; the event caused at least 135 fatalities, most of them in Kerr County. Economic losses in Jamaica due to hurricane *Melissa* and associated flooding ranked among the highest recorded in 2025, resulting in a loss of 41% of the gross domestic product (GDP) of the country. Cyclone *Ditwah* cost Sri Lanka around 4% of GDP. Severe drought gripped Eastern Europe, the Mediterranean and the Middle East, with Türkiye, Armenia, the Syrian Arab Republic and Jordan each recording their driest conditions in decades. Drought also returned to the Greater Horn of Africa after one of the driest October–December seasons on record linked to La Niña and a negative Indian Ocean Dipole, prompting a national emergency in Somalia.

Key advancement of the 2025 report

- **Observations**: Over the past five years, the number of observed data points received from WMO Members, the Global Runoff Data Centre (GRDC) and other partners for river discharge measurements increased dramatically: from just 14 stations in 7 countries in 2021 to 3 115 stations in 52 countries in 2025. However, despite improvements in observational data, Africa and Asia remain underrepresented in hydrological data availability in the report, representing only 7% of the stations included. This highlights the need for improved monitoring and data sharing, particularly in these areas. Similarly, the coverage of groundwater observational stations improved compared to the 2024 report, with data from 43 529 stations across 51 countries available in 2025. In contrast, soil moisture observations remained scarce, this year covering stations in the United States only (183 stations and 119 stations, depending on the depth of measurement).

- **Models and data sources:** Modelling, remote sensing and in situ observation-based data products all contributed to the 2025 report; among these, 13 global hydrological modelling systems (GHMSs) provided substantial input that strengthened the analysis of variables, especially river discharge, evapotranspiration, soil moisture, snow and ice, and TWS. This year,

[8] Only water temperature is presented in the main report. For other water quality variables, please refer to the annex.

for the first time, the report provides observations from the National Aeronautics and Space Administration–Centre national d'études spatiales (NASA–CNES) Surface Water and Ocean Topography (SWOT) mission. Though currently limited to a 2024–2025 comparison, SWOT data provide a new and promising source of satellite-based information helping to enhance future monitoring of surface water dynamics.

- **Coverage:** The 2025 edition of this report was enhanced by the addition of a new chapter providing an overview of lake ice extent and water quality parameters, both obtained from models (water temperature) and observed data.

- **Model validation:** Where validation was possible, modelled river discharge anomalies agreed with observations in 63% of the validated basins, in particular in the La Plata basin, North America, parts of India, Australia, the Middle East, southern Africa and Europe. Disagreement was found in parts of eastern North America, the Amazon Basin and parts of Australia. Moreover, the intra-model agreement was also robust: over 50% of the models agreed on the anomaly trend for 98% of the assessed area.

Introduction

Knowledge of water resources and hydrological extremes at the local, regional and global scales is fundamental to managing the risks of drought, flooding and cryosphere loss, as well as adapting to a changing climate. The State of Global Water Resources report, now in its fifth edition, is the most comprehensive standardized science-based annual assessment of water resources availability and variability at the global scale. Through its assessment of the key components of the hydrological cycle, including river discharge, groundwater, evapotranspiration, terrestrial water storage (TWS), snow and ice as well as high-impact events for the year 2025, the report provides an evidence base to support water-resources assessment, preparedness and planning, and the identification of monitoring and data-sharing priorities at national, regional and global levels.

The 2025 edition of the report continues to integrate both in situ observations and model-based data derived from modelling and space-based observations. In situ observations remain the foundation of hydrological assessment: modelling and space-based observations extend spatial coverage beyond what point measurements can provide, but depend on in situ records for calibration and validation.

The current edition expands the contribution of observed data from WMO Members and partners, with 68 countries providing river discharge, groundwater, water quality and soil moisture data (Figure 1). As shown in Figure 1, river discharge data were received from 3 115 stations across 52 countries, compared with 2 777 stations across 41 countries for the previous report. A similar increase was observed for groundwater data: measurements from 43 529 stations across 51 countries were collected for the fifth edition of the report, compared with 37 406 stations across 47 countries for the previous edition. This growing global cooperation, underpinned by the

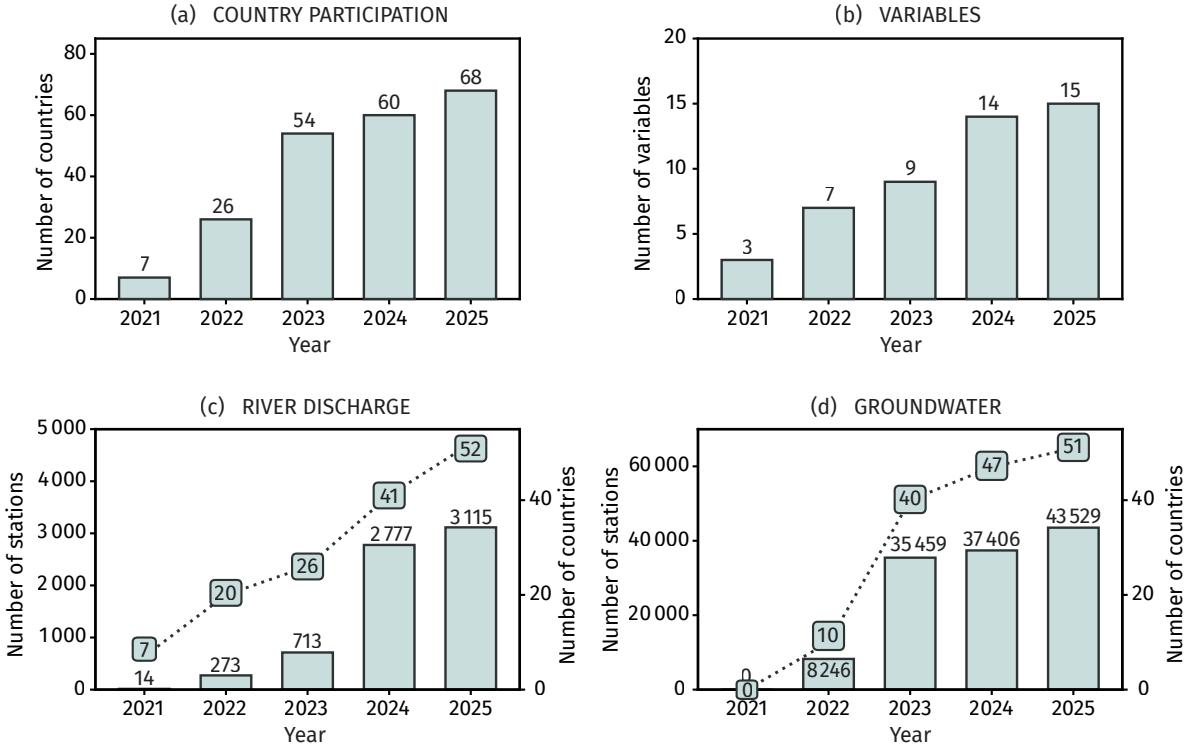


Figure 1. Growth in data sources/variables

continued commitment, engagement and interest of WMO Members and partners, highlights the report's value as a platform for strengthening the exchange of hydrological data worldwide.

In the 2025 report we have continued to use remote sensing-based discharge estimates to infill in situ observation records in river discharge. For the first time, this edition also introduces observations from the National Aeronautics and Space Administration–Centre national d'études spatiales (NASA–CNES) Surface Water and Ocean Topography (SWOT) mission. While the available record is currently limited to a comparison between years 2024 and 2025, SWOT provides a new promising source of satellite-based information on river water surface elevation, width and slope, with strong potential to enhance global monitoring of surface water dynamics in the future.

The global hydrological modelling and space-based observation communities have made substantial contributions to the sections on river discharge, reservoir inflows and storage, lake levels, lake water temperature, lake ice cover duration, soil moisture, evapotranspiration, TWS, snow cover, glaciers and water quality. The soil moisture indicators are based on data obtained from space-based measurements and observed data obtained from the International Soil Moisture Network (ISMN). Observed water quality parameters are obtained from the GEMS Water Data Centre and modelled data are obtained from simulations performed using three models at the global scale.

Following this introduction, a semi-decadal statement provides a retrospective of the past five years' experience in data sharing and bringing different datasets under one methodology, an analysis of areas of recurring hydrological anomalies, a five-year record of global hydrological variability and future perspective. The main body of the report starts with a chapter providing an overview of climatic conditions covering precipitation patterns, including extreme precipitation, followed by chapters on river discharge, reservoirs, lakes, groundwater levels, soil moisture, evapotranspiration, terrestrial water storage, snow cover and glaciers, and water quality, each offering global and/or regional insights. The chapter on high-impact hydrological events provides a global overview of extreme and impactful hydrological events in 2025.

Strengthening data sharing and engagement from WMO Members will remain central for future editions of the report. A comprehensive understanding of hydrological processes and their impacts on water resources based on observed data is essential for improving the validation of model outputs across global river basins. In turn, modelling and space-based observation products can provide consistent data across space and time and fill gaps in regions with scarce (or no) observations, thus improving understanding of the state of water resources.

These efforts are supporting progress towards achieving the objectives of the Early Warnings for All (EW4All) initiative, particularly by promoting capacity building for regular status calculations at national and regional scales, and by encouraging data sharing (which is key for improving forecasting systems) and accessibility for effective water-related hazard monitoring, moving towards the provision of universal early warning systems by 2027. The report forms part of an integrated WMO framework for monitoring and reporting on the global water cycle. It complements the WMO Hydrological Observing System (WHOS), which enables the discovery and exchange of in situ hydrological observations, and the WMO Global Hydrological Status and Outlook System (HydroSOS), which produces standardized indicators of current hydrological status and sub-seasonal to seasonal outlook. Together, these components form an end-to-end chain than ranges from observation and data exchange through operational status and outlook products to the annual global assessment provided in this report, all underpinned by the WMO Unified Data Policy.

Data sources

The data used in the report were gathered from various sources to ensure a robust, spatially consistent and comprehensive analysis (refer to Box 1 and Data sources in the annex), including National Meteorological and Hydrological Services (NMHSs), global hydrological data collection centres (hereafter referred to as data centres), the space-based observation community and the global modelling community. The River discharge, Soil moisture and Water quality chapters are based on modelled and observed data, and the Groundwater levels chapter is based only on in situ observations. Where possible, in situ data were used to validate the modelled results. Global hydrological modelling systems (GHMSs) contributed to obtaining values for additional hydrological variables, in particular reservoir inflows and actual evapotranspiration.

BOX 1. DATA SOURCES

- *Precipitation:* Global Precipitation Climatology Centre (Becker et al., 2013; GPCC, 2025; Schneider et al., 2014) and daily and monthly EUMETSAT CM SAF Global Interpolated RAinFall version 1 (GIRAFE v1) (Konrad et al., 2025) datasets.
- *Observed river discharge data:* National Meteorological and Hydrological Services (NMHSs), Global Runoff Data Centre (see GRDC Data Portal), extended river discharge estimates using remote sensing data (Elmi et al., 2024; Saemian et al., 2025, 2026).
- *Modelled river discharge data:* Thirteen global hydrological modelling systems (GHMSs) – CaMa-Flood with Dam (Hanazaki et al., 2022; Yamazaki et al., 2011), Conjunctive Surface–Subsurface Process version 3 (CSSPv3) (Yuan et al., 2026), DHI-GHM (Murray et al., 2023), ecLand (Boussetta et al., 2021), Global Flood Awareness System (GloFAS) (Alfieri et al., 2013; Grimaldi et al., 2023), HBV-PML (Huang et al., 2022; Zhang et al., 2019), mesoscale Hydrologic Model (mHM) (Kumar et al., 2013; Samaniego et al., 2010, 2019; Shrestha et al., 2025), PCR-GLOBWB 2 (Sutanudjaja et al., 2018), GEOGLOWS River Forecast System (RFS) (Hales et al., 2022), WaterGAP 2.3 (Nyenah et al., 2026), World-Wide HYPE v1.3.9 (Arheimer et al., 2020), Today's Earth – Global (JRA-55) (Ma et al., 2024; Yoshimura et al., 2008) and Wflow_sbm (Eilander et al., 2021; Imhoff et al., 2020; Verseveld et al., 2024).
- *Inflow into selected reservoirs globally:* Four GHMSs – CaMa-Flood with dams (Hanazaki et al., 2022; Yamazaki et al., 2011), World-Wide HYPE (Arheimer et al., 2020), CSSPv3 (Yuan et al., 2026) and Wflow_sbm (Eilander et al., 2021; Imhoff et al., 2020; Verseveld et al., 2024).
- *Reservoir volume anomalies:* Texas A&M University (TAMU) (Li et al., 2023).
- *Lake levels, ice cover duration and temperature:* European Space Agency (ESA) (Lake CCI project).
- *Groundwater level data*: International Groundwater Resources Assessment Centre (IGRAC).
- *Soil moisture:* Exploitation of Meteorological Satellites (EUMETSAT) Satellite Application Facility on Support to Operational Hydrology and Water Management (H SAF) Root Zone Soil Moisture Data Record version 3 (H SAF, 2026) and observed data for the United States from the International Soil Moisture Network (ISMN).
- *Evapotranspiration:* Six GHMSs – CSSPv3 (Yuan et al., 2026), mHM (Kumar et al., 2013; Samaniego et al., 2010, 2019; Shrestha et al., 2025), WaterGAP 2.3 (Nyenah et al., 2026), World-Wide HYPE v1.3.9 (Arheimer et al., 2020), HBV-PML (Huang et al., 2022; Zhang et al., 2019) and Wflow_sbm (Eilander et al., 2021; Imhoff et al., 2020; Verseveld et al., 2024).
- *Terrestrial water storage:* GRACE/GRACE Follow-On satellites (Landerer et al., 2020; Tapley et al., 2004).
- *Glaciers:* WMO Member States and Territories, World Glacier Monitoring Service (WGMS).
- *Snow water equivalent:* Environment and Climate Change Canada (Mudryk et al., 2025, 2026).

- *Water quality:* NMHSs and National Environmental Agencies, UNEP Global Environment Monitoring System for Freshwater (GEMS/Water) through the Global Freshwater Quality Database (GEMStat – The global water quality database) and three global water quality model based products: DynQual (Jones et al., 2023), DyER-TM (Jones et al., 2025; Mohseni and Stefan, 1999) and CoSWAT-WQ (Chawanda et al., 2025; Nkwasa et al., 2025).
- *High-impact events:* Communication from WMO Members for WMO State of the Global Climate report, open data sources, such as the EM-DAT database (CRED, 2026), ReliefWeb, World Bank and others.
- *Water surface elevation data:* The Surface Water and Ocean Topography (SWOT) mission (Getirana et al., 2024, 2026).

Note: See Table A.3 in the annex for a list of GHMSs contributing to each variable.

Anomaly calculation

For each of the variables presented, the anomaly was calculated by comparing the annual, seasonal or monthly mean value in 2025 to the distribution of the corresponding (annual, seasonal to monthly) means obtained from the historical period as described in Box 2 and presented in Figure 2. Note that in this report, the term "anomaly" is used to describe the status of water resources in each basin in comparison with the long-term historical near-normal conditions for that basin, and that historical periods differ from variable to variable refer to Table A.2 in the annex), as well as spatially for observed discharge data. Further details on the methods (including an overview of all data sources), the GHMSs used in the analysis, the definitions of the indicators used in the report, and additional results are documented in the annex.

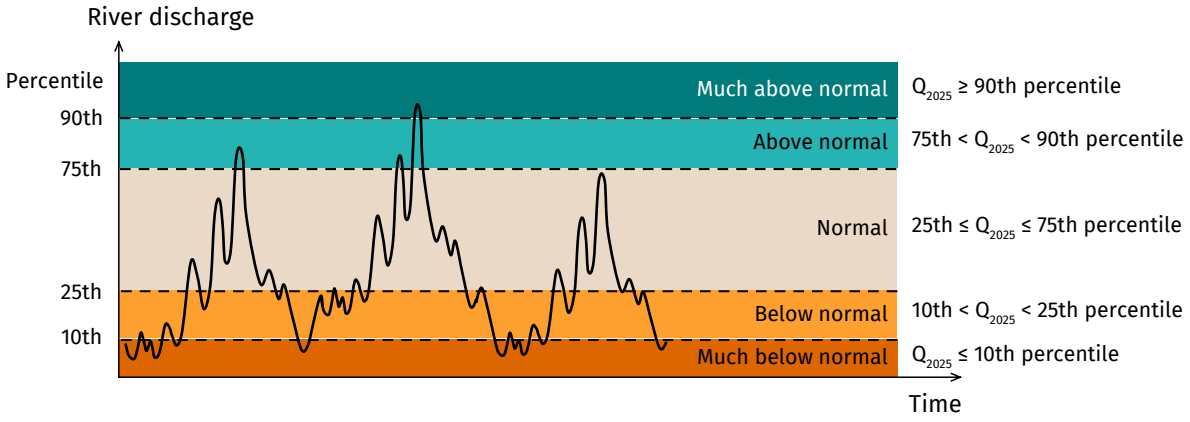


Figure 2. Conceptual diagram illustrating the classification of variable conditions (for example, river discharge) in 2025 relative to the historical reference period. Percentile thresholds define five categories: much above normal (≥90th percentile), above normal (75th–90th percentile), normal (25th–75th percentile), below normal (10th–25th percentile), and much below normal (≤10th percentile).

BOX 2. ANOMALY CALCULATION

For each hydrological variable, mean annual (seasonal or monthly) values were calculated for every year in the reference period, using either modelled or observed data. The mean 2025 value was then compared with the reference-period distribution and assigned to one of five percentile-based categories:

much below normal:	$Q_{2025} \leq$ 10th percentile (referring to exceptionally dry conditions)
below normal:	10th $< Q_{2025} <$ 25th percentile
normal:	25th $\leq Q_{2025} \leq$ 75th percentile
above normal:	75th $< Q_{2025} <$ 90th percentile
much above normal:	$Q_{2025} \geq$ 90th percentile (referring to exceptionally wet conditions)

Where results are obtained from several models, the above-specified categories were assigned an integer ("much below normal" = 1, "below normal" = 2, "normal" = 3, "above normal" = 4, "much above normal" = 5), then an average was calculated across the outputs of the ensemble of models for each of the basins. The resulting number was rounded and translated back into one of the categories listed above.

Note that the reference period varies for the different variables based on data availability. For example, 30 or 20 years (1991–2020 or 2001–2020) is the reference period for river discharge, whereas 20 or 10 years (2001–2020 or 2015–2024) is used for groundwater. While the historical period used differs from variable to variable, as well as spatially for observed discharge data (refer to Table A.2 in the annex), the classification of the anomaly ranking remains the same. Note that the selection of different reference periods is likely to influence the calculated results.

Semi-decadal statement

A five-year retrospective of the State of Global Water Resources

- In five years, the report has expanded from 3 to 15 hydrological variables, while country coverage increased more than sevenfold for river discharge and more than fivefold for groundwater. However, Asia and Africa are still among the least represented regions in terms of hydrological observations in the report.
- The share of global basin area experiencing normal discharge conditions has remained below the historical mean in each of the past seven years (34%–38%, against a 1991–2020 mean of 46%). Terrestrial Water Storage (TWS) shows a persistent decline since 2014–2016, with increasing area under below-normal conditions.
- Across the five reporting years, recurring below-normal river discharge was observed in major parts of the Amazon and La Plata basins, North America, Central and East Africa, Central Asia and the Middle East.
- Between 2021 and 2025, below-normal TWS repeatedly affected the south-western United States, Patagonia and the subtropical Andes, the Ganges–Indus headwaters, northern Africa, the Middle East, Central Asia and eastern China, while persistent positive anomalies occurred in parts of sub-Saharan Africa, the Sahel and the Tibetan Plateau.
- Between 2023 and 2025, glaciers lost mass in each reporting year, with cumulative global glacier mass loss at 1 400 Gt of water. The year 2025 marked the fourth consecutive year where all major glaciated regions experienced glacier mass loss. Some small-glacier regions (the European Alps, Scandinavia, the Caucasus and others) may already have passed "peak water".[9]
- Persistent groundwater deficits were observed during 2022–2025 in parts of the Americas, Europe, the Middle East, India, southern Africa and Australia, with over-abstraction identified as an important driver in several regions.
- The La Plata and Amazon basins, the Middle East and the Greater Horn of Africa experienced persistent multi-year drought conditions, while severe floods repeatedly affected West and Central Africa and South-East Asia.
- Over the past five years, Asia and Africa together accounted for nearly half of all recorded water-related extreme events and more than 80% of reported associated deaths.[10] Assessing the economic losses from these disasters remains challenging because losses are not reported systematically, particularly in countries with limited insurance coverage and disaster-loss accounting capacity.

[9] Peak water refers to the threshold where the glacier reaches its maximum runoff due to melting.

[10] As reported in EM-DAT. (Events like floods, droughts, glacial lake outburst, landslides (wet), heavy rainfall events leading to floods, and tropical cyclones were selected. Also, events defined as Storm, Severe weather and Extra-tropical cyclone were included if their primary associated hazard was defined as flooding.)

Report background and developments

Over five editions, the report has expanded substantially in scope, methodology, data coverage and institutional engagement. The first edition, covering 2021, focused on three variables: river discharge, TWS and high-impact events. The current 2025 edition covers fifteen essential hydrological variables and draws on contributions from WMO Members, represented by their National Meteorological and Hydrological Services (NMHSs), as well as from global hydrological data centres, hydrological modelling groups, space-based observation centres, international experts and scientists.

One of the most important developments over the five editions has been the growth in observed data contributions.

As shown in Figure 1, both the geographical coverage and the density of observations have expanded substantially since the 2021 edition. The number of countries providing river discharge data increased approximately 7.5-fold, from 7 in 2021 to 52 in 2025, while the number of river discharge stations rose from 14 in the first edition to 3 115 in the current one. River discharge observations are now also complemented by data on a further ~500 stations derived from space-based observations that help to address spatial and temporal gaps. Groundwater coverage increased more than fivefold from 10 to 51 countries, and from around 8 000 sites in the second edition to more than 43 000 in the current edition. This expansion has been driven by the growth in Member participation and enabled, in parallel, by progressive improvements in the methods used to request, collect, process and integrate the data.

However, significant gaps still remain. Africa and Asia together accounted for only about 7% of the stations included in the assessment, while South America accounted for 10%. Continued data sharing is therefore essential to improve the geographical representativeness and robustness of the global assessment, validate modelled and satellite-based information, and strengthen the evidence base for water resource management, early warning and climate adaptation.

Data from GHMS simulations and space-based observation datasets were used from the first edition of the report to fill in the gaps in observed datasets and enable a truly global analysis of the different components of the hydrological cycle. Participation from the modelling community has increased from seven GHMSs in the first edition to 13 in the latest edition, with 29 partners now contributing across modelling, space-based observation and data provision.

Observed data, where available, are used to validate modelled outputs. Regional discrepancies between observations and models remain, particularly in parts of south-eastern Europe, Africa and India. The current validation approach generally uses the gauge located closest to the basin outlet and representing the largest catchment area. However, suitable gauges are not always available near the outlet. In large basins, comparisons between modelled discharge at the outlet and observations from an upstream gauge may be affected by substantial inflows from downstream tributaries or sub-basins, leading to additional uncertainty in the validation results. This underlines the importance of combining multiple sources of information, while continuing to invest in stronger in situ observing networks as well as model development and improvement.

The report has become a platform for bringing scientific innovation into global hydrological assessment practice. Recent editions have included emerging river discharge estimates based on space-based observations, which have significant potential to complement in situ records

and help fill gaps in observational time series. This makes the State of Global Water Resources report more than a synthesis of annual conditions – it is also becoming a curated entry point to scientifically-based hydrological datasets and information for WMO Members, researchers and the global water community.

Semi-decadal status

In meteorological terms, the period 2021–2025 was characterized by exceptional warmth, record-high greenhouse gas concentrations, and continued accumulation of heat in the ocean (see the WMO State of the Global Climate reports for the period). Each year from 2021 to 2025 ranked among the warmest years on record. The five-year period was also influenced by variability in the El Niño–Southern Oscillation (ENSO): moderate La Niña conditions affected 2021 and 2022, then 2023 was affected by El Niño, after which La Niña conditions returned again in 2025. Ocean heat content continued to increase over the past five years, reaching unprecedented levels in 2023 and then again in 2024. These conditions affected the global water cycle by altering evaporation, precipitation patterns, snow and ice storage, soil moisture and runoff generation.

Figure 3 presents the share of global basin area under below-normal, normal and above-normal river discharge conditions (derived from GHMSs) and TWS (derived from satellite gravimetry;

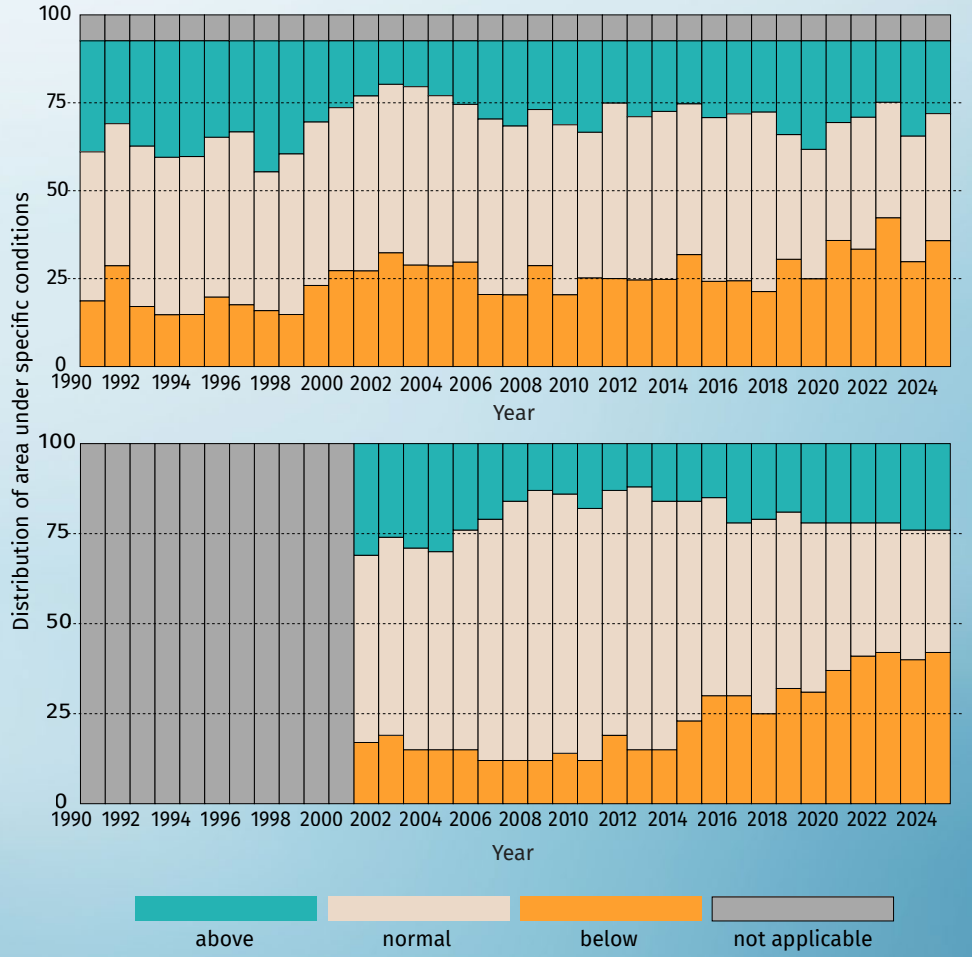


Figure 3. The distribution of global basin area under different river discharge (top) and terrestrial water storage (TWS) (bottom) conditions for the years 1991–2025 for river discharge and 2002–2025 for TWS. Note that the percentage distribution excludes the 7% of global basin area for which no data were available.

see also Huggins et al. (2022)) for each year from 1991 to 2025 for river discharge and from 2002 to 2025 for TWS, using fixed historical reference periods of 1991–2020 and 2002–2020, respectively. The below-normal conditions are defined as values below the 25th percentile, normal conditions as values between the 25th and 75th percentiles, and above-normal conditions as values above the 75th percentile, in line with Box 2. TWS integrates water held in snow and ice, surface water, soil moisture and groundwater. Unlike river discharge, which responds more strongly to short-term rainfall, snowmelt and seasonal variability, TWS captures slower changes in water storage, including groundwater depletion, drought-related reservoir storage losses and global-warming-driven ice loss.

These two variables provide complementary perspectives on recent global hydrological conditions. The share of global basin area experiencing normal discharge conditions has remained below the historical mean in each of the past seven years (34%–38%, against a 1991–2020 mean of 46%).[11] TWS shows a persistent decline since 2014–2016 (as discussed by Rodell et al. (2024) and Chandanpurkar et al. (2025)), with increasing area under below-normal conditions, indicating that, on balance, land is holding less fresh water than before.[12]

Across the five editions of the State of Global Water Resources report, there is a set of persistent and recurring hydrological anomalies. Recurring below-normal river discharge has been recorded in large parts of South America (particularly the Amazon and La Plata basins), in North America (parts of the Fraser, Colorado, Missouri, Mississippi and Nelson basins), in Central and East Africa (parts of the Congo, Nile and Zambezi basins), as well as across territories of Central Asia and the Middle East.

Below-normal TWS anomalies are repeatedly observed in the south-western United States, Patagonia and the subtropical Andes, the Ganges–Indus headwaters, northern Africa, the Middle East, Central Asia and eastern China. In contrast, positive TWS anomalies are observed in parts of sub-Saharan Africa, the Congo–Nile region, the Sahel, the Tibetan Plateau and, more variably, northern South America and the Murray–Darling Basin.

Over all five reporting years glaciers worldwide lost mass: during 2023–2025 global glacier mass loss amounted to around 1 400 Gt of water (see the Glaciers chapter in *State of Global Water Resources 2023* (WMO-No. 1362) and *State of Global Water Resources 2024* (WMO-No. 1380)), with 2025 marking the fourth consecutive year in which all major glaciated regions experienced glacier mass loss (see the Glaciers chapter). Some small-glacier regions, including the European Alps, Scandinavia, Caucasus, western Canada and USA, South Asia West and New Zealand Global Terrestrial Network for Glaciers (GTN-G) regions, may have already passed peak water (see *State of Global Water Resources 2024* (WMO-No. 1380) and the Glaciers chapter).

Groundwater conditions during 2022–2025 indicate several areas with persistent below- to much-below-normal groundwater levels. Northern and central Chile, Central/Eastern Europe, the Middle East, north-western India, northern South Africa, southern/western Australia, California and the southern high plains of the United States, and Mexico stand out as regions with persistent multi-year groundwater deficits. Brazil and Southern Europe show recurring groundwater stress, with some areas recovering temporarily, but others continuing to experience below-normal or worsening conditions (see *State of Global Water Resources 2022* (WMO-No. 1333),

---

[11] The normal range is defined as the 25th–75th percentile. Under stationary conditions, the share of area under normal conditions averages around 50% in the long term, though the share in any individual year may fluctuate around this value. In addition, around 7% of the global catchment area is not represented because of model-resolution limitations.

[12] These records describe recent changes relative to the reference period; however, the period over which these changes have been observed is too short (7–10 years) to determine whether they represent a long-term trend.

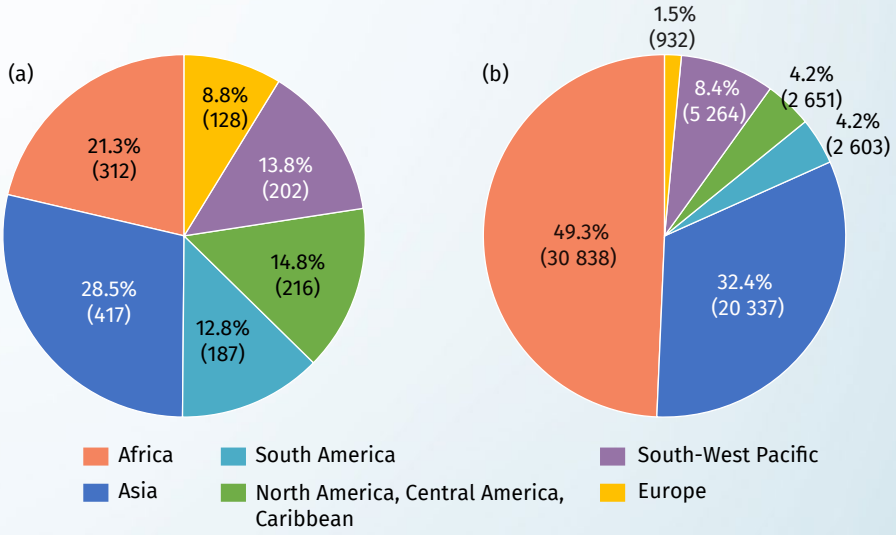


Figure 4. Total reported by EM-DAT number of events (a) and deaths (b) caused by water-related disasters per WMO Region.

Note: Not all disasters and not all their impacts are captured in the EM-DAT database.

Source: EM-DAT

State of Global Water Resources 2023 (WMO-No. 1362), *State of Global Water Resources 2024* (WMO-No. 1380) and the Groundwater chapter). Groundwater level anomalies respond to both climate variability and over-abstraction, with regional differences in the relative contribution of each driver.

Between 2021 and 2025, about 1 500 water-related extreme events were reported by EM-DAT (CRED, 2026; Delforge et al., 2025) globally.[13] These events caused at least 62 500 deaths, with Asia and Africa together accounting for nearly half of recorded water-related extreme events and over 80% of deaths (Figure 4). WMO Region I (Africa) was the most affected region in terms of human losses, accounting for nearly half of all reported fatalities, or approximately 30 800 deaths. This included around 16 700 deaths in sub-Saharan Africa and 14 100 fatalities in northern Africa, latter largely driven by the catastrophic floods in Libya in 2023, which caused approximately 13 500 deaths. WMO Region II (Asia) was the second most affected region, with approximately 20 200 reported deaths.[14,15]

Assessing the economic losses associated with water-related disasters remains challenging. Available EM-DAT data do not support a comprehensive assessment because such losses are not reported systematically, particularly in countries with limited insurance coverage and disaster-loss accounting capacity (Delforge et al., 2025). This highlights the need for more systematic

---

13 Events like floods, droughts, glacial lake outbursts, landslides (wet), heavy rainfall events leading to floods, and tropical cyclones were selected. Also, events defined as Storm, Severe weather and Extra-tropical cyclones were included if their primary associated hazard was defined as Flooding or Dam break.

14 Excluding the mortality from the 2023 Libya floods, WMO Region II (Asia) becomes the region with the highest reported water-related mortality over the period.

15 Figures in this paragraph were derived from country-level records in EM-DAT (CRED, 2026), re-aggregated to WMO Regional Associations. They should be read as minimum estimates. EM-DAT registers only events meeting impact-based entry criteria, so recorded occurrences and losses reflect national reporting and disaster-loss accounting capacity and are systematically under-recorded where that capacity is limited (Delforge et al., 2025). Mortality attributed to drought is incomplete, since deaths arising from prolonged water scarcity and associated food insecurity are rarely attributed to a discrete event; the mortality figures presented here therefore predominantly reflect flood- and storm-related deaths. Droughts are recorded by year of declaration, so multi-year events spanning the reporting period are counted once at onset.

assessment and reporting in these regions, which is essential for tracking progress, identifying trends and directing risk-reduction and adaptation finance where it is most needed.

Several persistent drought events stand out across the five-year review period. The La Plata basin is the site of the most consistently documented multi-year drought, unprecedented in the last 50 years (Rivera, 2024), with conditions deteriorating from 2019 onwards and persisting until 2023, while some areas remained under drought conditions in late 2024 (Toreti, 2024). The Paraguay and Paraná Rivers experienced all-time record low water stages in the second half of 2021 (see Annex 2 in the *State of Global Water Resources 2022* (WMO-No. 1333)). Multi-year, record-breaking (Bai et al., 2026) drought conditions have also affected the Amazon basin, starting in 2022 and deteriorating through 2023–2024. On 26 October 2023 the Rio Negro at Manaus saw the lowest level recorded since 1902 (Espinoza et al., 2024).

Other persistent drought hotspots include the Middle East, where the Islamic Republic of Iran, Iraq, the Syrian Arab Republic and Jordan experienced repeated dry years and consistently below-normal TWS. The year 2025 was the driest year since 1964 in Türkiye. In the Islamic Republic of Iran, spring rainfall was 44% below normal, a situation that led to severe water shortages. Armenia recorded its driest winter (2024/2025) since 1935, with seasonal rainfall at 52% of average. In the Syrian Arab Republic, the 2024/2025 rainy season was the poorest in 60 years nationally.

The Greater Horn of Africa was affected by the multi-year 2020–2022 drought, with the most severe drought conditions ever recorded (*State of the Global Climate 2022* (WMO-No. 1316)), following five consecutive seasons of below-normal rainfall. Late in 2023 the region experienced significant flooding due to heavy rains linked to El Niño and the positive Indian Ocean Dipole. In 2025 new drought conditions started to develop in the region, triggering a state of emergency in Somalia in November. West and Central Africa were affected by severe floods in 2022, 2024 and 2025, claiming almost 3 000 lives in total.

Countries in South-East Asia were repeatedly affected by flooding triggered by tropical cyclones and typhoons, leading to hundreds of deaths each year. In 2025 the Philippines and Viet Nam were badly affected; Viet Nam was hit by 11 typhoons and tropical cyclones throughout one of the country's most severe and prolonged typhoon seasons in decades (Extreme events chapter).

In the central-western United States, multi-year drought persisted from 2020 to 2022, in 2023 centring on the central-southern United States – specifically Texas – where it persisted until 2024 (see the Extreme events chapter in *State of Global Water Resources 2022* (WMO-No. 1333), *State of Global Water Resources 2023* (WMO-No. 1362) and *State of Global Water Resources 2024* (WMO-No. 1380)). In 2025, the same region was hit by a catastrophic and historic flash flood that claimed 135 lives.

Perspective

After five editions, the central lesson of the State of Global Water Resources report is clear: global hydrological assessment is possible, and it depends on sustained cooperation. The strength of the State of Global Water Resources report lies in bringing together in situ observation data, modelling products, space-based observation datasets and expert knowledge into a common, regularly updated assessment framework. The report has shown that fragmented and unevenly distributed hydrological information can be translated into a coherent global picture, while also revealing where the critical observation and data sharing gaps are.

The State of Global Water Resources report has demonstrated that WMO Members can undertake consistent hydrological status assessments at national scales. As the WMO Hydrological Observing System (WHOS) and the Global Hydrological Status and Outlook System (HydroSOS) mature, they will increasingly underpin future editions of the report and support wider WMO and United Nations priorities, including Early Warnings for All and the water-, climate- and disaster-related Sustainable Development Goals.

Five years is a short span in hydrology. This report will continue to document the latest state of water resources, monitor and add the latest reliable data sources, build on solid, scientific hydrological data products and seek answers to the questions:

- How are water resources changing at the global scale?
- Are recent changes part of variability, emerging trends or more structural shifts?
- Are we measuring and sharing the data well enough to tell?

Overview of climatic conditions in 2025

- The year 2025 was one of the warmest years on record, at 1.43 °C (±0.13 °C) above the 1850–1900 pre-industrial baseline. Significant warm anomalies affected many regions, including Greenland, northern Canada, Western Europe, Fennoscandia, the Mediterranean, and parts of Asia, Africa, Australia and South America.
- In terms of the El Niño–Southern Oscillation (ENSO), neutral conditions prevailed for most of 2025, though a weak La Niña re-emerged toward year end. At the same time, a predominantly negative Indian Ocean Dipole favoured reduced rainfall over East Africa and increased rainfall over Indonesia, Australia and the south-western Arabian Peninsula.
- Annual precipitation was near normal across many major basins, including much of the Amazon, Paraná, Mackenzie, Nelson, St. Lawrence and Fraser basins, although with some seasonal and sub-basin variability.
- Much-above-normal precipitation affected several regions, including the upstream Mississippi basin, the Limpopo and Orange basins, parts of the Niger and Lake Chad basins, the Volga, Ob, Ural and Yenisei basins, and major basins in India and South-East Asia.
- Precipitation was below to much below normal in the September–October–November (SON) period across northern Africa, the Mediterranean coast and the Greater Horn of Africa. The Middle East experienced persistent dry conditions, with below- to much-below-normal precipitation throughout the year and drought developing during March–April–May (MAM) and June–July–August (JJA).
- Extreme precipitation events were observed in southern Africa and Asia, particularly across the Zambezi, Limpopo and Orange basins, and in the headwaters of the Indus basin.

This chapter is based on the key findings from the WMO flagship report *State of the Global Climate 2025* (WMO-No. 1391), as well as Global Precipitation Climatology Centre (GPCC) and Global Interpolated RAinFall (GIRAFE) (Konrad et al., 2025) precipitation and drought data products.

The year 2025, slightly cooler than the record-warm 2024, was the second warmest year on record (or third, depending on the global temperature dataset, see *State of the Global Climate 2025* (WMO-No. 1391) for the full list of products) at 1.43 °C (±0.13 °C) above the 1850–1900 pre-industrial baseline. The past 11 years (2015–2025) are now the 11 warmest on record. ENSO-neutral conditions prevailed through most of the year; a weak La Niña present at the end of 2024 dissipated in early 2025, re-emerged toward the end of 2025 and persisted into 2026. The Indian Ocean Dipole was predominantly negative throughout 2025, reaching the third most negative monthly index value in the 45-year record. These climate drivers shape regional rainfall patterns globally, although outcomes vary with the strength and timing of each event and concurrent meteorological factors. La Niña typically favours drier conditions across the Middle East, the Greater Horn of Africa, southern South America and the southern United States and wetter conditions across southern and Central Africa, South-East Asia and northern India. The negative phase of the Indian Ocean Dipole is characterized by strengthened westerly equatorial winds, cooler-than-normal sea-surface temperatures in the western Indian

Ocean and warmer-than-normal temperatures in the east. This pattern is typically associated with reduced rainfall over East Africa and increased rainfall over Indonesia, Australia and the south-western Arabian Peninsula.

Significant warm anomalies in 2025 affected Greenland, northern Canada, Western Europe, Fennoscandia and the Mediterranean, as well as parts of western, central and eastern Asia. Other regions of significant warmth included Central America and the Caribbean, western North America and Mexico, tropical and northern Africa, southern Australia, southern South America, and an area centred on the Antarctic Peninsula.

The ocean, which absorbs around 91% of the excess energy trapped in the Earth system, continued to accumulate heat. Ocean heat content reached the highest level in the 66-year observational record, exceeding the previous record set in 2024.

Precipitation

Figure 5 presents the annual precipitation anomalies for 2025, and Figure 6 shows the seasonal anomalies in precipitation, both expressed as percentiles and derived from:

- The GPCC product (GPCC, 2025), which provides global gridded (1° resolution, ~111 km at the Equator) monthly near-real-time precipitation data;

- Remote sensing-based GIRAFE v1 (Konrad et al., 2025), which provides gridded (global 1°) monthly and daily resolution, extended continuously to the present day.

Annual precipitation was near normal across much of the Amazon and Paraná basins, with some areas experiencing much-above-normal precipitation, particularly during JJA.

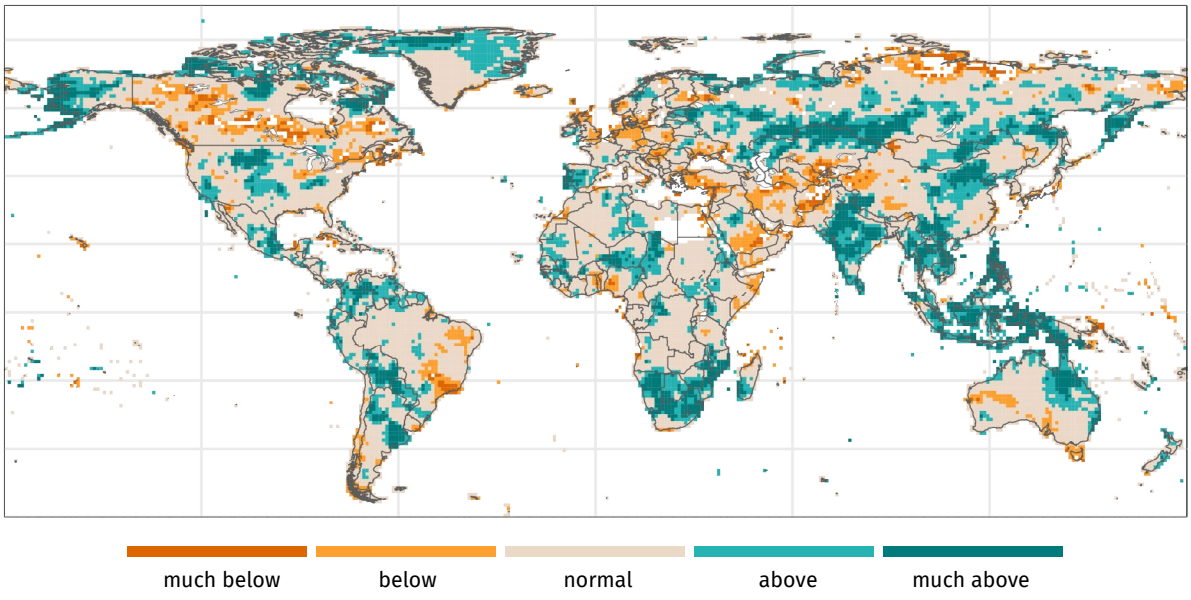


Figure 5. Total annual precipitation in 2025 expressed as anomalies compared with the 2002–2022 reference period

Note: The boundaries and names shown, and the designations used do not imply official endorsement or acceptance by WMO or the United Nations

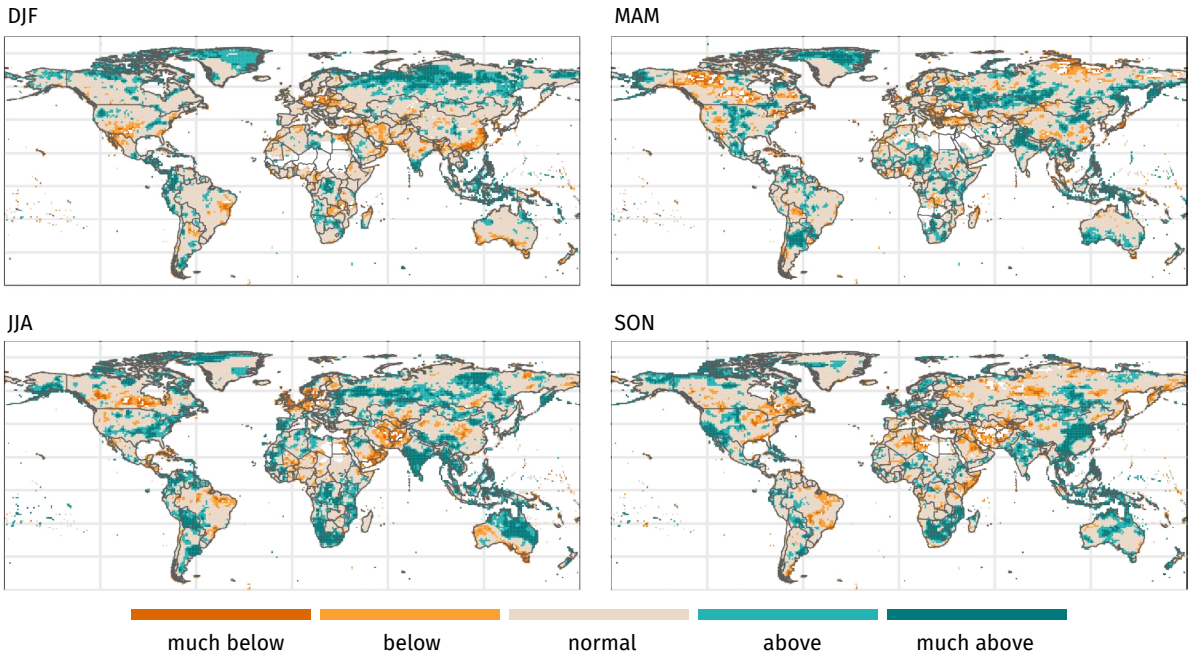


Figure 6. Seasonal precipitation in 2025 expressed as anomalies compared with the 2002–2022 reference period. DJF = December–January–February (includes December 2024), JJA = June–July–August, MAM = March–April–May; SON = September–October–November.

Note: The boundaries and names shown and the designations used do not imply official endorsement or acceptance by WMO or the United Nations.

In North America, the Mackenzie, Nelson, St. Lawrence and Fraser basins recorded near-normal precipitation overall, although some areas experienced below- to much-below-normal conditions, especially during MAM and JJA. In contrast, the upstream parts of the Mississippi basin saw much-above-normal precipitation during most of the year, except in December–January–February (DJF).

In Africa, the Limpopo and Orange basins recorded much-above-normal precipitation across their entire basin areas, mainly during JJA and SON. Parts of the Niger and Lake Chad basins also experienced much-above-normal precipitation. In the Greater Horn of Africa, where drought began to unfold in 2025, precipitation was normal to below-normal, becoming much-below-normal in SON.

In Europe, the Iberian Peninsula experienced above-normal precipitation in JJA. During the same season, Northern Europe recorded much-below-normal precipitation, which shifted to much-above-normal conditions in SON. Large parts of the Volga, Ob, Ural and Yenisei basins recorded much-above-normal annual precipitation, while the Middle East experienced below- to much-below-normal precipitation throughout the year.

In Asia, the Krishna, Godavari and Ganges basins, as well as the upstream parts of the Indus basin, recorded much-above-normal precipitation, especially during MAM and JJA. Countries in South-East Asia that were severely affected by floods also experienced much-above-normal precipitation.

Extreme precipitation

Extreme precipitation is defined here as the daily precipitation amount exceeding the 95th percentile based on the reference period 1991–2020. Figure 7 presents a schematic representation of the variable, and Figure 8 presents the fraction of the annual total precipitation in 2025 that was extreme.[16]

Extreme precipitation events were observed across several southern African basins, including the Zambezi, Limpopo and Orange, as well as in the headwaters of the Indus basin and across parts of Murray–Darling Basin, and across western and northern Australia.

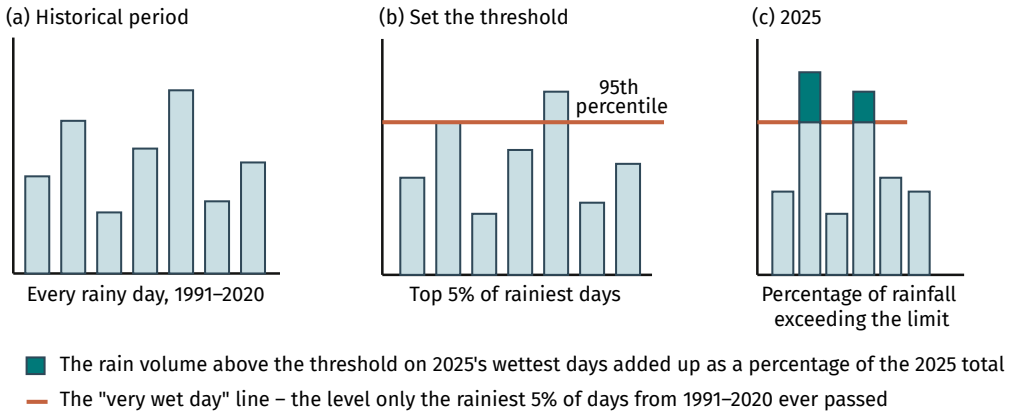


Figure 7. Schematic representation of the calculation of the extreme precipitation variable: (a) observed daily precipitation amounts for each grid cell and all wet days in the reference period 1991–2020; (b) based on the data from (a), the 95th percentile of wet-day precipitation during the reference period was calculated and used as the threshold; (c) daily precipitation totals recorded in 2025 that exceeded the 95th percentile threshold calculated in (b) were aggregated and expressed as a percentage of the annual total precipitation in 2025.

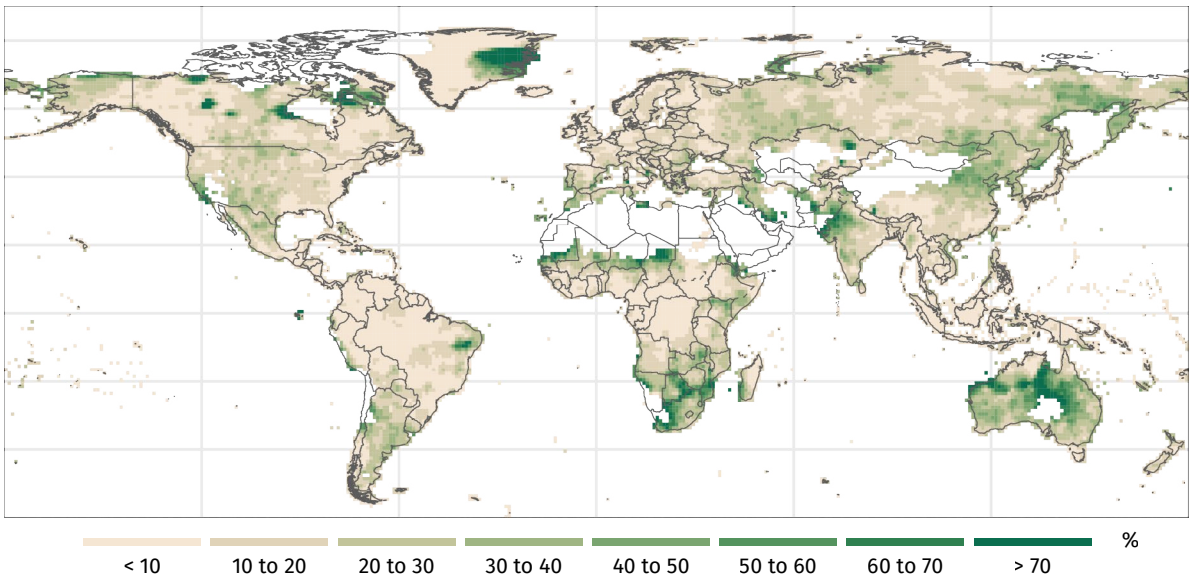


Figure 8. Percentage of the precipitation in 2025 that was above the annual 95th percentile for the historical period 1991–2020
Note: The boundaries and names shown and the designations used do not imply official endorsement or acceptance by WMO or the United Nations.

[16] Areas with annual precipitation below 300 mm were masked and shown as white in Figure 8.

River discharge

- Observed daily river discharge data were available for 3 611 stations in total: 3 115 stations provided in situ observations, while discharge records for 496 stations were infilled using space-based observations. Most of these stations are located in Europe (36.9%); North America, Central America and the Caribbean (27.2%); the South-West Pacific (19.2%); and South America (9.6%). The smallest proportion of stations with available data for the report are found in Africa and Asia (7.1% in total).
- Modelled anomalies agreed with observations in 63% of the validated basins in 2025, including the La Plata basin, North America, parts of India, Australia, the Middle East, southern Africa and Europe. Disagreement between modelled and observed anomalies was found in parts of eastern North America, the Amazon Basin and parts of Australia.
- In 2025, approximately 36% of the global catchment area experienced below-normal annual river discharge conditions, 36% was within the normal range and 21% was above normal.[17] Overall, 2025 was a dry year for river discharge worldwide, and one of the driest in 35 years (1991–2025).
- Annual river discharge in 2025 was above to much above normal across South and South-East Asia, parts of northern South America, and selected African and north-eastern and eastern Australian basins.
- Below- to much-below-normal river discharge affected several major regions, including much of North America, the La Plata and São Francisco basins of South America, Eastern European basins, the Middle East and Central Asia.
- Africa showed contrasting river discharge conditions, with above-normal flows in the Senegal, Niger, Lake Chad, Orange and Limpopo basins, but much-below-normal discharge in the Nile, Congo and Zambezi basins.
- Major basins in South, South-East and East Asia recorded above- to much-above-normal discharge, while across the Middle East the discharge was below to much below normal.

This 2025 edition of the State of Global Water Resources report uses the same HydroBASINS level 4 spatial delineation adopted by the previous reports (Lehner et al., 2008). This delineation represents approximately 986 river basins (with a minimum upstream area of 10 000 km^2) around the globe (Figure A.1 in the annex).

The river discharge analysis in the 2025 report is based on in situ data received from WMO Members represented by NMHSs, primarily obtained via the GRDC database (see GRDC Data Portal). These data were supplemented with substantial contributions from GHMSs, the Remote Sensing-based Extension of GRDC (RSEG) dataset, the Satellite Altimetry-based Extension of global-scale in situ river discharge Measurements (SAEM) dataset and SWOT Water Surface Elevation (WSE)-based discharge observations, which provide extended time series of river

[17] Based on results of simulations performed using GHMSs. Note: The normal range is defined as the 25th–75th percentile. Under stationary conditions, the share of area under normal conditions averages around 50% in the long term, though the share in any individual year may fluctuate around this value. In addition, around 7% of the global catchment area is not modelled because of model-resolution limitations.

discharge observations using products based on space-based observation (Elmi et al., 2024; Saemian et al., 2025, 2026). The 13 GHMSs listed in Box 1 and in Table A.3 in the annex were used for this year's report. For more information about the models, the input data used and other details, please refer to the Global hydrological modelling systems section in the annex.[18]

Only in situ stations with no more than 10% missing values for the period covering at least the first 10 months of 2025 (until 31 October 2025) and the historical period of 30 years (1991–2020) or at least 20 years (2001–2020) were selected for the analysis (Figure 9 provides a breakdown by the type of data received). Non-verified data were accepted. At the time of preparation

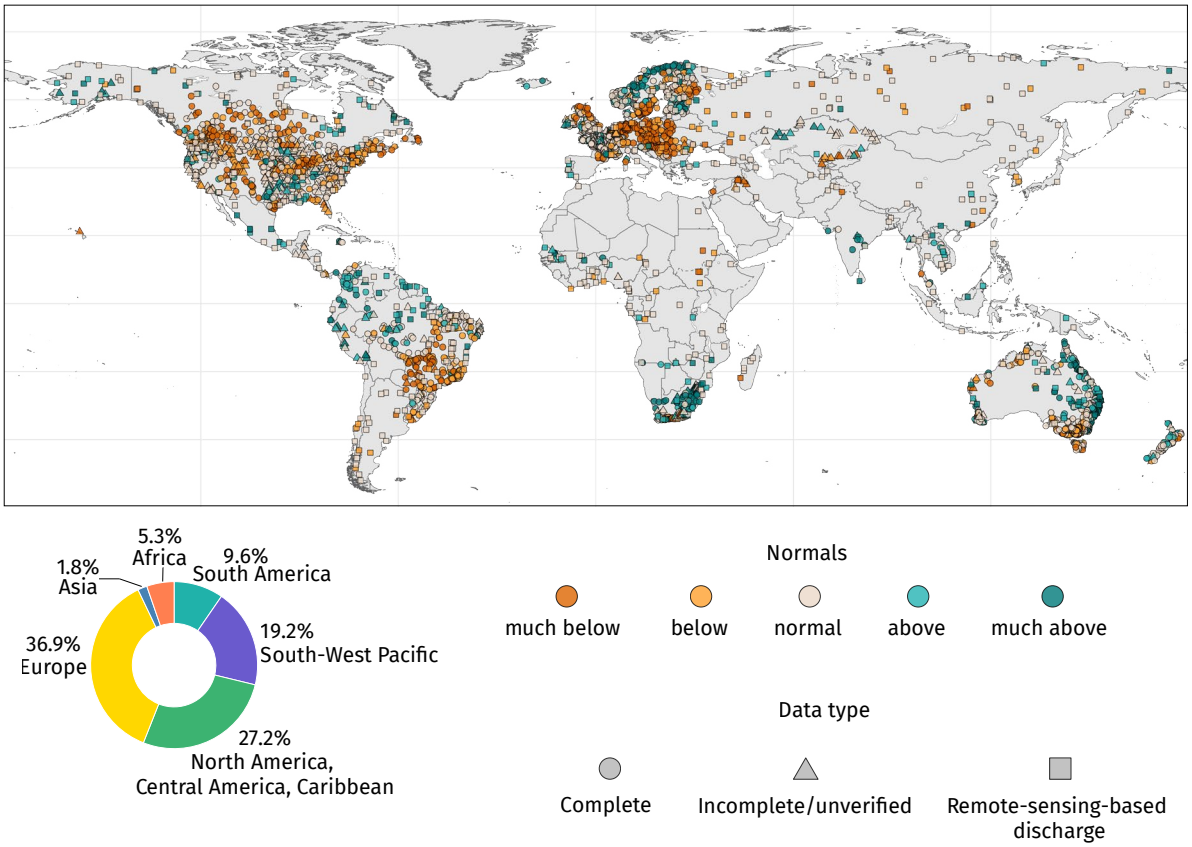


Figure **9.** Observed mean river discharge for the year 2025 compared to the period 1991–2020 or 2001–2020. The results are based on observed river discharge data: circles indicate stations with 30 years of observations and full coverage of the year 2025, triangles indicate stations with at least 20 years of observations and/or coverage including at least first 10 months of 2025, and squares represent infilled time series of river discharge data derived from satellite-based products (RSEG and SAEM datasets and SWOT WSE-based discharge observations). Observations were obtained from NMHSs and GRDC. The inset chart (bottom left) shows the data distribution excluding the 496 points with satellite-based infilling. The observed data were used to validate the GHMS simulations shown in Figure 10, where the reference period was adjusted to match the available in situ records (see Figure A.6 in the annex). Regions shown on the map correspond to the official WMO regions.

Note: The boundaries and names shown and the designations used do not imply official endorsement or acceptance by WMO or the United Nations.

[18] Simulations from GHMSs may contain uncertainties arising from model structure, input data or configuration. To capture a broader range of these uncertainties, an ensemble of GHMSs was used. Intercomparison of the models and validation against in situ data is provided in the annex.

of this report, observed daily river discharge data (corresponding to the selection criteria, as described) were available for 3 611 stations in total – 3 115 stations providing in situ observations and 496 stations from the RSEG and SAEM datasets and SWOT WSE-based discharge observations.

Most of the stations with in situ observations collected for analysis are located in Europe (36.9%); North America, Central America and the Caribbean (27.2%); the South-West Pacific (19.2%); and South America (9.6%). The smallest proportion of stations with available data are found in Africa and Asia (7.1% in total).

For observed river discharge stations, the 2025 mean was compared with available data (that is, at least 20 years of data 2001–2020), while for the modelled data obtained from GHMSs, the annual mean river discharge for 2025 was compared with historical values from 1991 to 2020. The annual discharge was then classified as normal, above normal, below normal, much above normal or much below normal relative to these historical values (refer to Anomaly calculation for more details). Table A.3 in the annex provides details on each of the GHMSs used, together with information on their set-up and calibration with historical data, and on how simulations for 2025 were produced. Modelled data from GHMSs were validated using observed data in basins where observed river discharge data were available and covered a 30-year historical period.

Figure 9 presents the observed mean river discharge for the year 2025 against the selected historical period (1991–2020 or 2001–2020) derived from three data sources (in situ observations from Members, GRDC data and infilled river discharge data based on space-based products), and Figure 10 presents the modelled mean river discharge for the year 2025 against the selected historical period (1991–2020) based on ensemble results from the GHMSs (see the annex for details on the methods of calculation). In cases where observational data were available,

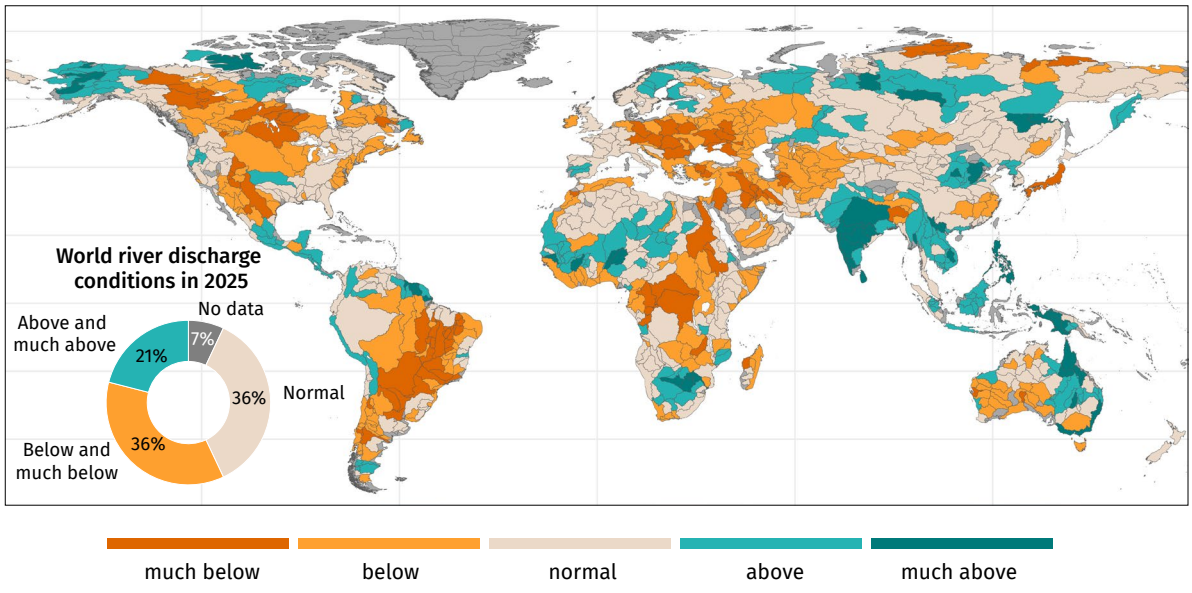


Figure 10. Mean river discharge in 2025 expressed as anomalies relative to the 1991–2020 reference period for basins larger than 10 000 km^2. The results presented here are derived from the modelled river discharge data obtained from an ensemble of 13 GHMS simulations (see Methods section in the annex). Inset (bottom left) shows the percentage distribution of the modelled catchment area under the given conditions. Dark grey areas indicate no modelling data. The results were validated against hydrological observations wherever available (see Figure A.6 in the annex).

Note: The boundaries and names shown and the designations used do not imply official endorsement or acceptance by WMO or the United Nations.

they were used to validate the model results shown in Figure 10. A detailed presentation of the validation showing basins where the GHMS simulations agreed with the observed data is provided in Figure A.6 in the annex.

Where validation was performed, there was agreement between observed and simulated anomalies[19] for 63% of basins in 2025, particularly in the eastern parts of South America (the La Plata basin), North America, parts of India (the Godavari basin), Australia, the Middle East, Kazakhstan, Myanmar, southern Africa and across Europe. At the same time, modelled anomalies disagreed with observations in parts of eastern North America and northern South America (the Amazon basin), and in Queensland in Australia. Note that discrepancies between modelled and observed hydrological flows may arise from modelling uncertainties, complex topography, such as high mountains that create localized discharge anomalies unrepresentative of wider regional conditions, or validation methodology – see Semi-decadal statement as well as the annex for further details. The locations of the gauges used to validate the modelled results are presented in Figure A.3 in the annex (for full validation results refer to Figure A.6 in the annex). The locations of the gauges with observed river discharge data are critical for reliable model validation, as presented in Figure A.5 in the annex.

In 2025 river discharge exhibited deviations from normal conditions in approximately 57% of the global catchment area (Figure 10). With respect to the historical period, the year 2025 was characterized by below-normal conditions in approximately 36% of the area globally, while conditions in another 36% were normal (compared with a 1991–2020 mean of 46%), and in another 21% they were above normal.[20] Overall, 2025 was a dry year for river discharge worldwide. A comparison of the areas under different river discharge conditions for every year from 1991 to 2025, using a constant historical normal (1991–2020), shows that 2025 was one of the driest years in the last 35 years (see the top panel in Figure 3, which is derived from GHMS simulations).

In North and Central America, basins across much of the United States and Canada, including the Churchill, Nelson, Fraser, Colorado (see information from the US National Integrated Drought Information System) and Mackenzie rivers, experienced below- to much-below-normal discharge conditions (Figures 9 and 10). The Yukon basin was an exception, with above-normal discharge.

In the northern part of South America, the Amazon basin and coastal basins in Peru recorded normal to above- and much-above-normal discharge (Figure 9). In contrast, large parts of the La Plata system, including the Paraná basin, as well as the São Francisco basin, experienced below- to much-below-normal discharge (Figures 9 and 10).

Across Eastern Europe, including southern Greece and Türkiye, below- to much-below-normal discharge conditions prevailed (Figures 9 and 10). Much-below-normal discharge was recorded across the Danube basin. Similar conditions were observed in the Dnieper, Don and Volga basins, contrasting with the much-above-normal discharge recorded in the previous year. Across Central and Western Europe, including parts of France and Germany, discharge conditions varied from below to above normal (Figure 9), while in Southern Europe they remained mostly near normal (Figure 10).

---

[19] Based on multi-model mean; validation was performed for the categories “above”, “below” and “normal”.

[20] The normal range is defined as the 25th–75th percentile. Under stationary conditions, the share of area under normal conditions averages around 50% in the long term, though the share in any individual year may fluctuate around this value. In addition, around 7% of the global catchment area is not represented because of model-resolution limitations.

In Asia and South Asia, the Indus, Ganges, Godavari and Krishna basins recorded above- to much-above-normal discharge. Similarly, above-normal flows were observed in the Irrawaddy, Salween and Mekong basins in South-East Asia. In East Asia, the Yellow River basin in China showed above- to much-above-normal discharge, while discharge in the Yangtze basin ranged from normal to much below normal in some areas.

The Tigris–Euphrates system and the Aral Sea basin in the Middle East and Central Asia recorded below- to much-below-normal discharge, reflecting drought conditions across the region.

In Africa, above- to much-above-normal discharge was recorded in the Senegal, Niger and Lake Chad basins, as well as in the Orange and Limpopo basins in southern Africa. By contrast, the Nile, Congo and Zambezi basins experienced much-below-normal discharge. The Greater Horn of Africa, affected by drought towards the end of 2025, recorded normal to below-normal discharge conditions.

In Oceania, discharge conditions in New Zealand were near normal. In Australia, basins along the north-eastern coast recorded above- to much-above-normal discharge, as did parts of the Murray–Darling basin, while in the south-east there was below-normal discharge.

Reservoirs

- Reservoir inflows in 2025 were below to much below normal across the Middle East, Eastern Europe, Central Asia, and parts of North America and South America (across Patagonia, as well as the La Plata and São Francisco basins). In contrast, South and South-East Asia recorded above- to much-above-normal inflows.
- Reservoir storage was below to much below normal across Eastern Europe, Central Asia, the Middle East and parts of the United States, broadly reflecting inflow deficits. Above-normal storage was observed in parts of Central America and West Africa (the Niger and Senegal basins).
- Reservoirs in the Orange river basin (Africa) and across parts of South and South-East Asia (India, Myanmar and Thailand) showed normal to below-normal storage despite above-normal inflow anomalies (likely due to reservoir operations, withdrawals, and the timing of inflow events).

This chapter presents the state of reservoirs in 2025. It includes inflow into selected reservoirs across the globe modelled by GHMSs and anomalies in reservoir volumes obtained from Texas A&M University (TAMU). The number of reservoirs included differed across data sources. The current results cover a total of 913 reservoirs, consisting of reservoirs with a capacity greater than 100 million m^3 included in the TAMU dataset that were also modelled by at least two GHMSs.

Inflow into selected reservoirs

The inflow data were obtained from four GHMS products, namely, the Wflow_sbm (also includes space-based observations) (Eilander et al., 2021; Imhoff et al., 2020; Verseveld et al., 2024), CaMa-Flood with Dam (Hanazaki et al., 2022; Yamazaki et al., 2011), World-Wide HYPE (Arheimer et al., 2020) and CSSPv3 (Yuan et al., 2026) models (more details are available in Table A.3 in the annex).

Daily inflow data for the reservoirs were computed for the historical period between 1991 and 2020 and for the year 2025. Inflow anomalies were then calculated following the same method as for the river discharge anomalies (see Box 2). The results are presented in Figure 11. Water inflow into the reservoirs was selected as an indicator because it is less influenced than other reservoir-related indicators by water resource management strategies, such as reservoir operations.

Reservoir inflow conditions in 2025 showed widespread below-normal patterns across several regions. In the Middle East, including parts of the Islamic Republic of Iran, Türkiye and the Syrian Arab Republic as well as Central Asia, including Uzbekistan, Tajikistan, Kyrgyzstan and Afghanistan, reservoir inflows were below to much below normal, consistent with the drought conditions affecting the region.

Similar below- to much-below-normal inflows were observed across parts of the United States, Canada and South America. In South America, reservoirs in the La Plata and São Francisco basins and across Patagonia showed much-below-normal inflows.

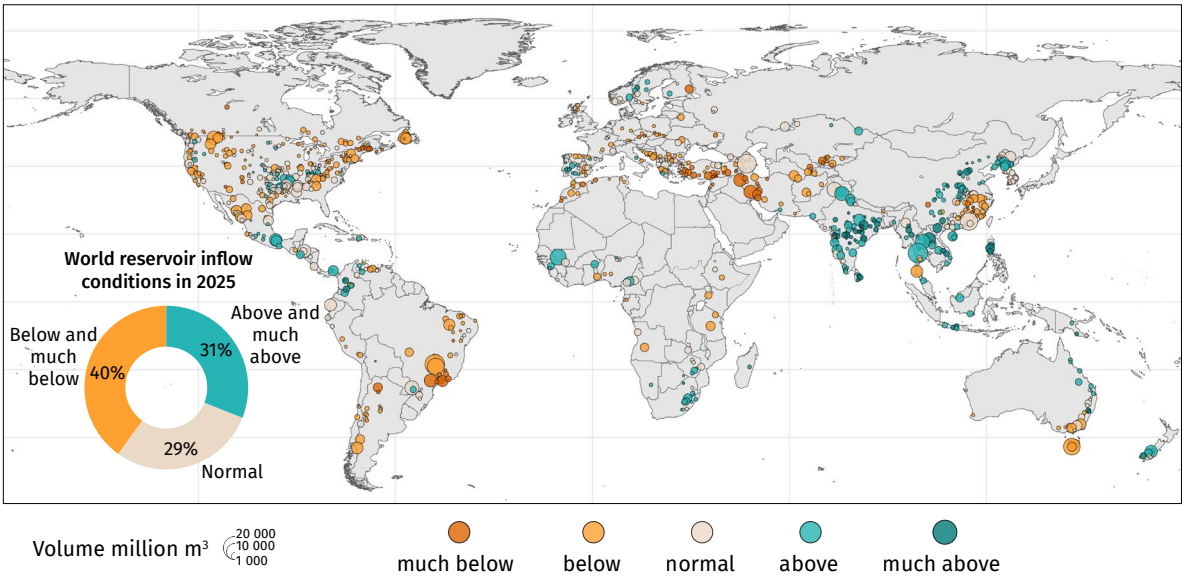


Figure 11. Annual mean inflow into selected reservoirs in 2025 expressed as anomalies compared with the 1991–2020 reference period. The size of the dots corresponds to the maximum storage volume of the reservoirs. The inset (bottom left) shows the percentages of reservoir volumes under the given conditions.

Note: The boundaries and names shown, and the designations used do not imply official endorsement or acceptance by WMO or the United Nations.

In Europe, reservoir inflows were generally below normal across much of the continent, with the exception of the Tagus River basin on the Iberian Peninsula, and Northern Europe, including parts of Norway, Sweden and Finland, where conditions were closer to or above normal.

Reservoirs across South and South-East Asia, including India, Myanmar, Thailand and Viet Nam, recorded above- to much-above-normal inflows, consistent with the above-normal river discharge conditions observed in the region.

Reservoir storage

Reservoir storage volumes were estimated by measuring each reservoir's water surface area using a space-based observation product (OPERA, 2023), correcting for cloud coverage (Yadav et al., 2025) and then converting the area to stored volume with reservoir-specific relationships from Li et al. (2023). The 2025 storage anomaly with respect to the historical period of 1999–2018 is presented in Figure 12.

Reservoir storage conditions in 2025 were generally below to much below normal across Eastern Europe, Central Asia and the Middle East, including areas around Türkiye, Armenia, the Syrian Arab Republic, the Islamic Republic of Iran and Iraq, and neighbouring regions. These storage deficits broadly coincided with below- to much-below-normal anomalies in inflow into selected reservoirs. In the United States, many reservoirs also showed below- to much-below-normal storage and inflow conditions, although both storage and inflow anomalies were spatially mixed.

In Central America, reservoir storage was generally above normal, consistent with above-normal inflow conditions at several reservoirs. In South America, reservoirs in the La Plata and São Francisco basins, as well as those in Patagonia, recorded below-normal volumes.

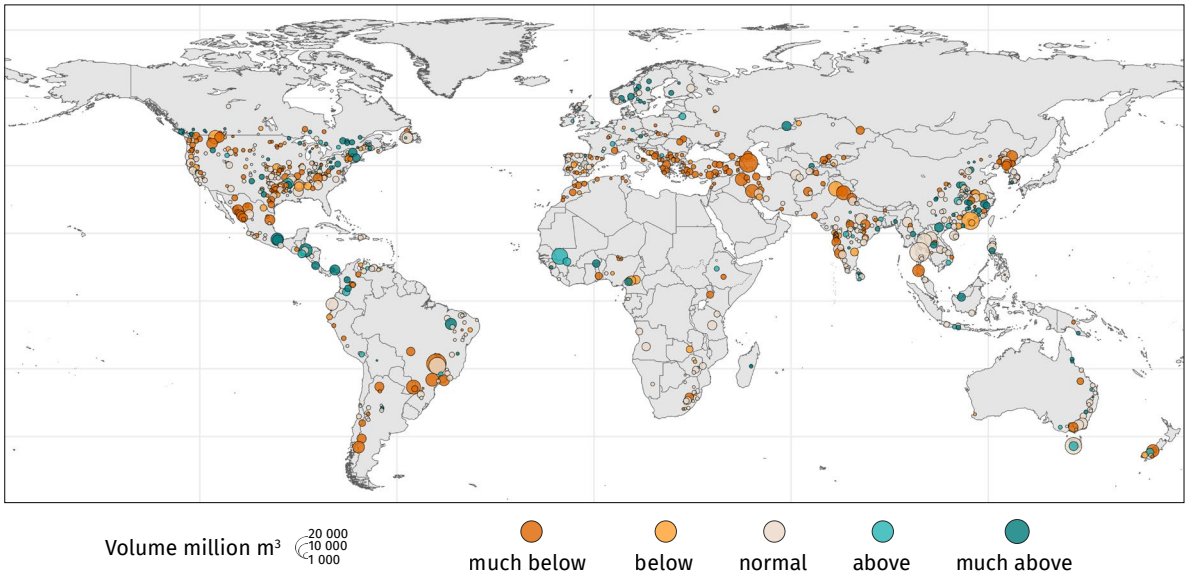


Figure 12. Reservoir storage in 2025 expressed as the annual mean of monthly anomalies compared with the 1999–2018 reference period

Note: The boundaries and names shown and the designations used do not imply official endorsement or acceptance by WMO or the United Nations.

In Africa, reservoirs in parts of southern Africa, including the Orange River basin, showed normal to below-normal storage, while some reservoirs in West Africa, including the Niger and Senegal basins, showed above-normal storage volumes.

Across parts of South and South-East Asia (for example, India, Myanmar and Thailand), many reservoirs showed normal to below-normal storage despite above-normal inflow anomalies. This contrast suggests that annual inflow anomalies alone do not fully explain reservoir storage volumes, which may also reflect reservoir operations, withdrawals and the timing of inflow events.

Lakes

- African lakes and reservoirs showed widespread much-above-normal water levels in 2025, including Lakes Malawi, Chad, Victoria, Tanganyika, Rukwa and Turkana, as well as Volta and Nasser reservoirs. Kariba reservoir remained much below normal.
- In Europe, water levels in Lakes Peipus and Ladoga remained near normal, while water levels in Lake Beyşehir in Türkiye and Lake Urmia in the Islamic Republic of Iran were below to much below normal. Across Canada, lake levels were generally below to much below normal.
- Lake surface water temperature in July 2025 was above normal in Lake Michigan and Lake Erie and across selected African lakes, normal in Lakes Victoria, Ladoga, Peipus, Superior, Huron and Ontario and much below normal in Lakes Chad and Malawi. In January 2025, Lakes Tanganyika, Nasser and Malawi in Africa, together with selected lakes in South America, recorded above- to much-above-normal surface water temperatures, while in Lake Victoria it remained normal.
- Lake ice cover duration was generally below to much below normal across the assessed Eurasian and North American lakes, with some exceptions, including normal conditions in Lakes Peipus and Michigan and much-above-normal duration in Lakes Huron and Erie.

This chapter provides anomalies in lake levels, lake ice cover duration and water temperatures in January and July 2025 for 75 selected lakes with respect to the historical period of 1995–2020. The 75 selected lakes consisted of 55% near-natural lakes, 12% regulated lakes and 33% reservoirs. The data were derived from the European Space Agency (ESA) Lake CCI project, which aims to provide consistent essential climate variables. Three such climate variables are: (a) lake water level, which is critical to understanding the balance between water inputs and water loss and their connection with regional and global climate changes; (b) lake surface water temperature, which reflects regional air temperatures, and hence mixing regimes, driving biogeochemical cycling and seasonality; and (c) lake ice cover duration, which is a sensitive indicator of changes in air temperature and climate and supporting aquatic ecosystems.

Lake levels

Lake levels (Figure 13) were much above normal in 2025 in Africa, specifically in Lakes Malawi, Chad, Victoria, Tanganyika, Rukwa and Turkana, as well as in Volta and Nasser reservoirs. At the same time, Kariba, the world largest reservoir by volume, on the Zambezi River, had much-below-normal levels. In Europe, water levels in lakes Peipus and Ladoga were normal. In Türkiye Lake Beyşehir had below-normal levels. Lake Baikal had much-above-normal levels, while Lake Urmia in the Islamic Republic of Iran saw much-below-normal levels. Lakes across Canada saw below- to much-below-normal levels, however Superior and Michigan in North America had normal levels. In Argentina, Lake Argentino saw below-normal levels.

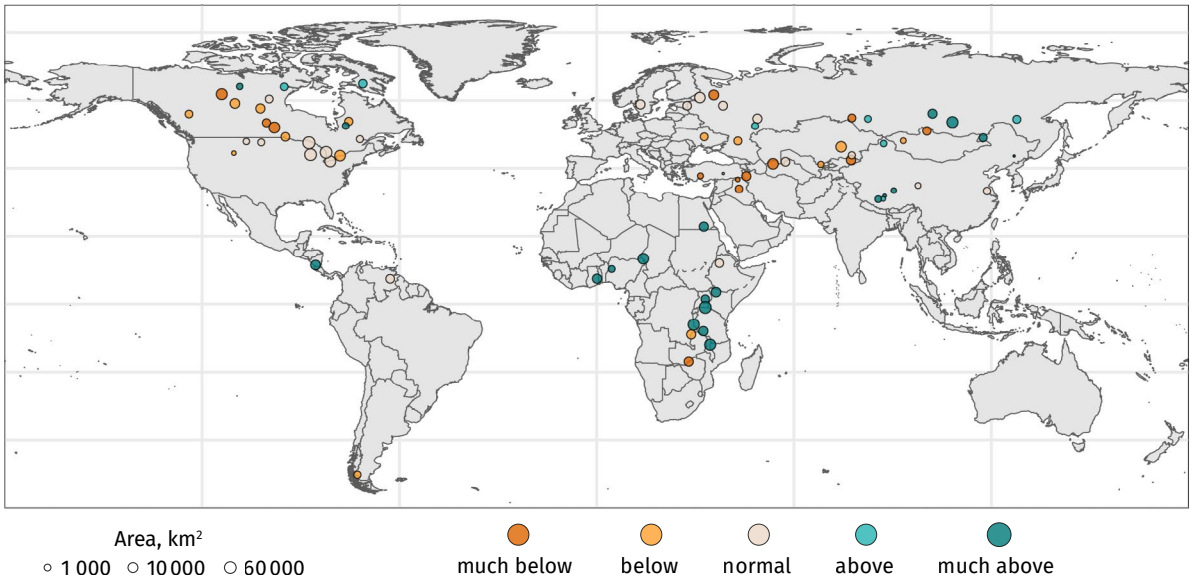


Figure 13. Lake water levels in 2025 expressed as anomalies compared with the 1995–2020 reference period. The selected 75 water bodies consist of 55% near-natural lakes, 12% regulated lakes and 33% reservoirs.

Note: The boundaries and names shown and the designations used do not imply official endorsement or acceptance by WMO or the United Nations.

Lake water temperature

In July, the majority of selected lakes in Africa saw much-above-normal temperatures, except for Lake Chad, which had much-below-normal temperatures (Figure 14). Lakes Tanganyika and Nasser saw much-above-normal water temperature in July and January 2025, while Lake Malawi had much-above-normal temperatures in January and much-below-normal temperatures in July. Lake Victoria saw normal temperatures, both in July and January. Temperatures in Lake Beyşehir in Türkiye were much above normal in July.

Lakes in South America had much-above-normal temperatures in January. In July, temperatures in Lakes Ladoga and Peipus in Europe were normal, and in Lake Baikal they were much above normal. In July, most of the Great Lakes (Lakes Superior, Huron and Ontario) saw normal surface water temperatures, while Lakes Michigan and Erie saw above- to much-above-normal surface water temperatures.

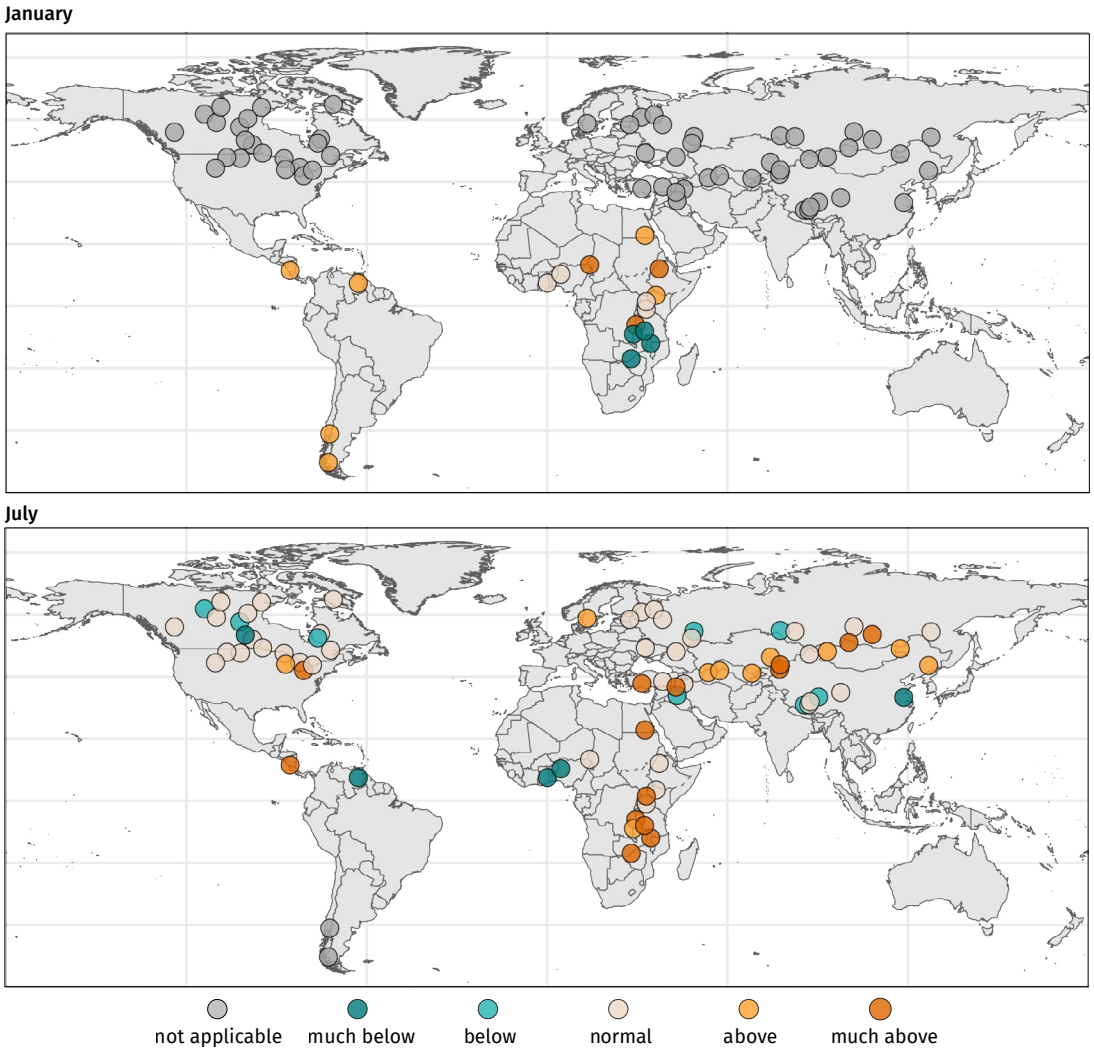


Figure 14. Lake surface water temperature in January and July 2025 expressed as anomalies compared with the 1995–2020 reference period. Gray dots for January indicate no data for lakes where winter effects can skew the temperature data.

Note: The boundaries and names shown and the designations used do not imply official endorsement or acceptance by WMO or the United Nations

Ice cover duration

Lake ice cover duration was below to much below normal for Lakes Ladoga, Onega, Baikal and Balkhash, while Lake Peipus showed normal conditions (Figure 15). Lakes in North America also generally experienced below- to much-below-normal ice cover duration, with some exceptions, like Lakes Huron and Erie, where ice cover duration was much above normal, and Lake Michigan, where it was normal.

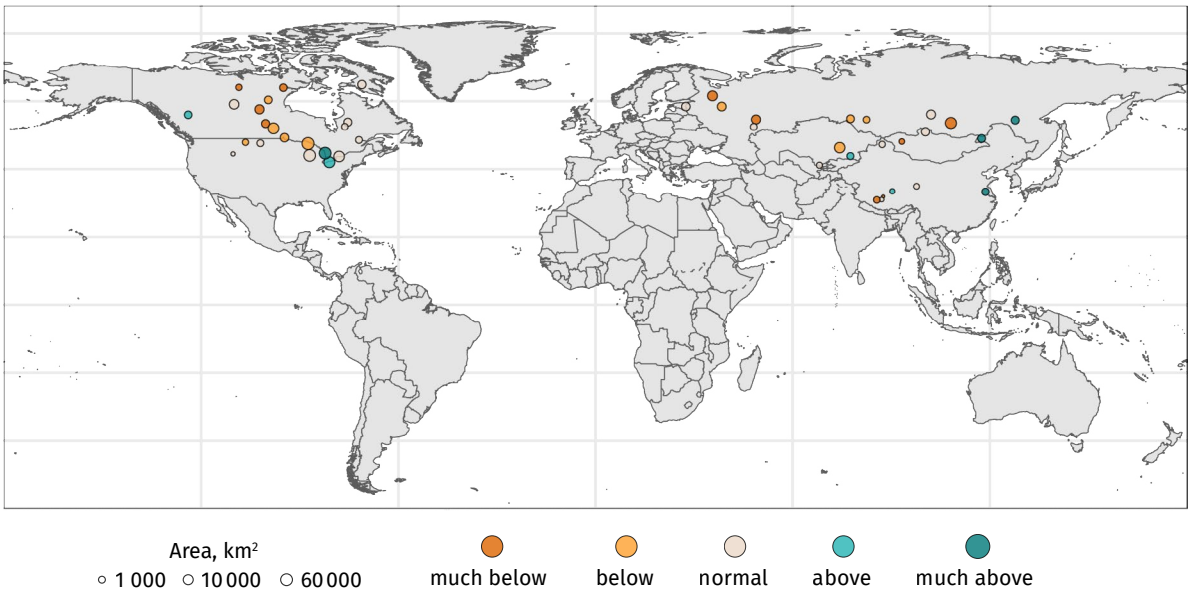


Figure 15. Lake ice cover duration in 2025 expressed as anomalies compared with the 1995–2020 reference period

Note: The boundaries and names shown and the designations used do not imply official endorsement or acceptance by WMO or the United Nations.

Groundwater levels

- In 2025, 65% of groundwater observation stations recorded annual mean levels outside the normal range, with below- to much-below-normal levels observed at 34% of stations (25% in 2024), and above- to much-above-normal levels at 31% (37% in 2024). The percentages are derived from regions with available groundwater monitoring data, and indicate a shift towards more widespread below-normal groundwater conditions compared to 2024.
- Persistent and widespread below- to much-below-normal groundwater levels were observed across Central and Eastern Europe, the central United States, parts of Mexico, northern and central Chile, north-eastern and central-western Brazil, northern South Africa, north-western India and parts of southern Australia, pointing to a cumulative depletion with a multi-year drying trend (Jasechko et al., 2024; Cao et al., 2026).
- Several regions shifted from below normal in 2024 to normal or above normal in 2025, including parts of the Caribbean (Cuba, Jamaica), central to northern Brazil, and northern New Zealand.
- Additional areas with above- to much-above-normal conditions include parts of France, much of Northern Europe, the south-eastern United States, large parts of South Africa, South-East Asia and eastern Australia.

This chapter presents the status of groundwater levels in 2025, compared to the 20-year reference period 2001–2020, based on in situ monitoring data shared by national and subnational institutions responsible for groundwater monitoring. Where longer time series were not available, a 10-year reference period (2015–2024) was used.[21]

After data filtering and processing (see the annex for methodology), the analysis includes data from a total of 43 529 groundwater stations across 51 countries (see the annex for country list and data sources). As in previous reports, station-level anomaly rankings were averaged over 0.5° grid cells to improve visualization on the global map, particularly in regions with dense monitoring networks, where overlapping points can obscure local patterns and lead to misleading visual interpretations.[22] Station-level maps are provided in the annex to enable more detailed local insights.

Groundwater-level and river discharge data were also provided by several countries, including Malawi, Rwanda, Somalia, Nigeria and Malaysia, but could not be included in the analysis because the available time series were shorter than selected historical periods or the target year was not covered sufficiently. These contributions nevertheless reflect continued improvements in hydrological monitoring and data sharing.

In 2025, 65% of groundwater observation stations recorded annual mean levels outside the normal range, and normal levels were observed at 35% of monitoring stations (38% in 2024).[23]

---

[21] The countries where a 10-year reference period was used are Benin, Brazil, Colombia, Costa Rica, El Salvador, Georgia, Greece, Ireland, Kenya, Luxembourg, Qatar, Senegal, Thailand and The Gambia. For countries with a historical period of less than 10 years, the results should be interpreted with caution.

[22] Note that spatial representativeness (the number and distribution of wells) within each grid cell is not captured, which may introduce minor biases (for example, the results for a cell with only one or a few stations may not represent overall conditions).

[23] The normal range is defined as the 25th–75th percentile. Under stationary conditions, the share of stations under normal conditions averages around 50% in the long term, though the share in any individual year may fluctuate around this value.

Below- to much-below-normal levels were observed at 34% of stations (25% in 2024), and above- to much-above-normal levels at 31% (37% in 2024), indicating a clear shift toward more widespread below-normal groundwater conditions compared to 2024.

Central and Eastern Europe stands out as one of the most affected regions, with below-normal groundwater conditions that not only persisted but intensified in 2025 (Figure 16). Sustained below-normal levels were also observed in the central United States, parts of Mexico, northern and central Chile, north-eastern and central-western Brazil, northern South Africa, north-western India and parts of southern Australia. The persistent and widespread groundwater deficits point to a cumulative depletion that a single normal or wet year may not be sufficient to reverse. Below-normal groundwater levels also prevailed along the north-western coast of the United States, across the eastern Mediterranean region (for example, in Greece) and in the southern fringes of Northern Europe (for example, in southern Sweden and Norway), where they were also compounded by intensified seasonality, with more pronounced extremes in low and high groundwater levels (Cao et al., 2026).

While drought and dry conditions contributed to many of these declines (see the Precipitation chapter), below-normal groundwater levels in some regions occurred despite the absence of significant drought, highlighting the role of intensive groundwater abstraction, such as in the central United States, central Mexico and northern South Africa. These declines may also reflect delayed aquifer responses to previous stresses.

Signs of rising groundwater levels were observed in several regions, with a shift from below normal in 2024 to normal or above normal conditions in 2025, including in parts of the Caribbean (Cuba, Jamaica), central to northern Brazil and northern New Zealand. In Europe, although the pronounced wet conditions of 2024 did not persist in the west, groundwater levels in parts of France and most of Northern Europe remained above normal. Other regions with above-normal levels include the south-eastern United States, large parts of South Africa, South-East Asia and eastern Australia (Figure 17).

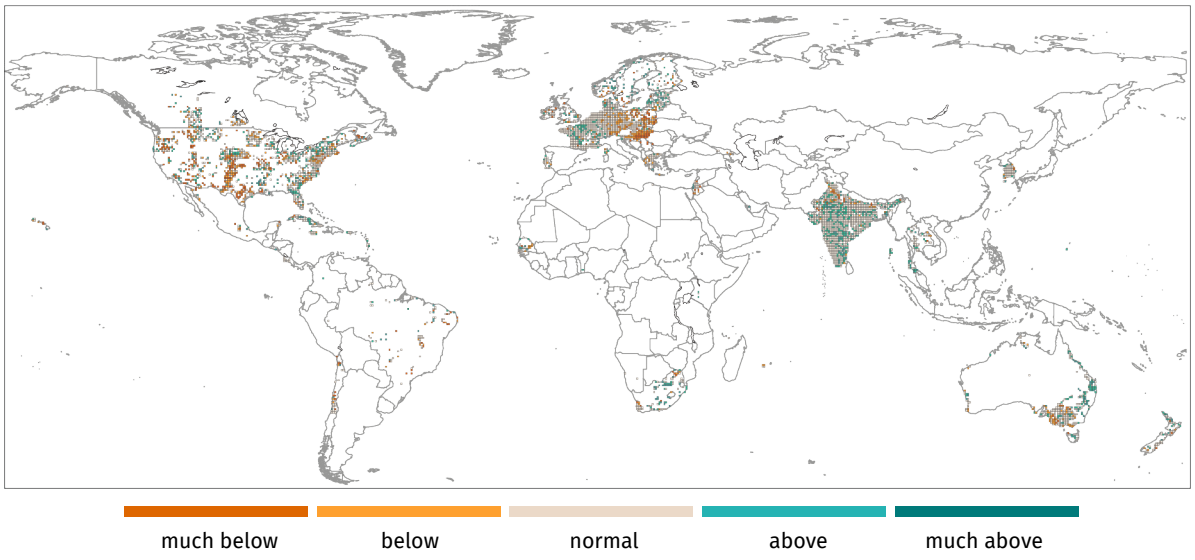


Figure 16. Mean groundwater levels in 2025 expressed as anomalies (averaged over 0.5° grid cells) as compared to the 2001–2020 reference period (2015–2024 for Benin, Brazil, Colombia, Costa Rica, El Salvador, Georgia, Greece, Ireland, Kenya, Luxembourg, Qatar, Senegal, Thailand, and The Gambia)

Note: The boundaries and names shown and the designations used do not imply official endorsement or acceptance by WMO or the United Nations.

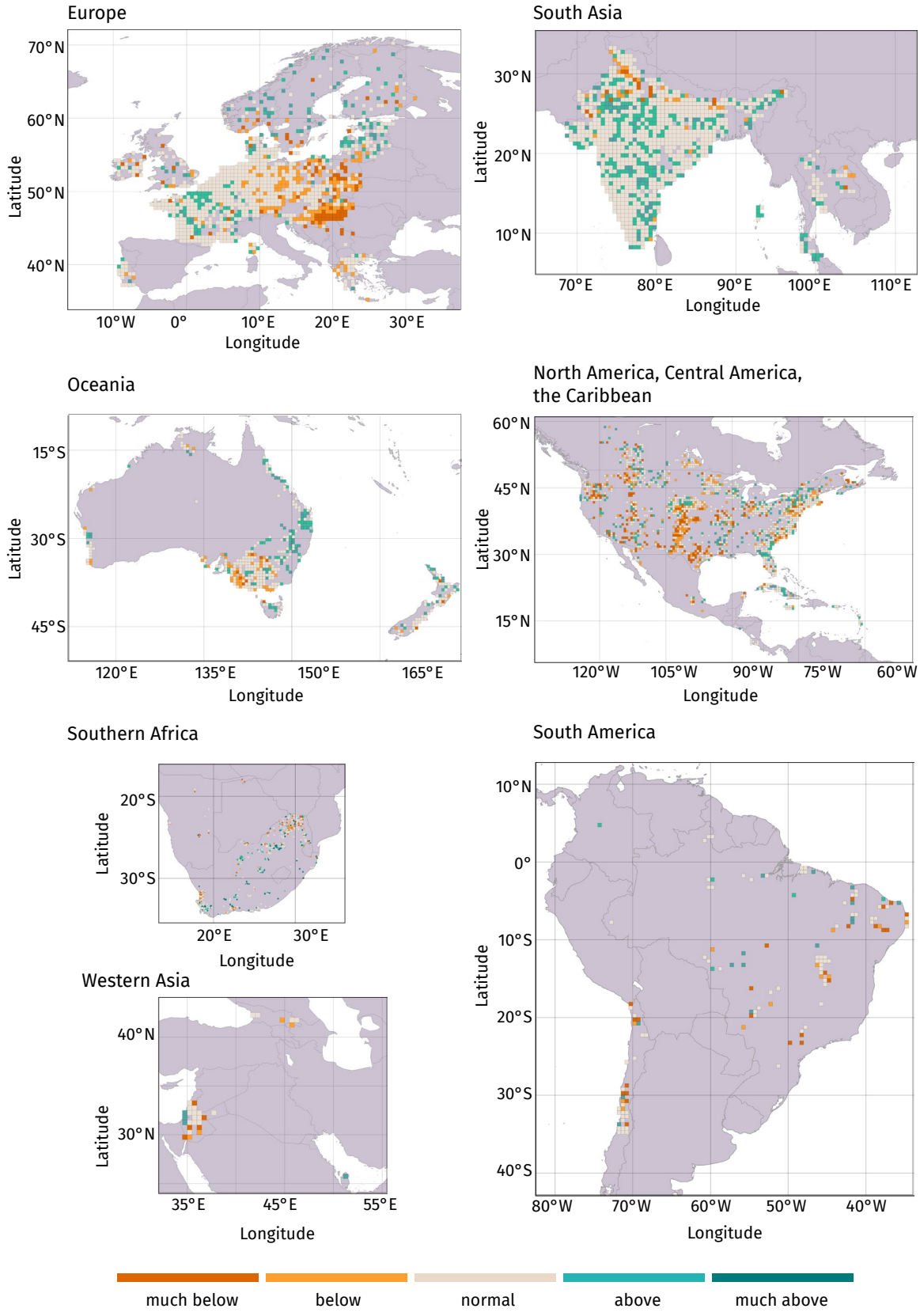


Figure 17. Snapshots for selected countries showing mean groundwater levels in 2025 expressed as anomalies

Note: The boundaries and names shown and the designations used do not imply official endorsement or acceptance by WMO or the United Nations.

Soil moisture

- Soil moisture was below normal across much of South America and the Middle East during DJF and JJA, while northern Africa shifted from much-below-normal conditions in DJF to much-above-normal conditions in JJA. Above-normal conditions prevailed in India during both seasons and in southern Africa during JJA.
- In Europe, below-normal soil moisture conditions developed during JJA. In North America, large areas experienced much-above-normal soil moisture during DJF, followed by widespread much-below-normal conditions during JJA.
- In the United States, after a mostly dry spring and summer, soil moisture started recovering in September and continued to improve over the subsequent months.
- In the current edition, the number of stations providing observed soil moisture data has increased, however the geographical coverage has decreased; for this report only data from the United States were available (183 stations and 119 stations, depending on the depth of measurement).

Surface soil moisture is one of the crucial variables driving hydrological processes. It influences the exchange of water and energy fluxes at the land surface/atmosphere interface, impacts river discharge generation, is important for biogeochemical cycles and co-controls vegetation development. Understanding soil moisture patterns is essential for sustainable water resource management and for the assessment and understanding of food production (see Soil moisture deficit and Essential Climate Variables).

Global root zone soil moisture anomaly for 2025 was obtained from the European Organisation for the Exploitation of Meteorological Satellites (EUMETSAT) Satellite Application Facility on Support to Operational Hydrology and Water Management (H SAF) Root Zone Soil Moisture Data Record version 3 (H SAF, 2026). The global root-zone soil moisture product is expressed as a liquid soil wetness index and is sampled at 0.1° resolution. The historical reference period is 1991–2020. The dataset was validated using around 800 in situ soil moisture measurements from the International Soil Moisture Network (ISMN) in North America, Europe and Australia.

In December, much-below-normal soil moisture was detected over almost the whole of South America (Figure 18). This extended into January, though it eased partially in February over the Amazon basin. In JJA, however, below-normal soil moisture conditions dominated in the Amazon basin and other parts of South America once again.

In December–January, soil moisture was much below normal across northern Africa, shifting to much-above-normal conditions in July and August. During JJA, large areas of southern Africa also experienced much-above-normal soil moisture.

In India, soil moisture was above and much above normal throughout the DJF and JJA seasons, and the Middle East, which was affected by drought, saw much-below-normal soil moisture in the same seasons.

In Europe, negative soil moisture anomalies developed during the summer months, reaching much-below-normal levels across Central and Eastern Europe. In North America, large areas experienced much-above-normal soil moisture during the DJF season, followed by widespread much-below-normal conditions during JJA.

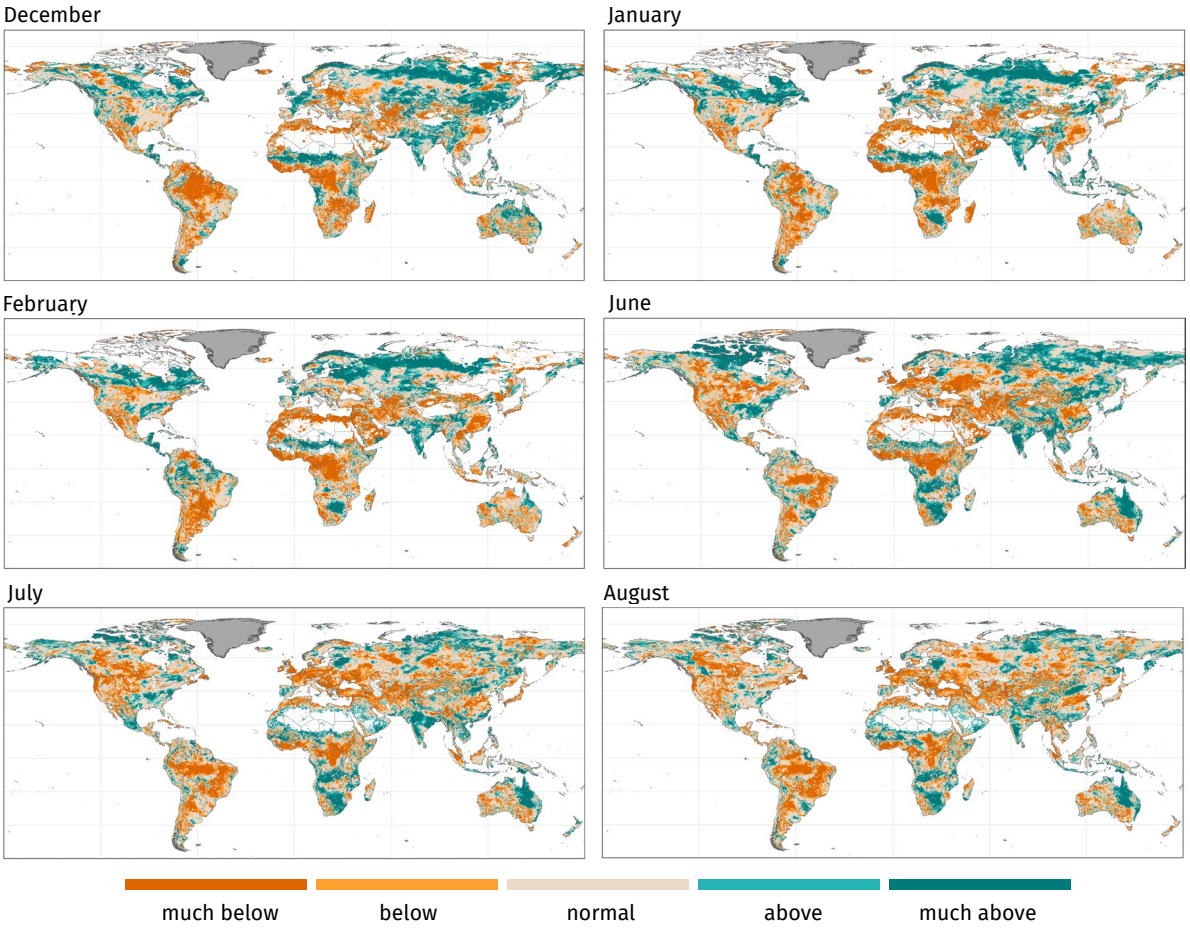


Figure 18. Monthly root zone soil moisture conditions in 2025 (Dec. 2024–Feb. 2025 and Jun.–Aug. 2025) expressed as anomalies compared with the 1991–2020 reference period. Greenland is masked in accordance with Global Land Ice Measurements from Space (GLIMS).

Note: The boundaries and names shown and the designations used do not imply official endorsement or acceptance by WMO or the United Nations.

BOX 3. OBSERVED SOIL MOISTURE: UNITED STATES CASE STUDY

Figure 19 shows anomaly in situ soil moisture from the International Soil Moisture Network (ISMN) (Dorigo et al., 2013, 2021) for September 2025 across the United States. The top and bottom panels depict the soil moisture measurements at depths of 11 and 51 cm, respectively. After a mostly dry spring and summer, soil moisture started recovering in September and continued to improve over the subsequent months.

The number of stations available for this report series has slowly grown with each edition, but the number of represented countries decreased to just the United States for this year's report (Bell et al., 2013; Leavesley et al., 2008, 2010; Schaefer et al., 2007).

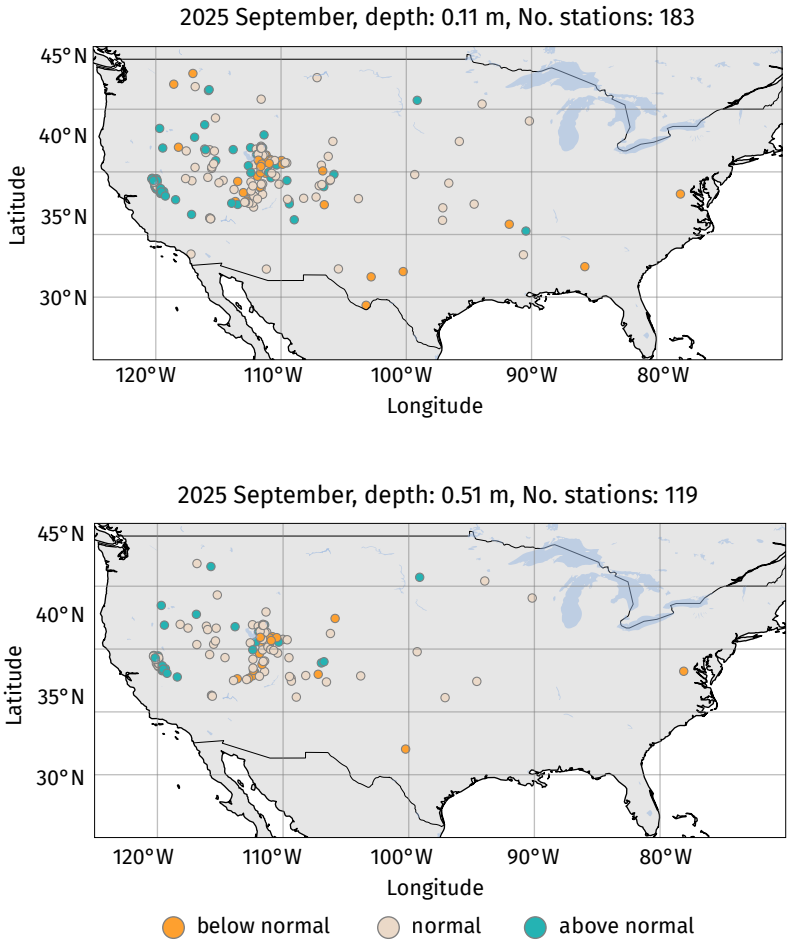


Figure 19. September 2025 observed soil moisture anomaly for the United States at 0.11 m depth (top) and 0.51 m depth (bottom)

Note: The boundaries and names shown and the designations used do not imply official endorsement or acceptance by WMO or the United Nations.

Evapotranspiration

- Persistent negative actual evapotranspiration (AET) anomalies affected several regions, including the Middle East, Central Asia, south-eastern Europe and the Greater Horn of Africa, with below- to much-below-normal conditions continuing through JAJ and SON.
- South America experienced below-normal AET in DJF and JJA, particularly across the Paraná and São Francisco basins. In North America, AET shifted from above-normal conditions in MAM to much-below-normal conditions in several basins during JJA.
- Much-above-normal AET persisted across large parts of Asia, affecting China, India and major South and South-East Asian basins from MAM into JJA and, in some areas, SON.

Actual evapotranspiration (AET), one of the key elements in the hydrological cycle, refers to the process by which water is evaporated, including evaporation from the soil and from vegetation surfaces (including interception evaporation), and transpiration from plants. Elements influencing the rate of evapotranspiration include the level of solar radiation, atmospheric vapour pressure, humidity, air temperature, wind speed, soil moisture content (water availability) and vegetation type and cover. This process is responsible for a large part of the water loss from the soil during a crop's growth cycle and is critical for understanding the state of water resources. The rates of AET are controlled by the amount of water that is available (which is dependent on the existing hydrological conditions) in addition to the present weather conditions.

This chapter presents AET anomalies at the global scale for four seasons in 2025 with respect to the 1991–2020 historical period (Figure 20), derived from six GHMSs (listed in Table A.3 in the annex) and averaged over the river basins derived from the HydroBASINS level 4 delineation.

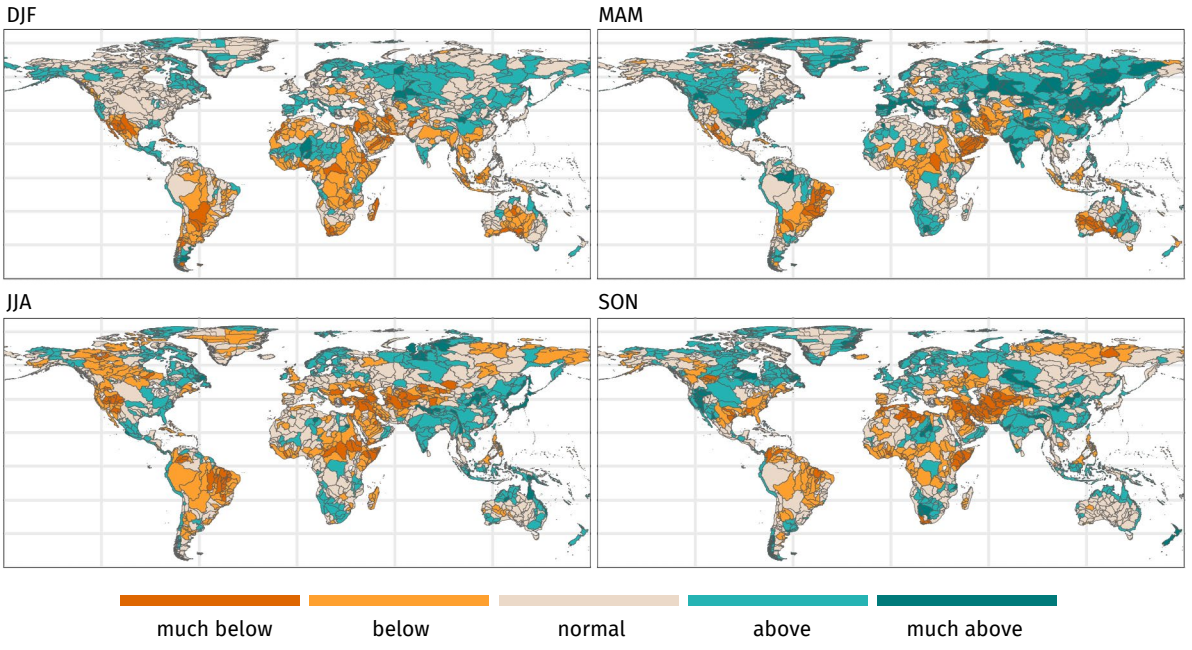


Figure 20. Seasonal actual evapotranspiration (AET) in 2025 expressed as anomalies compared with the 1991–2020 reference period based on an ensemble of six GHMSs

Note: The boundaries and names shown and the designations used do not imply official endorsement or acceptance by WMO or the United Nations.

In northern Eurasia, above- to much-above-normal AET extended across the Ob, Yenisei, Lena and Amur basins during DJF and MAM, extending to the Kolyma basin in MAM. In JJA and SON, below- to much-below-normal AET became widespread across Central Asia and the Middle East. In the Middle East and south-eastern Europe, below- to much-below-normal AET developed during JJA and continued into SON, indicating persistent warm-season deficits.

Much-above-normal AET was observed across China (Yangtze, Yellow River basins) and India in MAM. In India it persisted into JJA and, partially, SON, including the Ganges, Krishna and Godavari basins, as well as the Irrawaddy and Mekong basins in South-East Asia. Much-above-normal AET occurred in the Niger, Senegal and Lake Chad basins in DJF, while the Greater Horn of Africa recorded much-below-normal AET from JJA through SON, coinciding with developing drought conditions. Southern African basins shifted from below-normal AET in DJF to above-normal conditions throughout March–November.

In South America, AET was below normal during DJF and JJA, especially across the Paraná and São Francisco basins.

In North America, AET shifted from much-above-normal conditions in the Mackenzie and Nelson basins in MAM to much-below-normal conditions across the Mackenzie, Churchill, Nelson and Colorado basins in JJA.

Terrestrial water storage

- Below-normal terrestrial water storage (TWS) persisted across several major regions in 2025, including northern and south-western North America, Patagonia, Eastern Europe, the Middle East, Central Asia, eastern Brazil, northern India, parts of Northern Europe, the Russian Federation, China and northern Africa, continuing the pattern of the year 2024.
- South America showed signs of partial TWS recovery, with the area affected by below- to much-below-normal TWS in the La Plata basin decreasing and conditions mostly returning to normal.
- Much-above-normal TWS in Central and southern Africa continued from 2024 into 2025.

Satellite gravimetry is a remote-sensing-based method (used by Gravity Recovery and Climate Experiment (GRACE) and GRACE Follow-On (GRACE-FO) satellites (Landerer et al., 2020; Tapley et al., 2004) that is capable of observing all large-scale mass changes on and below the Earth's surface. This includes, in particular, those caused by water storage changes, including in surface water, soil moisture, groundwater, as well as snow and ice. Terrestrial water storage (TWS), defined as the sum of all these storage compartments, is expressed as an anomaly relative to its long-term mean in equivalent water heights in centimetres as an area-averaged height of the water column over the area being considered. This chapter provides results of the TWS anomaly in the year 2025 obtained from the GRACE/GRACE-FO-based product.

The section on Terrestrial water storage in the annex provides more details on TWS and how TWS anomalies were calculated.

Similar to 2024, below- to much-below-normal TWS persisted in 2025 in northern and south-western North America and Patagonia, the latter being affected by drought during the year (Figure 21). In South America, by contrast, the area affected by below- to much-below-normal TWS in the La Plata basin decreased, with conditions mostly returning to normal.

Much-below-normal TWS conditions were observed in northern Africa, Eastern Europe, the Middle East, Central Asia, northern India, parts of Northern Europe, the Russian Federation, and western China, broadly similar to 2024. In contrast, TWS remained within the normal range on the Iberian Peninsula. In Central and southern Africa, much-above-normal TWS conditions persisted from 2024 into 2025.

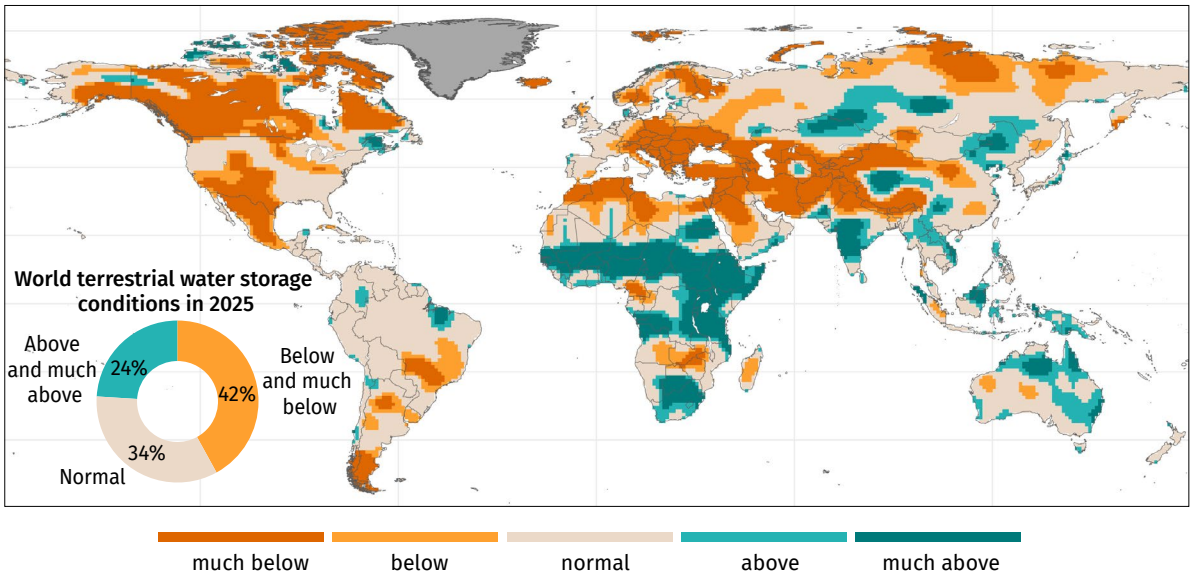


Figure 21. Terrestrial water storage (TWS) in 2025 expressed as anomalies compared with the 2002–2020 reference period. The inset chart (bottom left) shows the percentages of area under the different conditions.

Note: Greenland and Antarctica are excluded because mass change there reflects ice-sheet dynamics rather than TWS in the hydrological sense. There was also already a trend there during the reference period 2002–2020 and hence anomalies in 2025 would not be meaningful.

Note: The boundaries and names shown and the designations used do not imply official endorsement or acceptance by WMO or the United Nations.

Snow cover and glaciers

- Snow conditions were below normal across Europe, with Eastern European basins, including the Danube, Dnieper, Don and Volga, as well as those in Western and Northern Europe, recording below- to much-below-normal seasonal peak snow mass and March snow water equivalent (SWE).
- Snow cover in the Russian Federation showed strong regional contrasts in March SWE, with deficits in the upstream Yenisei and Ob basins, but above- to much-above-normal values in the Amur basin and downstream parts of the Ob and Yenisei basins; seasonal peak snow mass was generally near normal.
- North America had mostly near-normal seasonal peak snow mass, but mixed March SWE, with deficits in parts of the Mississippi and St. Lawrence basins and surpluses in portions of the Nelson, Mackenzie, Churchill and Yukon basins. Seasonal peak snow mass was much below normal in the Colorado basin as well as the Fraser basin and the surrounding Pacific seaboard along the western coast of Canada.
- In the hydrological year 2025,[24] glaciers lost 408 ± 132 Gt of mass, equivalent to 1.1 ± 0.4 mm of sea-level rise, marking the fourth consecutive year in which every major glaciated region recorded a net loss. In 2025, the Central Asia, South Asia West, Russian Arctic, Iceland, and Western Canada and USA Global Terrestrial Network for Glaciers (GTN-G) regions all recorded annual mass balances that ranked among the three most negative years on record for those regions.
- Some regions dominated by smaller glaciers, such as the Caucasus, Western Canada and USA, and Central Europe regions, experienced little or no increase, or even a decrease, in the 2025 summer balance despite greater annual mass loss compared with 1991–2020.[25] This indicates that these regions may already have reached peak water conditions.[26]

Snow water equivalent and peak snow mass

The March snow water equivalent (SWE) in the northern hemisphere was obtained as an ensemble mean over the 1991–2025 period from four individual gridded products:

- The ESA Snow CCI SWE version 3.1 product derived through a combination of satellite passive microwave brightness temperatures and climate station snow depth observations (Luojus et al., 2024);
- The Modern-Era Retrospective Analysis for Research and Applications version 2 (MERRA-2) (GMAO, 2015) daily SWE fields;
- SWE output from the ERA5-Land analysis (Muñoz Sabater, 2019);
- The physical snowpack model Crocus (Decharme and Barbu, 2024) driven by ERA5 meteorological forcing.

[24] The hydrological year used in glacier analysis ran from October 2024 to September 2025.

[25] Summer balance is a minimum approximation of summer runoff.

[26] Peak water refers to the threshold where the glacier reaches its maximum runoff due to melting.

March mean SWE data from each product were regridded to a common 0.5° × 0.5° regular grid and averaged together (Figure 22). This is the same suite of products currently used to produce annually updated SWE data for the *Arctic Report Card* (Mudryk et al., 2025) and the *Bulletin of the American Meteorological Society* (BAMS) State of the Climate Report (Mudryk et al., 2026). March 2025 SWE values were converted to anomalies using the 1991–2020 reference period on a pixel-wise basis, as per Box 1.

To produce daily snow mass time series, daily SWE output from the Crocus-ERA5 snow model (Decharme and Barbu, 2024) and ERA5-Land model output (Muñoz Sabater, 2019) were each aggregated over a given basin region. For each of the two products, peak snow mass values were then calculated for each calendar year, and the resulting series of values were used to calculate 2025 percentiles relative to the 1991–2020 reference period. The average of the two sets of percentiles is illustrated in Figure 23. Because they are calculated from daily snow mass totals specific to each basin, these percentiles can better represent the timing of peak snow mass than anomalies of March mean SWE.

In Eastern European basins, including the Danube, Dnieper, Don and Volga, as well as across Western and Northern Europe, March SWE and seasonal peak snow mass were below to much below normal. In contrast, large parts of the Amur basin recorded above- to much-above-normal March SWE, with seasonal peak snow mass remaining close to normal. In the northern basins of the Russian Federation, seasonal peak snow mass was near normal overall, with below- to much-below-normal March SWE across the upstream reaches of the Yenisei and Ob and above- to much-above-normal March SWE in the downstream parts of the Ob and Yenisei basins. Across parts of the Russian Federation (the European and southern regions), snow cover melted earlier than usual, consistent with anomalously warm conditions observed from January to March. The duration of snow cover, averaged across the Russian Federation, was significantly

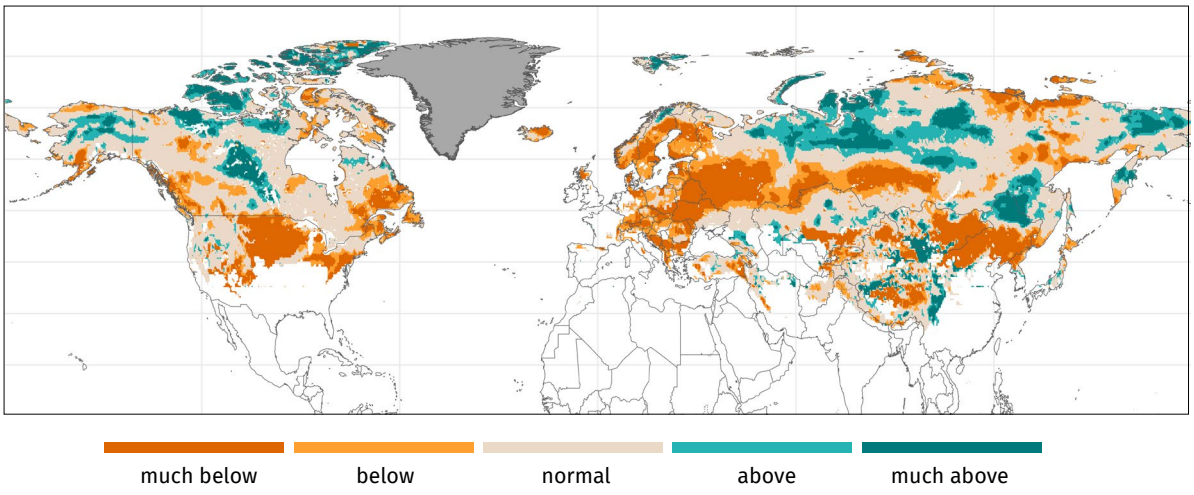


Figure 22. Snow water equivalent in March 2025 expressed as anomalies compared with the 1991–2020 reference period. Results are based on four gridded products (see the Snow water equivalent section in the annex for more details).

Note: The boundaries and names shown and the designations used do not imply official endorsement or acceptance by WMO or the United Nations.

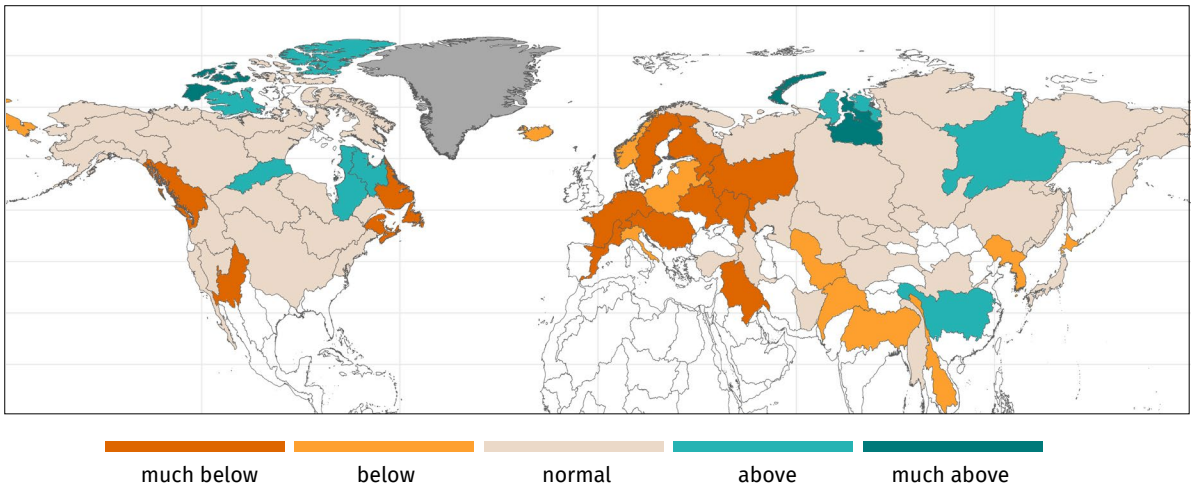


Figure 23. Seasonal peak snow mass over the entire northern hemisphere in 2025 expressed as anomalies compared to the 1991–2020 reference period

Note: The boundaries and names shown and the designations used do not imply official endorsement or acceptance by WMO or the United Nations.

shorter than the climatic norm, as was the case during the previous winter as well, with the negative anomaly becoming a record in the ranked series since 1967 (Roshydromet, 2026).

In North America, the Mississippi, St. Lawrence, Mackenzie, Columbia, Nelson and Yukon basins recorded near-normal seasonal peak snow mass. Seasonal peak snow mass was above normal in the Churchill basin and parts of the Arctic seaboard, and it was much below normal in the Colorado basin as well as the Fraser basin and surrounding Pacific seaboard along the western coast of Canada. March SWE was much below normal across parts of the Mississippi and St. Lawrence basins, while much-above-normal values were recorded across portions of the Nelson, Mackenzie and Churchill basins. In the Yukon basin, March SWE ranged from normal to much above normal.

Glaciers

The present assessment of global and regional glacier mass change (Figure 24) is based on observations compiled by the World Glacier Monitoring Service (WGMS) in the Fluctuations of Glaciers database (WGMS, 2026). Multi-year elevation changes from remote sensing (>200 000 glaciers or 96% of the world's glaciers) are temporally downscaled using selected annual mass changes from field measurements (149 glaciers or <1% of the world's glaciers) to estimate the annual mass change of every glacier (Dussaillant et al., 2025; RGI Consortium, 2017) and subsequently aggregated by region. For regions and years with sufficient observations, winter and summer mass changes are derived from the annual mass changes and measured seasonal mass changes (275 glaciers).

Since the 1990s, ice loss has been increasing in almost all regions, and it has considerably accelerated since 2000 (Hugonnet et al., 2021). This is mostly due to regions consistently presenting larger summer melt than winter accumulation after the 1990s (Figure 24).

During the hydrological year 2025, glaciers lost 408 ± 132 Gt of mass, equivalent to 1.1 ± 0.4 mm of sea-level rise. This marked a continuation of widespread glacier mass loss, with six of

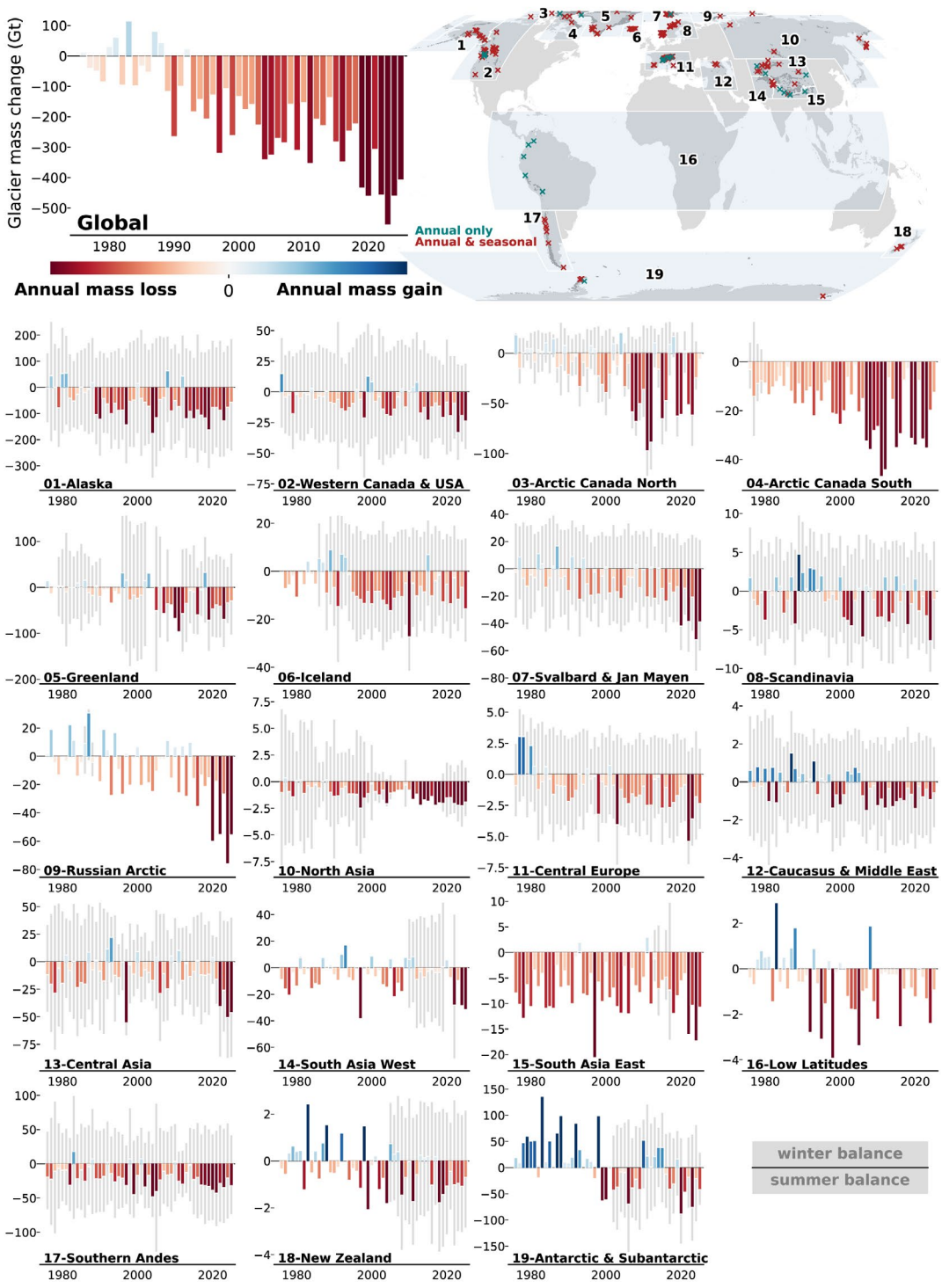


Figure 24. Annual and seasonal mass change for hydrological years 1976 to 2025 for the 19 GTN-G glacier regions. Hydrological years begin at the start of winter (mass gain) and continue through the end of the following summer (mass loss). They are labeled with the calendar year in which they end; thus, the 2025 hydrological year ended around September in the northern hemisphere (regions 1–15) and around March in the southern hemisphere (regions 17–19). At low latitudes (region 16), where seasons are less pronounced, calendar years are used instead. Note that summer and winter mass changes are only reported for years with at least one seasonal observation in a given region.

the seven largest annual losses on record occurring in the past seven years. Additionally, 2025 marks the fourth consecutive year in which all major glaciated regions experienced glacier mass loss (Figure 24). Specifically, in 2025, the Central Asia, South Asia West, Russian Arctic, Iceland, and Western Canada and USA regions all recorded annual mass balances that ranked among the three most negative years on record for those regions. Overall, the substantial loss of glacier mass throughout the twenty-first century represents a decline in global freshwater resources; mountain glaciers have lost 6.2% of their ice mass above sea level from 2000 to 2025 (WGMS, 2026), with relative mass loss reaching upwards of 40% for specific regions (The GlaMBIE Team, 2025). In the Russian Federation, glaciers in the Central Altai have shrunk substantially since the mid-1950s, losing 271.7 km², or 40.2% of their total area. In the twenty-first century alone, glacier area declined by 93.8 km², or 18.8% relative to 2001, with the strongest losses observed in the South Chuya Range (Roshydromet, 2026).

For regions with sufficient seasonal mass change observations over the reference climate period (1991–2020), the summer mass change in 2025 varies across regions, although most show greater summer runoff than during the reference period (Figure 24). The increased summer mass changes in 2025 compared to the reference climate period correspond with increased annual mass changes (Figure 24). Some regions dominated by smaller glaciers, such as the Caucasus, Western Canada and USA, and Central Europe regions, experienced almost no increase or a decrease in 2025 summer balance despite greater annual mass loss compared to 1991–2020,[27] indicating that these regions may have already reached peak water conditions (Huss and Hock, 2018).[28]

BOX 4. STATE OF PERMAFROST IN THE RUSSIAN FEDERATION IN 2025

Permafrost, which is recognized by WMO, through the Global Climate Observing System, as an Essential Climate Variable and is defined as ground that remains at or below 0 °C for at least two consecutive years, underlies extensive areas of the northern hemisphere. It plays an important role in the climate system by storing vast amounts of organic carbon, making its thaw an important indicator and driver of climate change impacts. Thawing of permafrost may adversely impact the stability of buildings, roads and infrastructure. Its state is monitored primarily by measuring permafrost temperature and active layer thickness, which describes the depth of seasonal thaw above the permafrost table.

In the Russian Federation, active layer thickness increased at 14 of the 21 sites analysed in 2025, meaning summer thaw penetrated deeper into the ground, with changes generally limited to 10 cm or less, across western and central Siberia and Chukotka. This contrasts with 2024, when most sites recorded a decrease of similar magnitude (Roshydromet, 2026).

Long-term observations indicate a widespread increase in active layer thickness across the Russian permafrost zone over 2005–2025, particularly in western regions. The strongest positive trends are observed in European Russia and western Siberia, reaching up to 39 cm per decade and locally even up to 60 cm per decade in western Siberia. In eastern Siberia, Chukotka and Kamchatka, trends are weaker and more variable, with slightly positive and slightly negative changes generally within 5–6 cm per decade (Roshydromet, 2026).

[27] Summer balance is a minimum approximation of summer runoff.

[28] Peak water refers to the threshold where the glacier reaches its maximum runoff due to melting.

Water quality

- January 2025 was characterized by widespread above- to much-above-normal river temperatures, particularly across Africa, Eastern Europe, Eurasia, Australia and parts of South America.
- In July 2025, the above-normal river-temperature anomalies persisted across Asia and the Middle East, affecting major basins including the Yangtze, Tarim, Brahmaputra and Amur.
- Several regions showed near-normal river temperatures in July, including much of South America and the Congo, Zambezi, Limpopo and Orange basins in Africa.
- In terms of the annual observed water temperature, in the United States, Switzerland, the United Kingdom and the Republic of Korea, most stations for which data were available recorded above- to much-above-normal river temperatures. The east coast of the United States was a notable exception.

This chapter presents 2025 water temperature anomalies at the station level provided by the GEMS/Water Data Centre (GEMStat – The global water quality database) and at the global scale provided by three global water quality model-based products: DynQual (Jones et al., 2023), DyER-TM (Jones et al., 2025; Mohseni and Stefan, 1999) and CoSWAT-WQ (Chawanda et al., 2025; Nkwasa et al., 2025). The historical period for modelled data was 1991–2020, and for observed data it was 2011–2023 for Switzerland, 2014–2023 for the United States, the Republic of Korea and the United Kingdom, and 2011–2020 for France (see Table A.5 in the annex).

Observed water quality

This chapter provides the status of observed water temperature in rivers in 2025 compared to the selected historical periods (which varied between 13 and 10 years). In order to align the assessment of river water quality with the methodologies used for other in situ variables as closely as possible, only water quality sensor data with daily or higher temporal resolution have been included in this year's report.

The data were obtained from national water agencies and subsequently filtered to comply with the data coverage requirements, limiting the amount of data available for analysis to 432 stations in five countries: the United States, the United Kingdom, the Republic of Korea, France and Switzerland, as presented in Table A.5 and Figure A.12 in the annex.

Further details on the methodology, as well as on further water quality variables – dissolved oxygen, pH and electrical conductivity – and the data being used are provided in the annex.

Observed water temperature

Water temperature is a key water quality variable because it directly affects the physical, chemical and biological processes in aquatic environments. Many aquatic species have narrow temperature tolerance ranges for growth and reproduction. Warmer water holds less oxygen than

cooler water, and this lack of oxygen can stress or kill aquatic species. Higher temperatures also accelerate chemical and biological processes, increasing the rates of decomposition and decay of organic matter, influencing nutrient cycling, and affecting the persistence and toxicity of pollutants, including pathogens.

Figure 25 presents water temperature anomalies for 2025 across the countries under consideration: except for the east coast of the United States, the majority of the stations where the data were available, in the United States, Switzerland, the United Kingdom and the Republic of Korea, reported above- to much-above-normal river temperatures.

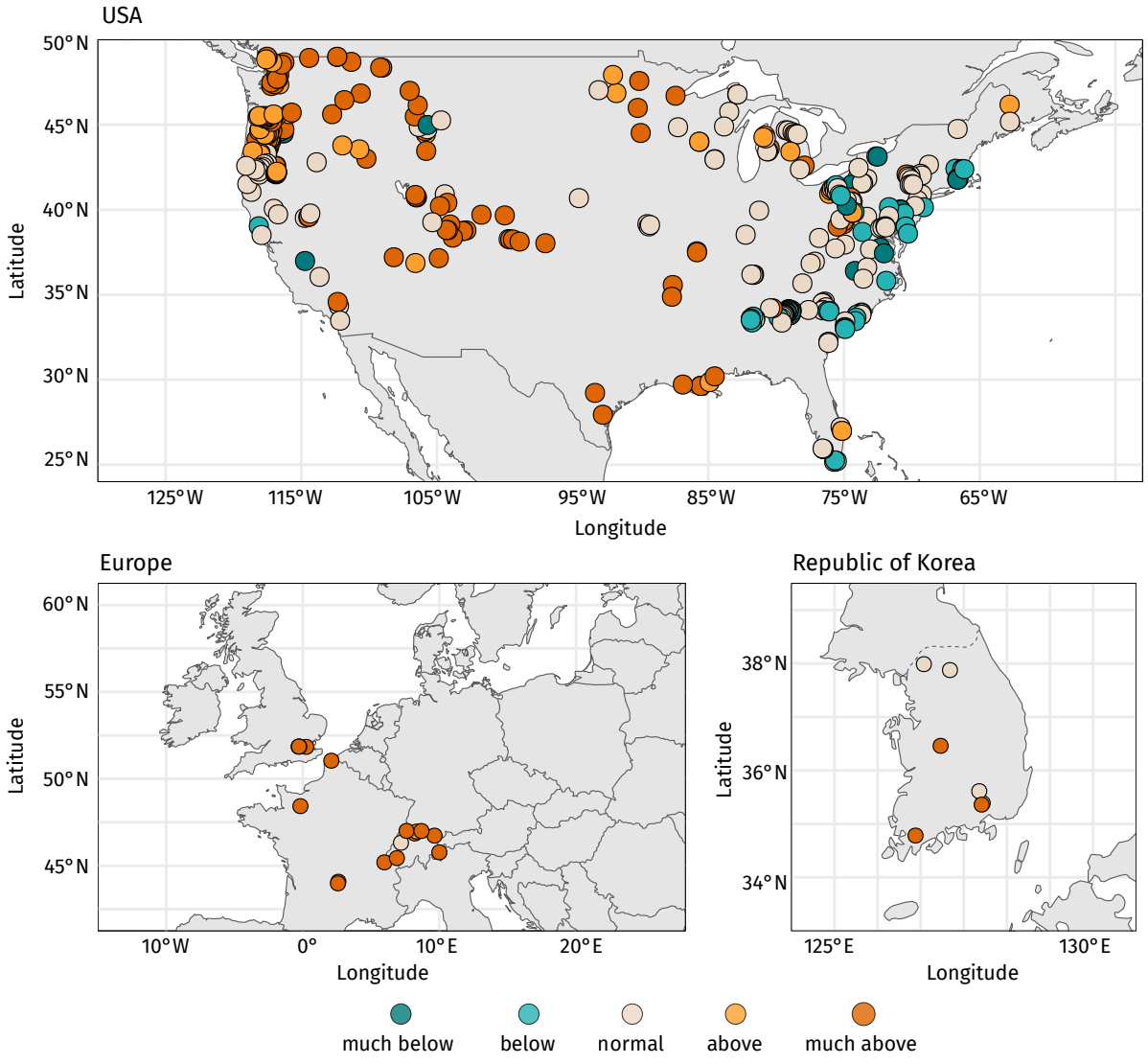


Figure 25. Water temperature anomalies in rivers in 2025 compared to a 10-year reference period between 2011 and 2023. Note: varying reference periods were applied depending on the data availability, see Table A.2 in the annex.

Note: The boundaries and names shown and the designations used do not imply official endorsement or acceptance by WMO or the United Nations.

Modelled river temperature

Figure 26 presents the modelled mean river temperature for 2025 relative to the selected historical reference period, 1991–2020. The calculation is based on ensemble results from three global water-quality model products: DynQual (Jones et al., 2023), DyER-TM (Jones et al., 2025; Mohseni and Stefan, 1999) and CoSWAT-WQ (Chawanda et al., 2025; Nkwasa et al., 2025). River temperature is simulated at the outlets of HydroBASINS.

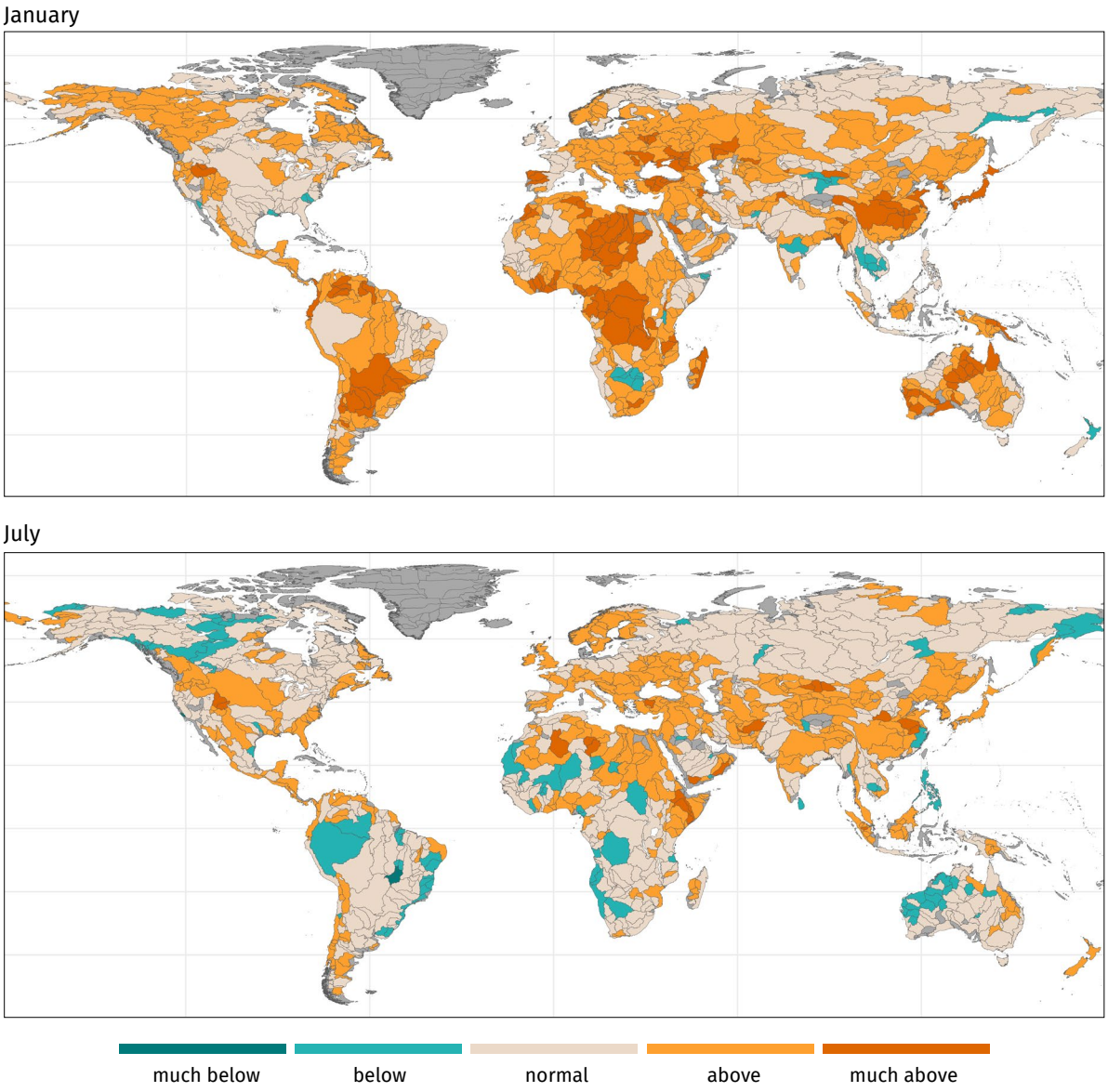


Figure 26. Mean river temperature for January and July 2025 relative to the selected historical reference period, 1991–2020

Note: The boundaries and names shown and the designations used do not imply official endorsement or acceptance by WMO or the United Nations.

Mean river temperature was above to much above normal across many regions in January 2025. The anomalies were especially pronounced across African basins, including the Volta, Niger, Lake Chad, Zambezi, Orange and Nile basins. In Europe, above-normal river temperatures were observed in southern Italy and across Eastern Europe, including the Danube basin. Above-normal conditions also extended across parts of Eurasia, including the Dnieper, Don, Volga, Ural, Ob and Yenisei basins, as well as across Australia and South America, particularly the Paraná and Amazon basins.

In July, above-normal river temperatures were observed mainly across Asia, including the Yangtze, Tarim, Ganges, Brahmaputra and Amur basins, as well as across the Middle East. In South America, river temperatures were generally near normal. Across Africa, the Congo, Zambezi, Limpopo and Orange basins also recorded near-normal river temperatures, while above-normal temperatures persisted in the Nile, northern African basins and parts of the Lake Chad basin.

High-impact hydrological events

- Asia and Africa were the regions most affected by extreme hydrometeorological events in 2025, with several African countries experiencing major flooding for two consecutive years (as in the case of Nigeria) or even three consecutive years (as in the Democratic Republic of the Congo).
- South and South-East Asia were hit by the compounded effects of tropical cyclones and intense monsoon rainfall, leading to more than 3 600 deaths across the affected countries – Sri Lanka, Pakistan, Viet Nam, Indonesia, Thailand, Malaysia and the Philippines.
- In the United States, catastrophic flash flooding hit the Texas Hill Country on 4 July 2025, when the Guadalupe River rose rapidly; the event caused at least 135 fatalities, most of them in Kerr County.
- Economic losses in Jamaica due to hurricane *Melissa* and associated flooding ranked among the highest recorded in 2025, resulting in a loss equivalent to 41% of the gross domestic product (GDP) of the country. Cyclone *Ditwah* cost Sri Lanka around 4% of GDP.
- Severe drought gripped Eastern Europe, the Mediterranean, and Middle East, with Türkiye, Armenia, the Syrian Arab Republic and Jordan each recording their driest conditions in decades.
- Drought also returned to the Greater Horn of Africa after one of the driest October–December seasons on record linked to La Niña and a negative Indian Ocean Dipole, prompting a national emergency in Somalia.

This chapter presents a non-exhaustive review of selected major extreme hydrological and weather events that occurred in 2025 (Figure 27). The events were selected from several sources, including the EM-DAT database (CRED, 2026; Delforge et al., 2025), the WMO *State of the Global Climate 2025* (WMO-No. 1391), direct communication from WMO Members to the WMO Secretariat (presented via the WMO Extremes Dashboard) and other public sources such as ReliefWeb. Events selected from the EM-DAT database were in the top 10th percentile either for number of casualties or for economic losses. From the WMO Extremes Dashboard, only events marked by the respective NMHS as "unprecedented" were considered.

In 2025, Asia and Africa were the regions most affected by extreme hydrometeorological events. Several African countries experienced widespread flooding, in some cases over consecutive years: Nigeria was affected by major flooding for the second year in a row, while the Democratic Republic of the Congo was hit by significant floods for the third consecutive year.

In South and South-East Asia, an unusual convergence of powerful weather systems produced compound impacts, leading to at least 1 969 fatalities across Viet Nam, the Philippines, Indonesia, Thailand and Malaysia and additional 640 deaths in Sri Lanka. Viet Nam and the Philippines were each struck by multiple typhoons, contributing to one of the most lethal sequences of hydrometeorological events in the region in recent years. In Pakistan, an unusually intense monsoon season resulted in over 1 000 additional fatalities.

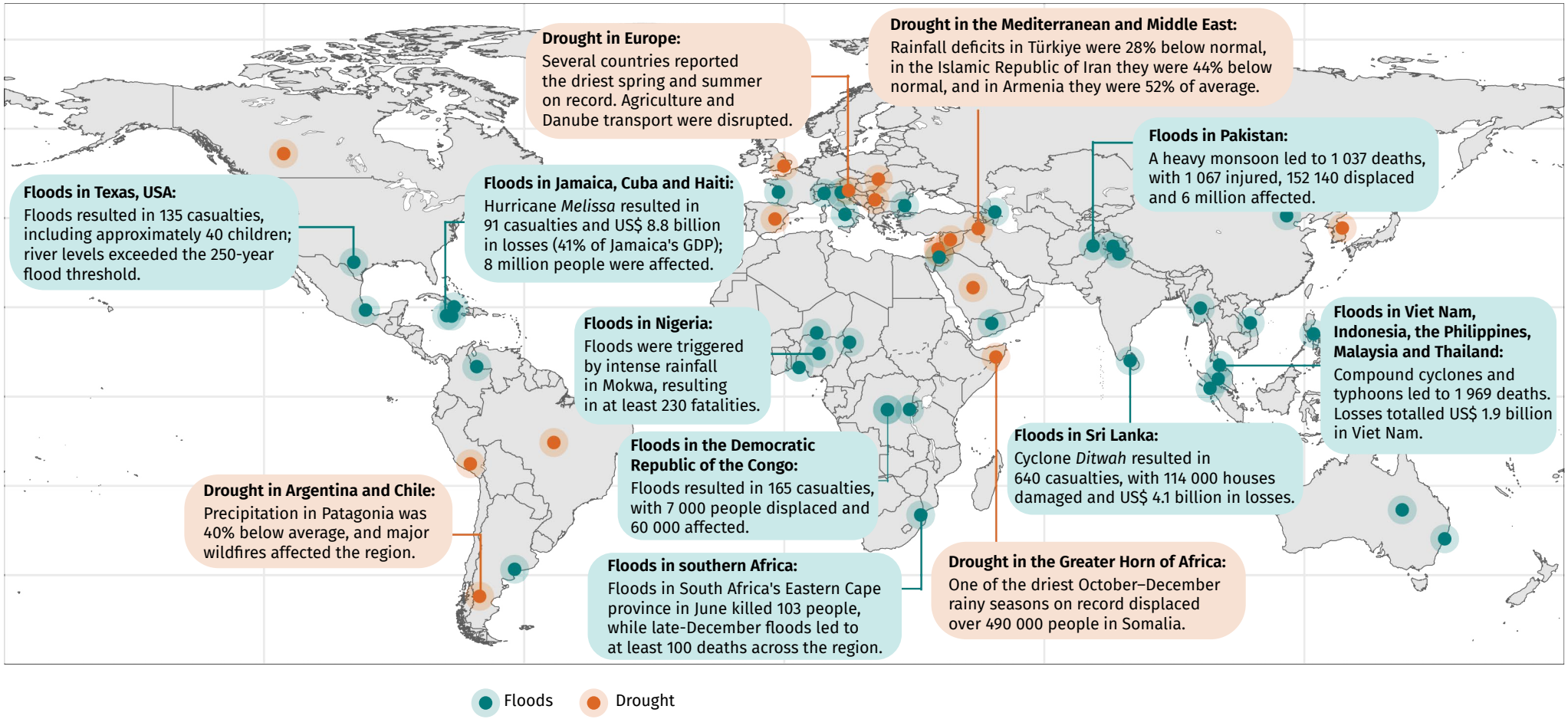


Figure 27. Selected most notable high-impact hydrological events across the globe in 2025 (obtained from EM-DAT database), the WMO *State of the Global Climate 2025* (WMO-No. 1391), direct communication from WMO Members to the WMO Secretariat and open sources, such as ReliefWeb, the World Bank and others). Note: additional information on the events can be obtained at the WMO Extremes Dashboard.

Note: The boundaries and names shown and the designations used do not imply official endorsement or acceptance by WMO or the United Nations.

Floods in the Democratic Republic of the Congo

The Democratic Republic of the Congo was severely hit by floods for the third year in a row. The catastrophic flash flooding combined with the Ndjili River inundation and landslides in Kinshasa in early April led to at least 165 deaths, with more than 7 000 people displaced and a total of over 60 000 affected in the city (*State of the Global Climate 2025* (WMO-No. 1391); ReliefWeb).

Drought in the Greater Horn of Africa

The year 2025 brought new widespread drought to the Greater Horn of Africa, with one of the driest October–December rainy seasons on record across much of Somalia, eastern Kenya and southern Ethiopia. The conditions are driven by La Niña conditions and a historically strong negative Indian Ocean Dipole (FEWS NET; *State of the Global Climate 2025* (WMO-No. 1391)). The Somali government declared a national emergency in November, with over 490 000 displacements reported in Somalia alone (*State of the Global Climate 2025* (WMO-No. 1391)). The drought conditions persisted into 2026.

Floods in Nigeria

The Nigeria Hydrological Services Agency (NIHSA) identified Mokwa Local Government Area, including the communities of Kpege and Ndakalowu, as being at high flood risk in its 2025 Annual Flood Outlook, issued in April 2025 and disseminated through the national flood early warning system.

On 29 May 2025, intense rainfall triggered a severe flood in Mokwa. A post-event field assessment conducted by NIHSA found that the impacts were exacerbated by a railway embankment associated with rehabilitation works initiated in 2018, which obstructed an ephemeral tributary of River Dingi. The absence of adequate culverts or bridge openings impeded natural drainage, creating an upstream impoundment that was subsequently breached. Settlement and development on the former floodplain further increased exposure. The flood caused over 230 fatalities, destroyed more than 300 houses, and inundated approximately 2.8 km^2 of farmland and residential areas, highlighting the importance of integrating flood-risk information into infrastructure design and land-use planning.

Floods in southern Africa

During the second week of June 2025, South Africa's Eastern Cape province was affected by floods, causing at least 103 deaths (*State of the Global Climate 2025* (WMO-No. 1391)). Recurrent extreme weather events affected Mozambique in late 2024 and throughout 2025. The country was severely affected by tropical cyclones *Dikeledi* and *Jude*, compounding the effects of *Chido*, which hit the country in late 2024 (*State of the Global Climate 2025* (WMO-No. 1391)), driving mass displacement across the country (UNHCR). Further, in late December 2025 another flooding event affected countries across southern Africa, including South Africa, Mozambique, Eswatini and Zimbabwe, killing at least 100 people (Al Jazeera).

Floods in Pakistan

The heavy monsoon led to 1 037 flood-related deaths (National Disaster Management Authority) in Pakistan during the 2025 monsoon season. A majority of the casualties were in Khyber Pakhtunkhwa (KP) and Punjab provinces (*State of the Global Climate 2025* (WMO-No. 1391)), with an additional 1 067 people injured, 152 140 people displaced, 6 million affected (ReliefWeb) and almost 230 000 houses damaged (National Disaster Management Authority).

Floods in Sri Lanka

Cyclone *Ditwah* in Sri Lanka led to 640 casualties, with over 114 000 houses damaged or destroyed (*State of the Global Climate 2025* (WMO-No. 1391); Disaster Management Center). Direct physical losses are estimated at 4.1 billion US dollars (US$), which is equivalent to about 4% of Sri Lanka's GDP (World Bank).

Floods in Indonesia, Thailand and Malaysia

Cyclone *Senyar* hit Indonesia, Thailand and Malaysia at the end of November 2025. In Indonesia 1 240 deaths were reported, and 276 were reported in Thailand (ReliefWeb).

Floods in Viet Nam

Viet Nam was struck by severe flooding during one of the country's most severe and prolonged typhoon seasons in decades (United Nations). Between May and early October, 11 typhoons and tropical cyclones either struck or influenced the country, bringing sustained heavy rainfall, flooding and landslides across northern and central provinces (United Nations). A site near Hue recorded 1 740 mm of rainfall in 24 hours on 26–27 October, and many rivers reached record-breaking levels (*State of the Global Climate 2025* (WMO-No. 1391)). At least 200 deaths were reported (*State of the Global Climate 2025* (WMO-No. 1391)), and overall economic losses are estimated at US$ 1.9 billion (*State of the Global Climate 2025* (WMO-No. 1391)).

Floods in the Philippines

The Philippines was impacted by several tropical cyclones in 2025. Typhoon *Kalmaegi* (known locally as *Tino*) and associated flooding on 4 November caused 253 deaths, mostly from flooding, with 5.4 million people affected (*State of the Global Climate 2025* (WMO-No. 1391)).

Drought in Armenia, Türkiye, the Islamic Republic of Iran, the Syrian Arab Republic and Jordan

Widespread drought continued to affect the Mediterranean and Middle East region in 2025. The year 2025 was the driest year since 1964 in Türkiye (TSMS, 2026), with national annual rainfall 28% below normal and rainfall in parts of the south-east more than 60% below normal (*State of the Global Climate 2025* (WMO-No. 1391)). In the Islamic Republic of Iran, spring rainfall was 44% below normal, leading to severe water shortages. Armenia recorded its driest winter (2024/2025) since 1935, with seasonal rainfall at 52% of average. In the Syrian Arab Republic, the 2024/2025 rainy season was the poorest in 60 years nationally.[29] Jordan reported its driest January–May since 1995 with significant crop impacts (*State of the Global Climate 2025* (WMO-No. 1391)).

[29] Contribution of the Syrian Arab Republic.

Floods in Jamaica, Cuba, Haiti and the Dominican Republic

Hurricane *Melissa* and associated flooding led to 45 deaths in Jamaica and 46 in Haiti, with a World Bank damage assessment placing Jamaica's direct losses at US$ 8.8 billion, which is almost 41% of the country's entire GDP (World Bank, 2025). The hurricane affected more than 8 million people, including more than 3 million children (Humanitarian Coalition).

In the Dominican Republic, rainfall associated with Tropical Storm *Melissa*, which passed south of the country towards Jamaica between 21 and 25 October, replenished reservoirs and improved water availability for drinking-water supply, agriculture and energy production. Rainfall peaked on 23 October, with 177.9 mm recorded at Santo Domingo Este and 175.6 mm at Centro de los Héroes in 24 hours. Accumulations of 300–435 mm over 120 hours were recorded in parts of the south-east and south.[30]

Floods in northern Australia

Northern Australia experienced a succession of major flood events between late January and April 2025. During 1–12 February, rainfall at several sites between Townsville and Ingham exceeded the previous records for any calendar month, most notably at Paluma Ivy Cottage, where 2 668.4 mm was recorded (54 years of data) (Australian Bureau of Meteorology). Between 22 and 31 March, widespread and persistent rainfall affected much of Queensland, with some parts of the west of the state recording up to 633 mm – making it the wettest March on record since 1900. The flooding cut major highways, isolated towns and remote communities, and caused substantial livestock losses (NASA).

Floods in the United States

(Note: Contribution of US Geological Survey (USGS))

Devastating flooding in Central Texas, including the Hill Country and the Concho Valley, began early on 4 July 2025. The historic and catastrophic flash flooding occurred as a result of widespread, heavy rainfall from the remnants of Tropical Storm *Barry*. The rainfall led to the rapid rise of the region's rivers. The Guadalupe River rose from less than one foot (approximately 30 cm) on 3 July to more than 34 feet (approximately 10 m) in Kerrville, Texas by 6.45 a.m. on 4 July. Total flood damages from the event are estimated to be between US$ 18 to US$ 22 billion (Billion-Dollar Weather and Climate Disasters), and the storm resulted in at least 135 direct fatalities.

In the immediate aftermath of the Central Texas flood event, the US Geological Survey (USGS) and the Texas Water Development Board (TWDB) initiated a cooperative study to collect and survey 681 high-water marks (HWMs) to evaluate the magnitude of the flood, determine the probability of occurrence at individual USGS streamflow-gauging stations, map the extent of the flooding in Central Texas, and understand geomorphic change along the Guadalupe River following the flood event. New peaks of record were recorded at 3 of the 17 USGS streamflow-gauging stations, with some sites reaching a 250-year flood event. HWMs and peak-stage data from USGS streamflow-gauging stations were used to create seven inundation maps which document the areal extent of the maximum depth of the flooding.[31]

---

[30] Contribution of National Institute of Hydraulic Resources, Dominican Republic.

[31] Forthcoming USGS products include: (a) digital datasets of the inundation area, modelling boundaries, water-depth rasters and final map products, available in the USGS data release associated with this report (https://doi.org/10.5066/P14DESPF), and (b) digital datasets, maps and documentation for the geomorphic change analysis associated with this report, available in the USGS data release (https://doi.org/10.5066/P1OPA3GE).

Drought in Argentina and Chile

Drought conditions have been developing across the Patagonia region since approximately mid-2024. The 3-month Standardized Precipitation Index (SPI) indicates that drought persisted throughout 2025 and continued to intensify in 2026, reaching the “severe” SPI category (SPI –1.5 to –1.99). In Patagonia, annual precipitation in 2025 was approximately 40% below the long-term average. The prolonged rainfall deficit contributed to extensive wildfires in both Argentina and Chile during the 2025/2026 austral summer (*State of the Global Climate 2025* (WMO-No. 1391)).

Drought in Europe

Significant drought was reported through many parts of Europe in the spring and summer of 2025. Serbia and Slovenia had their driest Junes on record, while the Republic of Moldova, Hungary and Slovakia also reported summer drought that impacted agriculture and transport on the Danube River (*State of the Global Climate 2025* (WMO-No. 1391)). Persistently warm and dry conditions in autumn 2025 sustained drought across the Iberian Peninsula (European Union). Portugal recorded its driest summer since 1931, and rainfall was also well below normal across western and north-western Spain, with summer totals more than 75% below normal in parts of the north-west (*State of the Global Climate 2025* (WMO-No. 1391)).

Floods in France

(Note: Contribution of France)

Three major storms (*Eowyn*, *Herminia* and *Ivo*) struck the Vilaine River basin in Brittany, north-western France, in January 2025. The rainfall in the Vilaine basin was three times the average: up to 200 mm during the month, while the average (referring to the 1991–2020 period) is around 65 mm. Up to 110 mm of rain fell within the basin in just one week. As a result, a significant flood occurred on the Vilaine and several of its tributaries; in some places (the cities of Guichen and Guipry-Messac), the flood reached the highest levels ever recorded. Severe damage was observed in those places as well as in the city of Redon, the lowest-lying city of the basin.

Outlook

The 2025 edition of the State of Global Water Resources report reflects significant progress in both reach and content. Continued engagement from WMO Members, data centres and international partners demonstrates the sustained relevance of the report and the importance of strengthening global cooperation on water data sharing. This is evident in the growing number of participating countries, the increase in data contributions, and the expanding list of partner organizations involved.

However, progress has not been uniform across all variables. For the soil moisture observations – while the number of stations has increased, the geographical coverage has declined over the five-year reporting period, due to the closure of some station networks. This year saw losses in the soil moisture network landscape: SMOSMANIA (southern France) could not deliver data on time due to staff shortages, and REMEDHUS (Spain) closed after 20 years of operation. On the other hand, several newer networks (COSMOS-UK, ROMPS in Central Asia and XMS-CAT in Catalonia) are now approaching the 15-year observational threshold and can be included in future editions of the report.

This edition further reflects the increasing role of complementary methods, including remote sensing and modelling, alongside in situ hydrological observations. Remote-sensing-based discharge estimates are used to support the interpretation and infilling of river discharge observation records in selected cases, particularly where ground-based data are limited or discontinuous. These approaches do not replace in situ observations, but can provide useful additional context for assessment in data-scarce regions.

As a glance into the future of global hydrological monitoring, Figure 28 depicts observations from the Surface Water and Ocean Topography (SWOT) mission, launched in December 2022

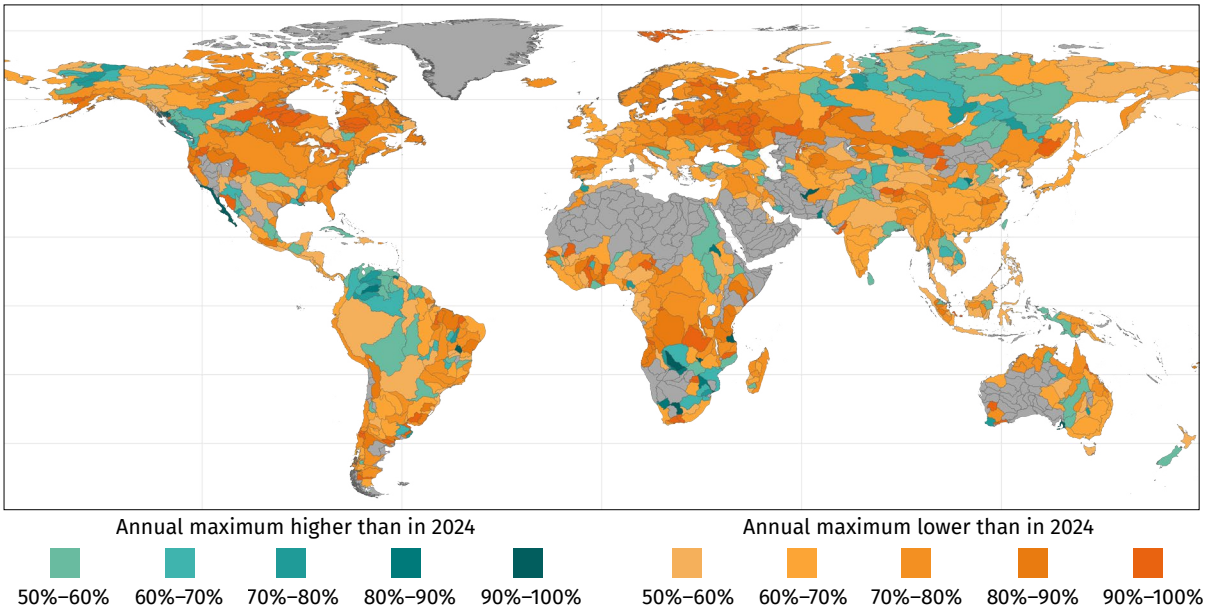


Figure 28. Annual maximum water surface elevation in 2025 relative to 2024, from the Surface Water and Ocean Topography (SWOT) mission. Green denotes basins where most SWOT reach lengths showed a 2025 annual maximum that was higher than in 2024, orange where most were lower; shading gives the percentage of reach lengths in that direction (50%–100%). Grey: insufficient SWOT data.

Note: The boundaries and names shown and the designations used do not imply official endorsement or acceptance by WMO or the United Nations.

(Getirana et al., 2024, 2026). SWOT provides a new satellite-based capability to observe inland surface water dynamics, including changes in water surface elevation and extent across rivers, lakes, reservoirs, wetlands and floodplains. In this report, SWOT observations are presented as comparisons between annual maximum water surface elevations in 2025 and those in 2024. Although the record is still short, the dataset illustrates the increasing potential of space-based observations to support operational water management, including the monitoring of floods, droughts, reservoir dynamics and basin-scale water availability, particularly in remote and transboundary basins where ground-based monitoring remains limited.

Looking ahead, we aim to enhance the automation of data flows through our data centres and the WMO Hydrological Observing System (WHOS), streamlining integration for future reporting cycles. The ongoing operationalization of the WMO Global Hydrological Status and Outlook System (HydroSOS) and associated capacity development activities will enable countries to produce monthly water resources status updates. This will provide WMO Members and stakeholders with timely, actionable information for water-related decision-making in an increasingly dynamic climatological and hydrological environment, in addition to the annual snapshot the State of Global Water Resources provides.

References

Alfieri, L.; Burek, P.; Dutra, E. et al. GloFAS – Global Ensemble Streamflow Forecasting and Flood Early Warning. *Hydrology and Earth System Sciences* **2013**, *17* (3), 1161–1175. https://doi.org/10.5194/hess-17-1161-2013.

Arheimer, B.; Pimentel, R.; Isberg, K. et al. Global Catchment Modelling Using World-Wide HYPE (WWH), Open Data, and Stepwise Parameter Estimation. *Hydrology and Earth System Sciences* **2020**, *24* (2), 535–559. https://doi.org/10.5194/hess-24-535-2020.

Bai, H.; Liu, X.; Yang, H. et al. Unprecedented Amazonian Rainforests Damage during the 2023–2024 Droughts. *Proceedings of the National Academy of Sciences* **2026**, *123* (13), e2514066123. https://doi.org/10.1073/pnas.2514066123.

Becker, A.; Finger, P.; Meyer-Christoffer, A. et al. A Description of the Global Land-Surface Precipitation Data Products of the Global Precipitation Climatology Centre with Sample Applications Including Centennial (Trend) Analysis from 1901–Present. *Earth System Science Data* **2013**, *5* (1), 71–99. https://doi.org/10.5194/essd-5-71-2013.

Bell, J. E.; Palecki, M. A.; Baker, C. B. et al. U.S. Climate Reference Network Soil Moisture and Temperature Observations. *Journal of Hydrometeorology* **2013**, *14* (3), 977–988. https://doi.org/10.1175/JHM-D-12-0146.1.

Boussetta, S.; Balsamo, G.; Arduini, G. et al. ecLand: The ECMWF Land Surface Modelling System. *Atmosphere* **2021**, *12* (6), 723. https://doi.org/10.3390/atmos12060723.

Cao, F.; Gerges, E.; Vargas, C. R. et al. In-Situ Groundwater Level Monitoring Reveals Worldwide Status, Trends and Impacts. *Environmental Research Letters* **2026**, *21*, 103002. https://doi.org/10.1088/1748-9326/ae651f.

Centre for Research on the Epidemiology of Disasters (CRED). *EM-DAT: The International Disaster Database*; CRED/UCLouvain: Brussels, 2026. https://www.emdat.be.

Chandanpurkar, H. A.; Famiglietti, J. S.; Gopalan, K. et al. Unprecedented Continental Drying, Shrinking Freshwater Availability, and Increasing Land Contributions to Sea Level Rise. *Science Advances* **2025**, *11* (30), eadx0298. https://doi.org/10.1126/sciadv.adx0298.

Chawanda, C. J.; van Griensven, A.; Nkwasa, A. et al. CoSWAT Model v1: A High-Resolution Global SWAT+ Hydrological Model. *Hydrology and Earth System Sciences* **2025**, *29*, 6901–6916. https://doi.org/10.5194/hess-29-6901-2025.

Decharme, B.; Barbu, A. Crocus-ERA5 Daily Snow Product over the Northern Hemisphere at 0.25° Resolution, Version 2023; *Zenodo*, **2024**. https://doi.org/10.5281/zenodo.10943718.

Delforge, D.; Wathelet, V.; Below, R. et al. EM-DAT: The Emergency Events Database. *International Journal of Disaster Risk Reduction* **2025**, *124*, 105509. https://doi.org/10.1016/j.ijdrr.2025.105509.

Dorigo, W. A.; Xaver, A.; Vreugdenhil, M. et al. Global Automated Quality Control of In-Situ Soil Moisture Data from the International Soil Moisture Network. *Vadose Zone Journal* **2013**, *12* (3), vzj2012.0097. https://doi.org/10.2136/vzj2012.0097.

Dorigo, W.; Himmelbauer, I.; Aberer, D. et al. The International Soil Moisture Network: Serving Earth System Science for over a Decade. *Hydrology and Earth System Sciences* **2021**, *25* (11), 5749–5804. https://doi.org/10.5194/hess-25-5749-2021.

Dussaillant, I.; Hugonnet, R.; Huss, M. et al. Annual Mass Change of the World's Glaciers from 1976 to 2024 by Temporal Downscaling of Satellite Data with In-Situ Observations. *Earth System Science Data* **2025**, *17* (5), 1977–2006. https://doi.org/10.5194/essd-17-1977-2025.

Eilander, D.; van Verseveld, W.; Yamazaki, D. et al. A Hydrography Upscaling Method for Scale-Invariant Parametrization of Distributed Hydrological Models. *Hydrology and Earth System Sciences* **2021**, *25* (9), 5287–5313. https://doi.org/10.5194/hess-25-5287-2021.

Elmi, O.; Tourian, M. J.; Saemian, P. et al. Remote Sensing-Based Extension of GRDC Discharge Time Series – A Monthly Product with Uncertainty Estimates. *Scientific Data* **2024**, *11* (1), 240. https://doi.org/10.1038/s41597-024-03078-6.

Espinoza, J.-C.; Jimenez, J. C.; Marengo, J. A. et al. The New Record of Drought and Warmth in the Amazon in 2023 Related to Regional and Global Climatic Features. *Scientific Reports* **2024**, *14* (1), 8107. https://doi.org/10.1038/s41598-024-58782-5.

Getirana, A.; Kumar, S.; Bates, P. et al. The SWOT Mission Will Reshape Our Understanding of the Global Terrestrial Water Cycle. *Nature Water* **2024**, *2* (12), 1139–1142. https://doi.org/10.1038/s44221-024-00352-0.

Getirana, A.; Collins, E.; Alcântara, E. et al. Floods in 2025. *Nature Reviews Earth & Environment* **2026**, *1–4*, 270–273. https://doi.org/10.1038/s43017-026-00779-x.

The GlaMBIE Team. Community Estimate of Global Glacier Mass Changes from 2000 to 2023. *Nature* **2025**, *639*, 382–388. https://doi.org/10.1038/s41586-024-08545-z.

Global Modeling and Assimilation Office (GMAO). *inst3_3d_asm_Cp: MERRA-2 3D IAU State, Meteorology Instantaneous 3-hourly (p-coord, 0.625x0.5L42)*, version 5.12.4. Goddard Space Flight Center Distributed Active Archive Center (GSFC DAAC): Greenbelt, USA, 2015. https://doi.org/10.5067/VJAFPLI1CSIV.

Global Precipitation Climatology Centre (GPCC). *GPCC Precipitation Quantiles at 1.0°: Monthly Land-Surface Precipitation as Quantiles from Rain-Gauges Built on GTS-Based and Historic Data*. Deutscher Wetterdienst, 2025. https://doi.org/10.5676/DWD_GPCC/QUANTILES_V2022_100.

Grimaldi, S.; Salamon, P.; Russo, C. et al. GloFAS v4.0: Towards Hyper-Resolution Hydrological Modelling at Global Scale (EGU23-3410). In *European Geosciences Union (EGU) Abstracts EGU General Assembly 2023*, Vienna, Austria, 23–28 April 2023. https://doi.org/10.5194/egusphere-egu23-3410.

EUMETSAT SAF on Support to Operational Hydrology and Water Management (H SAF). *Scatterometer Root Zone Soil Moisture Climate Data Record v3, 0.1° Sampling (H145) and Intermediate Climate Data Record (H146)*; H SAF: 2026.

Hales, R. C.; Nelson, E. J.; Souffront, M. et al. Advancing Global Hydrologic Modeling with the GEOGloWS ECMWF Streamflow Service. *Journal of Flood Risk Management* **2022**, *18* (1), e12859. https://doi.org/10.1111/jfr3.12859.

Hanazaki, R.; Yamazaki, D.; Yoshimura, K. Development of a Reservoir Flood Control Scheme for Global Flood Models. *Journal of Advances in Modeling Earth Systems* **2022**, *14* (3), e2021MS002944. https://doi.org/10.1029/2021MS002944.

Huang, Q.; Zhang, Y.; Ma, N. et al. Estimating Vegetation Greening Influences on Runoff Signatures Using a Log-Based Weighted Ensemble Method. *Water Resources Research* **2022**, *58* (12), e2022WR032492. https://doi.org/10.1029/2022WR032492.

Huggins, X.; Gleeson, T.; Kummu, M. et al. Hotspots for Social and Ecological Impacts from Freshwater Stress and Storage Loss. *Nature Communications* **2022**, *13*, 439. https://doi.org/10.1038/s41467-022-28029-w.

Hugonnet, R.; McNabb, R.; Berthier, E. et al. Accelerated Global Glacier Mass Loss in the Early Twenty-First Century. *Nature* **2021**, *592* (7856), 726–731. https://doi.org/10.1038/s41586-021-03436-z.

Huss, M.; Hock, R. Global-Scale Hydrological Response to Future Glacier Mass Loss. *Nature Climate Change* **2018**, *8* (2), 135–140. https://doi.org/10.1038/s41558-017-0049-x.

Imhoff, R. O.; van Verseveld, W. J.; van Osnabrugge, B. et al. Scaling Point-Scale (Pedo)Transfer Functions to Seamless Large-Domain Parameter Estimates for High-Resolution Distributed Hydrologic Modeling: An Example for the Rhine River. *Water Resources Research* **2020**, *56* (4), e2019WR026807. https://doi.org/10.1029/2019WR026807.

Jasechko, S.; Seybold, H.; Perrone, D. et al. Rapid Groundwater Decline and Some Cases of Recovery in Aquifers Globally. *Nature* **2024**, *625*, 715–721. https://doi.org/10.1038/s41586-023-06879-8.

Jones, E. R.; Bierkens, M. F. P.; Wanders, N. et al. DynQual v1.0: A High-Resolution Global Surface Water Quality Model. *Geoscientific Model Development* **2023**, *16*, 4481–4500. https://doi.org/10.5194/gmd-16-4481-2023.

Jones, E. R.; van Beek, R.; Cárdenas Belleza, G. et al. A Multi-Model Assessment of Global Freshwater Temperature and Thermoelectric Power Supply under Climate Change. *Environmental Research: Water* **2025**, *1* (2), 025002. https://doi.org/10.1088/3033-4942/addffa.

Konrad, H.; Roca, R.; Niedorf, A. et al. GIRAFE v1: A Global Climate Data Record for Precipitation Accompanied by a Daily Sampling Uncertainty. *Earth System Science Data* **2025**, *17*, 4097–4124. https://doi.org/10.5194/essd-17-4097-2025.

Kumar, R.; Samaniego, L.; Attinger, S. Implications of Distributed Hydrologic Model Parameterization on Water Fluxes at Multiple Scales and Locations. *Water Resources Research* **2013**, *49* (1), 360–379. https://doi.org/10.1029/2012WR012195.

Landerer, F. W.; Flechtner, F. M.; Save, H. et al. Extending the Global Mass Change Data Record: GRACE Follow-On Instrument and Science Data Performance. *Geophysical Research Letters* **2020**, *47* (12), e2020GL088306. https://doi.org/10.1029/2020GL088306.

Leavesley, G.; David, O.; Garen, D. et al. A Modeling Framework for Improved Agricultural Water Supply Forecasting. In *AGU Fall Meeting Abstracts*, San Francisco, USA, 15–19 December 2008.

Lehner, B.; Verdin, K.; Jarvis, A. New Global Hydrography Derived from Spaceborne Elevation Data. Eos, *Transactions American Geophysical Union* **2008**, *89* (10), 93–94. https://doi.org/10.1029/2008EO100001.

Li, Y.; Zhao, G.; Allen, G. H. et al. Diminishing Storage Returns of Reservoir Construction. *Nature Communications* **2023**, *14*, 3203. https://doi.org/10.1038/s41467-023-38843-5.

Luojus, K.; Venäläinen, P.; Moisander, M. et al. *ESA Snow Climate Change Initiative (Snow_cci): Snow Water Equivalent (SWE) Level 3C Daily Global Climate Research Data Package (CRDP) (1979–2022)*, Version 3.1; NERC EDS Centre for Environmental Data Analysis, 2024. https://doi.org/10.5285/9d9bfc488ec54b1297eca2c9662f9c81.

Ma, W.; Hibino, K.; Yamamoto, K. et al. A New Generation of Hydrological Condition Simulator Employing Physical Models and Satellite-Based Meteorological Data. *Earth and Space Science* **2024**, *11* (11), e2023EA003228. https://doi.org/10.1029/2023EA003228.

Mohseni, O.; Stefan, H. G. Stream Temperature/Air Temperature Relationship: A Physical Interpretation. *Journal of Hydrology* **1999**, *218* (3–4), 128–141. https://doi.org/10.1016/S0022-1694(99)00034-7.

Mudryk, L. R.; Elias Chereque, A.; Derksen, C. et al. *Terrestrial Snow Cover; Arctic Report Card 2025*; National Oceanic and Atmospheric Administration (NOAA), 2025. https://doi.org/10.25923/cfhv-c239.

Mudryk, L. R.; Elias Chereque, A.; Derksen, C. et al. Terrestrial Snow [in “State of the Climate in 2025”]. *Bulletin of the American Meteorological Society* **2026**, *107* (8), S328–S330. https://doi.org/10.1175/2026BAMSStateoftheClimate.1.

Muñoz Sabater, J. *ERA5-Land Hourly Data from 1950 to Present*; Copernicus Climate Change Service (C3S) Climate Data Store (CDS), 2019. https://doi.org/10.24381/cds.e2161bac.

Murray, A. M.; Jørgensen, G. H.; Godiksen, P. N. et al. DHI-GHM: Real-Time and Forecasted Hydrology for the Entire Planet. *Journal of Hydrology* **2023**, *620*, 129431. https://doi.org/10.1016/j.jhydrol.2023.129431.

Nkwasa, A.; Chawanda, C. J.; Nakkazi, M. T. et al. CoSWAT-WQ v1.0: A High-Resolution Community Global SWAT+ Water Quality Model. *EGUsphere* **2025** [preprint]. https://doi.org/10.5194/egusphere-2025-703.

Nyenah, E.; Hosseini-Moghari, S.-M.; Trautmann, T. et al. *WaterGAP v2.3 Documentation*; ReWaterGAP. https://hydrologyfrankfurt.github.io/ReWaterGAP/2.3/index.html.

OPERA. *OPERA Dynamic Surface Water Extent from Harmonized Landsat Sentinel-2 Product*, Version 1; Physical Oceanography Distributed Active Archive Center (PO.DAAC), 2023. https://doi.org/10.5067/OPDSW-PL3V1.

RGI Consortium. *Randolph Glacier Inventory – A Dataset of Global Glacier Outlines*, Version 6.0; Technical Report; Global Land Ice Measurements from Space (GLIMS): Boulder, USA, 2017. https://doi.org/10.7265/N5-RGI-60.

Rivera, J. A. Characterization of the Recent (2019–2022) La Plata Basin Hydrological Drought from a Centennial-Scale Perspective. *HydroResearch* **2024**, *7*, 140–153. https://doi.org/10.1016/j.hydres.2024.02.002.

Rodell, M.; Barnoud, A.; Robertson, F. R. et al. An Abrupt Decline in Global Terrestrial Water Storage and Its Relationship with Sea Level Change. *Surveys in Geophysics* **2024**, *45*, 1875–1902. https://doi.org/10.1007/s10712-024-09860-w.

Russian Federal Service for Hydrometeorology and Environmental Monitoring (Roshydromet). *A Report on Climate Features on the Territory of the Russian Federation in 2025*; Roshydromet: Moscow, 2026; 129 pp. ISBN 978-5-906099-58-7. https://meteoinfo.ru/novosti/21834-opublikovan-doklad-ob-osobennostyakh-klimata-na-territorii-rossijskoj-federatsii-za-2025-god.

Saemian, P.; Elmi, O.; Stroud, M. et al. Satellite Altimetry-Based Extension of Global-Scale In Situ River Discharge Measurements (SAEM). *Earth System Science Data* **2025**, *17*, 2063–2085. https://doi.org/10.5194/essd-17-2063-2025.

Saemian, P.; Tourian, M. J.; Ke, S. et al. SWOT-QQ: Global River Discharge Estimates at Gauging Stations from SWOT Observations (EGU26-17924). In *European Geosciences Union (EGU) Abstracts General Assembly 2026*, Vienna, Austria, 3–8 May 2026. https://doi.org/10.5194/egusphere-egu26-17924.

Samaniego, L.; Kumar, R.; Attinger, S. Multiscale Parameter Regionalization of a Grid-Based Hydrologic Model at the Mesoscale. *Water Resources Research* **2010**, *46* (5). https://doi.org/10.1029/2008WR007327.

Samaniego, L.; Kaluza, M.; Kumar, R. et al. Mesoscale Hydrologic Model; *Zenodo* **2019**. https://doi.org/10.5281/zenodo.3239055.

Schaefer, G. L.; Cosh, M. H.; Jackson, T. J. The USDA Natural Resources Conservation Service Soil Climate Analysis Network (SCAN). *Journal of Atmospheric and Oceanic Technology* **2007**, *24* (12), 2073–2077. https://doi.org/10.1175/2007JTECHA930.1.

Schneider, U.; Becker, A.; Finger, P. et al. GPCC's New Land Surface Precipitation Climatology Based on Quality-Controlled In Situ Data and Its Role in Quantifying the Global Water Cycle. *Theoretical and Applied Climatology* **2014**, *115* (1–2), 15–40. https://doi.org/10.1007/s00704-013-0860-x.

Shrestha, P. K.; Samaniego, L.; Rakovec, O. et al. A Novel Stream Network Upscaling Scheme for Accurate Local Streamflow Simulations in Gridded Global Hydrological Models. *Water Resources Research* **2025**, *61* (6), e2024WR038183. https://doi.org/10.1029/2024WR038183.

Sutanudjaja, E. H.; van Beek, R.; Wanders, N. et al. PCR-GLOBWB 2: A 5 Arcmin Global Hydrological and Water Resources Model. *Geoscientific Model Development* **2018**, *11* (6), 2429–2453. https://doi.org/10.5194/gmd-11-2429-2018.

Tapley, B. D.; Bettadpur, S.; Watkins, M. et al. The Gravity Recovery and Climate Experiment: Mission Overview and Early Results. *Geophysical Research Letters* **2004**, *31* (9), L09607. https://doi.org/10.1029/2004GL019920.

Toreti, Andrea; Bavera, Davide; Acosta Navarro, Juan et al. *Drought in the Amazon and the La Plata Basins: December 2024: GDO Analytical Report*; Publications Office of the European Union, 2024. https://data.europa.eu/doi/10.2760/9524487.

Turkish State Meteorological Service (TSMS). *Climate Assessment of Türkiye in 2025*; TSMS: Ankara, 2026. https://emcc.mgm.gov.tr/files/State_of_the_Climate_in_Turkey_in_2025.pdf.

van Verseveld, W. J.; Weerts, A. H.; Visser, M. et al. Wflow_sbm v0.7.3, a Spatially Distributed Hydrological Model: From Global Data to Local Applications. *Geoscientific Model Development* **2024**, *17* (8), 3199–3234. https://doi.org/10.5194/gmd-17-3199-2024.

World Bank. *Global Rapid Post-Disaster Damage Estimation (GRADE) Report: Hurricane Melissa 2025 Jamaica*; World Bank: Washington, DC, 2025. https://www.gfdrr.org/en/JamaicaGRADE.

World Glacier Monitoring Service (WGMS). *Fluctuations of Glaciers (FoG) Database*. WGMS: Zurich, Switzerland, 2026. https://doi.org/10.5904/wgms-fog-2026-02-10.

World Meteorological Organization (WMO). *State of Global Water Resources 2021* (WMO-No. 1308). Geneva, 2022.

World Meteorological Organization (WMO). *State of Global Water Resources 2022* (WMO-No. 1333). Geneva, 2023.
World Meteorological Organization (WMO). *State of Global Water Resources 2023* (WMO-No. 1362). Geneva, 2024.
World Meteorological Organization (WMO). *State of Global Water Resources 2024* (WMO-No. 1380). Geneva, 2025.
Yadav, A.; Zhang, S.; Zhao, B. et al. Mapping Reservoir Water Surface Area in the Contiguous United States Using the High-Temporal Harmonized Landsat and Sentinel (HLS) Data at a Sub-Weekly Time Scale. *Geophysical Research Letters* **2025**, *52* (11). https://doi.org/10.1029/2024GL114046.
Yamazaki, D.; Kanae, S.; Kim, H. et al. A Physically Based Description of Floodplain Inundation Dynamics in a Global River Routing Model. *Water Resources Research* **2011**, *47* (4). https://doi.org/10.1029/2010WR009726.
Yoshimura, K.; Sakimura, T.; Oki, T. et al. Toward Flood Risk Prediction: A Statistical Approach Using a 29-Year River Discharge Simulation over Japan. *Hydrological Research Letters* **2008**, *2*, 22–26. https://doi.org/10.3178/hrl.2.22.
Yuan, X.; Li, C.; Ji, P. et al. Development and Evaluation of the Conjunctive Surface-Subsurface Process Model Version 3 (CSSPv3) at Global Scale. *Journal of Advances in Modeling Earth Systems* **2026**, *18* (7). https://doi.org/10.1029/2025MS005440.
Zhang, Y.; Kong, D.; Gan, R. et al. Coupled Estimation of 500 m and 8-Day Resolution Global Evapotranspiration and Gross Primary Production in 2002–2017. *Remote Sensing of Environment* **2019**, *222*, 165–182. https://doi.org/10.1016/j.rse.2018.12.031.

Annex. Technical annex

Contents

Methods **62**
Data sources 63
Variable ranking (anomaly calculation) **69**
Global hydrological modelling systems **70**
Precipitation. **71**
Drought index **74**
River discharge **75**
Observed data and validation of modelled results 75
Validation of modelled results 76
Reservoirs **79**
Inflow into selected reservoirs 79
Reservoir fullness. 80
Groundwater **81**
Data collection and selection 81
Results visualization 85
Soil moisture modelled **86**
Snow water equivalent **87**
Terrestrial water storage **87**
Glaciers **88**
Glacier contribution to seasonal river runoff. 89
Water quality **91**
Observed river water quality 91
Dissolved oxygen 93
pH 94
Electrical conductivity 95
Water surface elevation data **95**
References **98**

METHODS

The present annex provides high-level information on the main methodological steps applied to portray the state of global water resources in the year 2025.

For the *State of Global Water Resources 2025* report, modelled data were based on 986 basins spanning the globe. The basin map was based on HydroBASINS level 4 data (Lehner and Grill, 2013). The original dataset contained about 1 300 basins. However, due to the resolution of global hydrological modelling systems (GHMSs), basins with a drainage area of less than 10 000 km^2 were removed in addition to basins in some areas with modelling limitations (such as Greenland), leaving 986 basins (presented in Figure A.1).

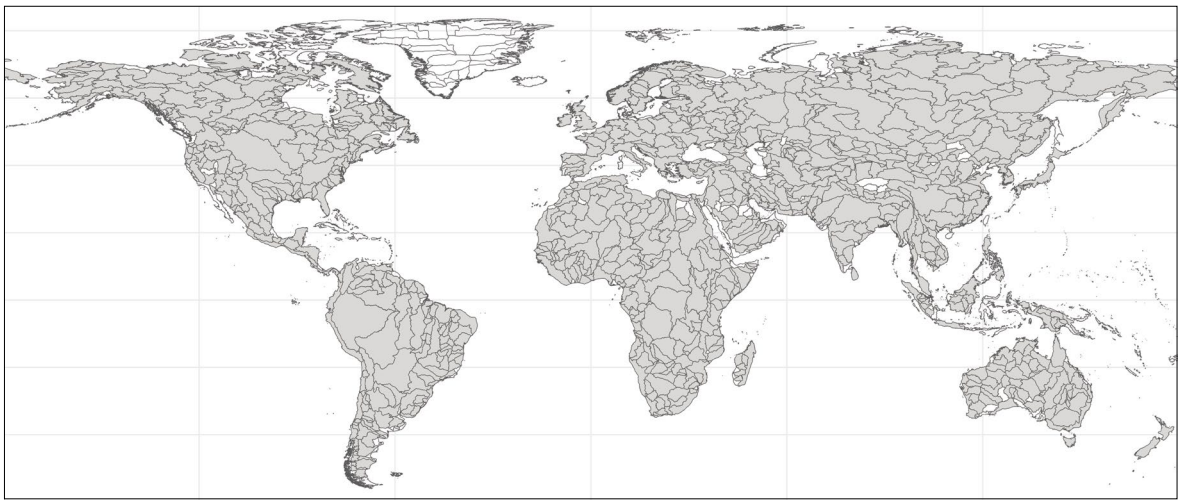


Figure A.1. Global coverage of selected hydrological basins for modelled data

Note: The boundaries and names shown and the designations used do not imply official endorsement or acceptance by WMO or the United Nations.

Data sources

Several sources of information on water resources were used to produce the *State of Global Water Resources 2025* report, in particular, the resources listed in Table A.1.

Table A1. Data sources per chapter

Institution	*Model/product name*	*Key reference*	*Streamflow*	*Reservoirs*	*Soil moisture*	*Actual evapotranspiration*	*Terrestrial water storage (TWS)*	*Snow and ice*	*Lakes*	*Glaciers*	*Groundwater*	*Water quality*	*Water surface elevation*	*Precipitation*
Observed datasets														
National Meteorological and Hydrological Services (NMHSs)			■											
Global Runoff Data Centre (GRDC)			■											
International Soil Moisture Network (ISMN)	**Observed soil moisture**				■									
International Groundwater Resources Assessment Centre (IGRAC)	**Observed groundwater levels**										■			
European Space Agency	**Lakes Climate Change Initiative (CCI) project**								■					

Institution	*Model/product name*	*Key reference*	*Streamflow*	*Reservoirs*	*Soil moisture*	*Actual evapotranspiration*	*Terrestrial water storage (TWS)*	*Snow and ice*	*Lakes*	*Glaciers*	*Groundwater*	*Water quality*	*Water surface elevation*	*Precipitation*
Observed datasets														
Global Environment Monitoring System for Freshwater (GEMS)/ Water Data Centre												■		
Global Precipitation Climatology Centre (GPCC)		Becker et al. (2013); GPCC (2025); Schneider et al. (2014)												■
World Glacier Monitoring Service (WGMS)										■				
Models and space-based observation datasets														
European Organisation for the Exploitation of Meteorological Satellites (EUMETSAT) Satellite Application Facility on Climate Monitoring (CM SAF)	**Daily and monthly Global Interpolated RAinFall Estimation (GIRAFE) dataset**	Konrad et al. (2025)												■
Goethe University Frankfurt, Johannes Gutenberg University Mainz	**WaterGAP 2.3**	Müller Schmied et al. (2021); Müller Schmied et al. (2024); Nyenah et al. (2026)	■			■								

Institution	*Model/product name*	*Key reference*	*Streamflow*	*Reservoirs*	*Soil moisture*	*Actual evapotranspiration*	*Terrestrial water storage (TWS)*	*Snow and ice*	*Lakes*	*Glaciers*	*Groundwater*	*Water quality*	*Water surface elevation*	*Precipitation*
Models and space-based observation datasets														
Institute of Atmospheric Physics (Chinese Academy of Sciences)	**Conjunctive Surface–Subsurface Process version 3 (CSSPv3)**	Yuan et al. (2026)	■	■	■	■	■	■						
Helmholtz Centre for Environmental Research – UFZ	**mesoscale Hydrologic Model (mHM)**	Kumar et al. (2013); Samaniego et al. (2010); Samaniego et al. (2019); Shrestha et al. (2025)	■		■	■	■	■						
Swedish Meteorological and Hydrological Institute (SMHI)	**World-Wide HYPE (WWH) version 1.3.9**	Arheimer et al. (2020)	■	■		■								
Danish Hydraulic Institute (DHI)	**DHI-Global Hydrological Model (GHM)**	Murray et al. (2023)	■											
University of Tokyo	**CaMa-Flood with Dam**	Hanazaki et al. (2022); Yamazaki et al. (2011)	■	■										
European Commission Joint Research Centre (JRC)	**Global Flood Awareness System (GloFAS)**	Alfieri et al. (2013); Grimaldi et al. (2023)	■											
European Centre for Medium-Range Weather Forecasts (ECMWF)	**ECLand: The ECMWF Land Surface Modelling System/ GloFAS**	Boussetta et al. (2021)	■											

Institution	*Model/product name*	*Key reference*	*Streamflow*	*Reservoirs*	*Soil moisture*	*Actual evapotranspiration*	*Terrestrial water storage (TWS)*	*Snow and ice*	*Lakes*	*Glaciers*	*Groundwater*	*Water quality*	*Water surface elevation*	*Precipitation*
Models and space-based observation datasets														
Deltares	**Wflow_sbm**	Eilander et al. (2021); Imhoff et al. (2020); van der Laan et al. (2024); van Verseveld et al. (2024)	■	■		■								
GEOGLOWS, Brigham Young University	**GEOGLOWS River Forecast System (RFS)**	Hales et al. (2022)	■											
Institute of Geographic Sciences and Natural Resources Research (Chinese Academy of Sciences)	**HBV-PML**	Huang et al. (2022); Zhang et al. (2019)	■			■	■							
Utrecht University	**PCR-GLOBWB 2**	Sutanudjaja et al. (2018)	■											
The University of Tokyo/ Japan Aerospace Exploration Agency	**Today's Earth – Global (JRA-55)**	Yoshimura et al. (2008); Ma et al. (2021)					■							
GFZ Research Centre for Geosciences (Germany)	**GRACE-based TWS**	Tapley et al. (2004); Landerer et al. (2020)					■							

Institution	*Model/product name*	*Key reference*	*Streamflow*	*Reservoirs*	*Soil moisture*	*Actual evapotranspiration*	*Terrestrial water storage (TWS)*	*Snow and ice*	*Lakes*	*Glaciers*	*Groundwater*	*Water quality*	*Water surface elevation*	*Precipitation*
Models and space-based observation datasets														
Environment and Climate Change Canada	**Multi-source daily snow water equivalent (SWE) including Crocus-ERA5 and ERA5-Land**	Mudryk et al. (2025) and (2026)						■						
University of Stuttgart	**The Remote-Sensing-based Extension for the GRDC (RSEG) dataset, the Satellite Altimetry-based Extension of global-scale in situ river discharge Measurements (SAEM) dataset and the Surface Water and Ocean Topography (SWOT) water surface elevation (WSE)-based discharge**	Elmi et al. (2024); Saemian et al. (2025); Saemian et al. (2026)	■											

Institution	*Model/product name*	*Key reference*	*Streamflow*	*Reservoirs*	*Soil moisture*	*Actual evapotranspiration*	*Terrestrial water storage (TWS)*	*Snow and ice*	*Lakes*	*Glaciers*	*Groundwater*	*Water quality*	*Water surface elevation*	*Precipitation*
Models and space-based observation datasets														
Texas A&M University (TAMU)	**Storage anomalies based on OPERA DSWx Level 3 product and Area/Volume/Water Surface Elevation (A/V/E) curves from Li et al. (2023)**	Li. et al. (2023); OPERA (2023); Yadav et al. (2025)		■										
National Aeronautics and Space Administration (NASA)	**SWOT**	Getirana et al. (2024), Getirana et al. (2026)											■	
Helmholtz Centre for Environmental Research – UFZ	**Dynamic Empirical River Temperature Model (DyER-TM)**	Mohseni and Stefan (1999); Jones et al. (2025)										■		
International Institute for Applied Systems Analysis (IIASA); Vrije Universiteit Brussel (VUB)	**Community Soil Water Assessment Tool-Water Quality (CoSWAT-WQ)**	Nkwasa et al. (2025); Chawanda et al. (2025)										■		
Utrecht University (Netherlands)	**The dynamical surface water quality model**	Jones et al. (2023)										■		

VARIABLE RANKING (ANOMALY CALCULATION)

To provide a coherent picture across the different datasets, a consistent method of variable ranking was applied to the variables listed in Table A.1, except for glaciers, where winter and summer balances are provided. Annual averages were calculated for each year for modelled and observed datasets over the given reference period. The resulting array was ranked. The annual average of the given variable for the year 2025 was then compared to this ranked array and classified according to the following rule:

much below normal: $Q_{2025} \leq$ 10th percentile (exceptionally dry)

below normal: 10th $< Q_{2025} <$ 25th percentile

normal: 25th $\leq Q_{2025} \leq$ 75th percentile

above normal: 75th $< Q_{2025} <$ 90th percentile

much above normal: $Q_{2025} \geq$ 90th percentile (exceptionally wet)

The historical reference period varied according to the variable in question, constrained by the data availability. Refer to Table A.2 for selected historical reference periods and to dataset-specific chapters of the main report for more details.

For the modelled data, where several data sources (ensembles of models) have been used, the averaging of the variable ranking results was done at the basin level. For each model in the ensemble, the above-specified rankings were assigned an integer ("much below normal" = 1, "below normal" = 2, "normal" = 3, "above normal" = 4, "much above normal" = 5), and then an average was calculated across the outputs of the ensemble of models for each of the basins. The resulting number was rounded, and the average discharge ranking was derived for each basin, according to the thresholds listed above.

Table A.2. Historical reference periods of selected datasets

Dataset	*Selected historical reference period*	*Length of historical reference period*
Precipitation	2002–2022	21 years
Extreme precipitation	1991–2020	30 years
Drought Index	1961–1990	30 years
Simulated river discharge from GHMSs	1991–2020	30 years
Observed river discharge from GRDC and NMHSs	Beginning between 1991 and 2001 (varies between NMHSs) and ending in 2020	Varies between 20 and 30 years
Inflow into reservoirs	1991–2020	30 years
Reservoir storage	1999–2018	20 years
Lake level	1995–2020	26 years

Dataset	*Selected historical reference period*	*Length of historical reference period*
Lake temperature	1995–2020	26 years
Lake ice cover duration	1995–2020	26 years
Groundwater level	2001–2020	20 years[a]
Evapotranspiration	1991–2020	30 years
Soil moisture	1991–2020	30 years
Soil moisture observed	2009–2023	15 years
Snow water equivalent	1991–2020	30 years
Glaciers	1976–2024	49 years
Terrestrial water storage	2002–2020	19 years
Water quality	2012–2023	12 years
Water surface elevation	2024	-

[a] 2015–2024 for Benin, Brazil, Colombia, Costa Rica, El Salvador, Georgia, Greece, Ireland, Kenya, Luxembourg, Qatar, Senegal, Thailand and the Gambia

GLOBAL HYDROLOGICAL MODELLING SYSTEMS

The *State of Global Water Resources 2025* report uses GHMSs sourced from the modelling community. Despite improved availability, observed discharge data were not sufficient to ensure a comprehensive global overview, resulting in the need for an alternative source for discharge data. The simulated discharge produced by multiple GHMSs was analysed using the sub-basin map obtained after processing the level 4 HydroBASINS dataset (Figure A.1).

In total, 13 GHMSs were used in the modelling exercise (in alphabetical order):

- CaMa-Flood with Dam (Hanazaki et al., 2022; Yamazaki et al., 2011)
- Conjunctive Surface–Subsurface Process version 3 (CSSPv3) (Yuan et al., 2026)
- DHI-GHM (Murray et al., 2023)
- ECLand (Boussetta et al., 2021)
- Global Flood Awareness System (GloFAS) (Alfieri et al., 2013; Grimaldi et al., 2023)
- HBV-PML (Huang et al., 2022; Zhang et al., 2019)
- mesoscale Hydrologic Model (mHM) (Kumar et al., 2013; Samaniego et al., 2010, 2019; Shrestha et al., 2025)

- PCR-GLOBWB 2 (Sutanudjaja et al., 2018)
- River Forecast System (GEOGLOWS) (Hales et al., 2022)
- Today's Earth – Global (JRA-55) (Yoshimura et al., 2008; Ma et al., 2024)
- WaterGAP 2.3 (Nyenah et al., 2026)
- World-Wide HYPE v1.3.9 (Arheimer et al., 2020)
- Wflow_sbm (Eilander et al., 2021; Imhoff et al., 2020; Verseveld et al., 2024)

The global hydrological modelling community was asked to provide historical simulations for the chosen 986 basins for the years 1991–2020 and the target year of 2025, using meteorological input data of their choice. Before submitting the outputs, the modelling teams were required to complete a modelling "fact sheet" to provide key information about the model, technical details and input data sources. An ensemble of models was used to address potential uncertainties in the simulations. The 2025 data were ranked for the simulated discharge and other variables (refer to Table A.1) from each model for each basin, then averaged across all models for each basin (refer to the Variable ranking (anomaly calculation) section for more details). GHMS simulations are subject to uncertainties, largely due to three factors: uneven data coverage and quality across regions and variables; insufficient measurement of human impacts on the water cycle; and difficulties in adapting processes to diverse regional hydrological systems (Reinecke et al., 2025).

Table A.3 shows a technical breakdown of the various GHMSs, and the Validation of modelled results section summarizes the models' spatial coverage and provides a graphical representation of trends simulated by each model for each basin. Regarding climate forcing, all GHMSs used ERA5 reanalysis data (Hersbach et al., 2020), except for the HBV-PML, World-Wide HYPE v1.3.9 and Today's Earth – Global (JRA-55) models, which were driven by the Multi-source Weighted-ensemble Precipitation (MSWEP) (Beck et al., 2019), Hydrological Global Forcing Data (HydroGFD) (Berg et al., 2021) and JRA-55 datasets (Kobayashi, 2015), respectively.

PRECIPITATION

The Global Precipitation Climatology Centre (GPCC) provides global precipitation analyses to support climate monitoring and research. It represents a contribution by Germany to the World Climate Research Programme (WCRP) and the Global Climate Observing System (GCOS). GPCC provides a gridded (1° resolution) monthly precipitation dataset, available from 1891 to the present, that is produced from quality-controlled, global station data.

The key objective of the EUMETSAT Satellite Application Facility on Climate Monitoring (CM SAF) is the generation and release of satellite-based products related to the Earth's energy budget and water cycle. CM SAF provides, among others, a global satellite-based precipitation data record called GIRAFE (Global Interpolated RAinFall Estimation) to support climate monitoring, climate analysis, model evaluation and climate services. Data from microwave sounders and imagers onboard polar orbiting satellites are merged with geostationary infrared observations. The data are available on a regular longitude/latitude grid with 1° spatial resolution and as daily accumulations and monthly means, with uncertainty characterized daily accumulations. GIRAFE covers the period January 2002 to the present day. More details are available in Konrad et al. (2025)

Table A.3. Characteristics of GHMSs used in the report

Model name	*Institution*	*Spatial coverage*	*Spatial model resolution*	*Climate data product used*
WaterGAP 2.3	Goethe University Frankfurt, Johannes Gutenberg University Mainz	Global	0.5° × 0.5°	Global Soil Wetness Project Phase 3 (GSWP3)-ERA5
Conjunctive Surface–Subsurface Process version 3 (CSSPv3)	Institute of Atmospheric Physics (Chinese Academy of Sciences)	Global	0.25°	ERA5, with precipitation replaced by MSWEPv2
mesoscale Hydrologic Model (mHM)	Helmholtz Centre for Environmental Research – UFZ	Two set-ups available: (1) Global; (2) Individually delineated and calibrated GRDC basins.	Last version was based on the 0.25° resolution	ERA5
World-Wide HYPE (WWH) version 1.3.9	Swedish Meteorological and Hydrological Institute (SMHI)	All continents except Antarctica	On average 1 000 km^2	HydroGFD
DHI-GHM	DHI	The model covers land surface of the globe between 60°S and 80°N	0.1° × 0.1°	ERA5
CaMa-Flood with Dam	University of Tokyo	60°S–90°N, 180°W–180°E (without Greenland)	0.25° lat./lon. deg.	ERA5-land runoff
Global Flood Awareness System (GloFAS)	European Commission Joint Research Centre (JRC)	Global except for Antarctica (60°S–90°N, 180°W–180°E)	0.05° (~5 km, gridded)	ERA5

Model name	*Institution*	*Spatial coverage*	*Spatial model resolution*	*Climate data product used*
River Forecast System	GEOGLOWS	Global	Irregular grid, ~150 km^2	ERA5
Wflow_sbm	Deltares	Global for reservoirs. Europe for hydrological model states and fluxes.	30 arcsec (0.0083° ~1 km)	ERA5, with precipitation replaced by MSWEPv2
ECLand	European Centre for Medium-Range Weather Forecasts (ECMWF)	Global	6 arcmin (~10 km)	ERA5
HBV-PML	Institute of Geographic Sciences and Natural Resources Research (Chinese Academy of Sciences)	Global	0.1° × 0.1°	MSWEP
PCR-GLOBWB 2	Utrecht University	Global	5 arcmin (10 km at the Equator)	ERA5 land, with precipitation correct to W5E5
Today's Earth-Global (TEJRA55)	The University of Tokyo/Japan Aerospace Exploration Agency	60°S–90°N, 180°W–180°E (without Greenland)	0.25° lat/lon deg.	JRA-55

DROUGHT INDEX

The Global Precipitation Climatology Centre Drought Index (GPCC-DI) (Ziese et al., 2014; Schneider et al., 2014) is presented in Figure A.2. The GPCC-DI is a combination of two drought indices – the Standardized Precipitation Index (SPI) and the Standardized Precipitation Evapotranspiration Index (SPEI) – and uses temperature and precipitation for the calculation of drought conditions. The combination of the two indices allows for an improved assessment of drought conditions at the global scale. Indeed, the SPEI performs better in dry, warm regions, whereas the SPI cannot be applied in such regions. The SPI is applicable in cold regions, where calculation of evapotranspiration is problematic. Still, dry and cold regions like the Tibetan Plateau and southern Andes cannot be covered by either index and are, therefore, left blank. The combined index is calculated on a regular grid with 1° spatial resolution with respect to the reference period of 1961–1990.

Drought conditions prevailed across northern Africa and along the Mediterranean coast during MAM, JJA and SON. In the Middle East, drought conditions developed during MAM and JJA and eased in SON, except over the Arabian Peninsula, where they persisted. In South America, parts of the Amazon basin were affected by drought conditions from JJA through SON. The Iberian Peninsula experienced moderate drought conditions during JJA.

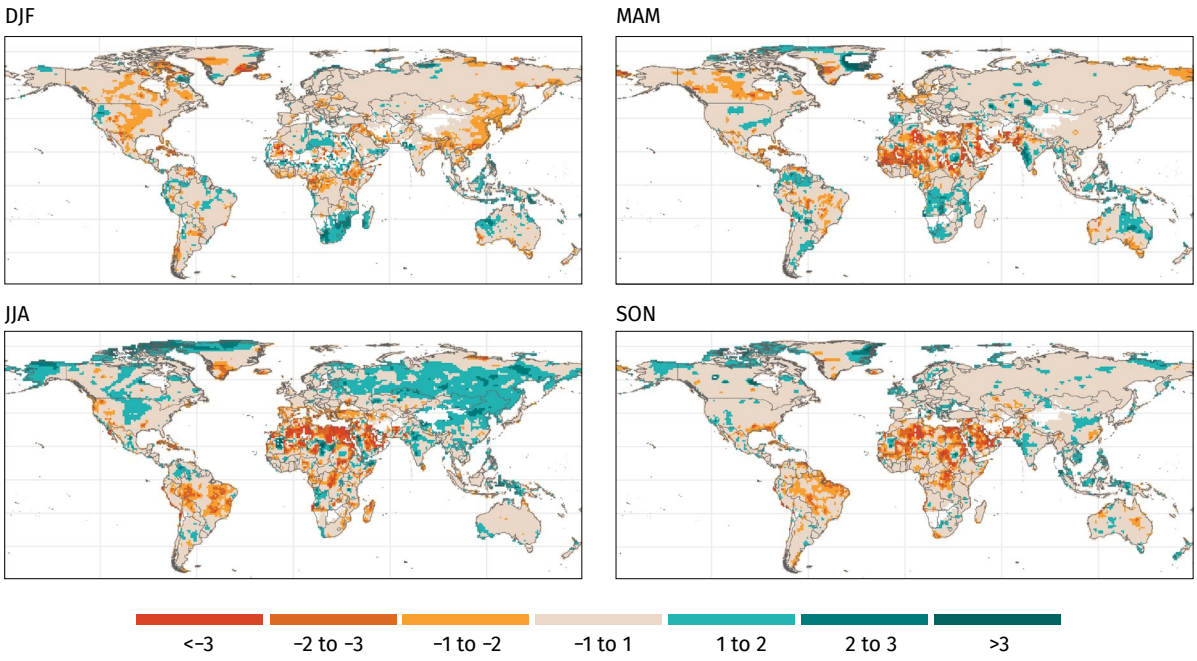


Figure A.2. GPCC-DI in 2025, with respect to the 1961–1990 reference period, over four seasons (DJF = December 2024, January, February; JJA = June, July, August; MAM = March, April, May; SON = September, October, November). Beige indicates normal precipitation, green shades indicate wetter-than-normal conditions and orange–red shades indicate drier-than-normal conditions.

Note: The boundaries and names shown and the designations used do not imply official endorsement or acceptance by WMO or the United Nations.

RIVER DISCHARGE

Observed data and validation of modelled results

Discharge data availability in Global Runoff Data Centre and from National Meteorological and Hydrological Services for the year 2025

Observed discharge data were received from NMHSs and GRDC (see GRDC Data Portal). Two selection criteria for the data were adopted: the number of missing values among the data points within the historical reference period had to be 10% or less, and for 2025 the data had to at least cover the 2025 hydrological year (until 31 October 2025). Similarly to last year, datasets not yet subjected to quality checks were included (in 2025, data from Austria, Canada, Croatia, Luxembourg, Poland, Serbia, Slovenia, Slovakia, Switzerland and the United Kingdom of Great Britain and Northern Ireland). NMHSs were also able to supply calculated anomalies.

Observational data were collected from 3 115 stations for the year 2025 from the GRDC database and NMHSs. Additionally, data from 509 stations were sourced from the Earth system-based infilled discharge product from space-based observations (Elmi et al., 2024; Saemian et al., 2025). The rationale for using space-based observation methods to infill data is as follows: the number of active GRDC river gauge stations has declined since the 1980s. However, the rise of space-based observation technologies offers possibilities to estimate river discharge from space. See more details below, in the Discharge data from space-based observations section.

The total pool of 3 624 stations was used for evaluating the 2025 discharge anomaly (Figure A.3, blue dots). A subset of 266 stations was identified for validating the GHMS results (Figure A.3, red dots), based on their proximity to the chosen HydroBASIN outlet, ensuring a closer match between the observed and modelled data. Given the spatial resolution of HydroBASINS outlets in the UK, an aggregated national UK outflow series was used to validate modelled outputs (Marsh et al., 2015), with the red dot being representative of this series and not reflecting the outlet of a gauged catchment.

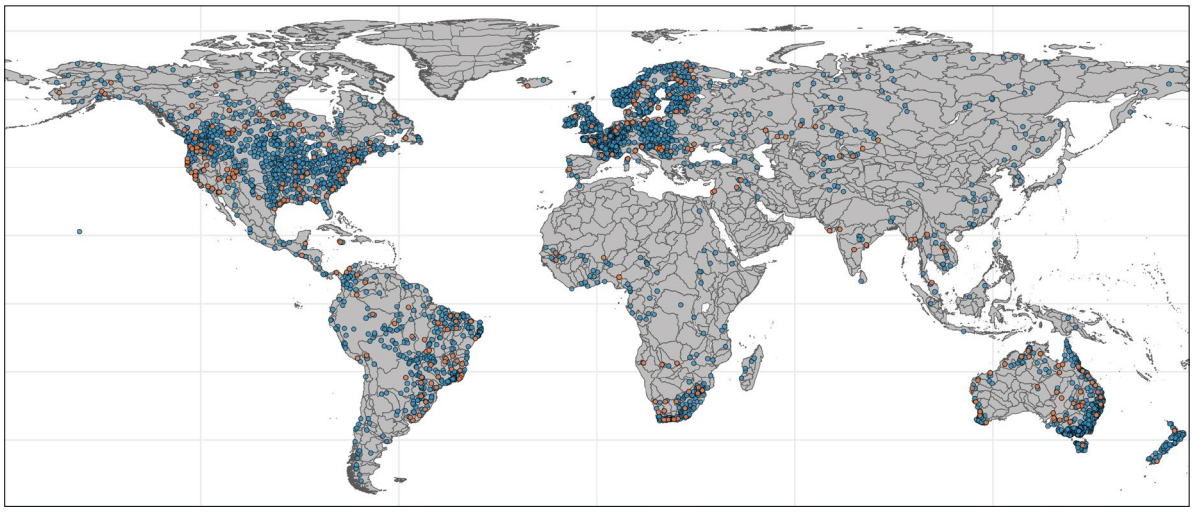


Figure A.3. Location of gauges with observed data used in this report, received from NMHSs and obtained from the GRDC database and from the discharge extension dataset from space-based observations (RSEG, SAEM and SWOT WSE-based discharge). Gauges selected to validate GHMSs are indicated by red dots.

Note: The boundaries and names shown and the designations used do not imply official endorsement or acceptance by WMO or the United Nations.

Note that the ranking of the streamflow for 2025, estimated from the ensemble of GHMSs, might differ from the results obtained from the observed streamflow data, depending on the catchment area of the observed data and model performance. Therefore, WMO emphasizes the importance of the availability of local in situ data to support water resource management and the production of hydrological status products at the regional, national and basin scales, as well as for producing accurate global products such as the assessments presented in the present report.

Discharge data from space-based observations

The number of active GRDC river gauge stations has declined since the 1980s. However, the rise of space-based observation technologies has created new opportunities to estimate river discharge from space. Developing a mapping function between satellite-based river width/height and historical gauge data is among the most straightforward solutions to estimate discharge from space. Building on this idea, Elmi et al. (2024) and Saemian et al. (2025) developed the extension of the GRDC discharge records from space-based observations.

For this year's contribution, most of the water height estimates for the target year 2025 are obtained from the RiverSP product of the Surface Water and Ocean Topography (SWOT) mission. SWOT observations strengthen the discharge extension by providing higher-quality river water height observations than traditional nadir-looking satellite altimetry, while also improving temporal sampling for many stations. These advantages increase the availability and reliability of space-based discharge estimates, providing a stronger basis for analysing river discharge variability beyond the active gauge network.

To derive the anomaly class for each station in 2025, the historical discharge records were compiled from the RSEG and SAEM datasets. For the target year 2025, space-based discharge estimates were first aggregated to monthly mean discharge values, as the satellite observations are available at overpass epochs rather than as continuous daily records. Annual mean discharge was then calculated for both the historical reference period and the target year 2025.

The 2025 annual mean discharge at each station was ranked against the distribution of annual mean discharge values from the historical reference period. The corresponding percentile rank was then used to assign the anomaly class following the classification scheme, described in Variable ranking (anomaly calculation) section.

Validation of modelled results

The discharge rankings derived from GHMS simulations were validated against rankings obtained from available observed discharge data from NMHSs and the GRDC database. Annual mean flow observations for 2025 were ranked against the hydrological normals, calculated from at least 20 years of flow observations, for each HydroBASINS basin where observed flow data were available. The simulated and observed discharge rankings for 2025 were then grouped according to the direction of change relative to the historical reference period – below normal, above normal or normal (three categories) – and compared to assess agreement between the modelled and observed results.

Note that, for validation, a gauge closest to the sub-basin outlet and with the largest upstream catchment area was chosen. However, it was not possible at all locations to find a gauge located in close proximity to the outlet, and in large basins, where some of the downstream units import a considerable amount of water resources from the upstream catchments,

the comparison/validations between results from modelled data at the outlet and observations at the upstream gauge might lead to inaccurate results. Therefore, including observations from additional gauges or redefining the catchment areas must be considered in the future to minimize uncertainties in the results.

Figure A.4 presents the agreement among GHMSs on the river discharge anomalies for each basin (only three categories considered: below normal, above normal or normal), indicating percentage of models simulating the same anomaly category relative to the historical reference period. The results show that more than 50% of GHMSs agree on the sign of trends for 98% of the area globally. The agreement for Australia, South and North America, South Africa, Northern Europe and many other regions lies even higher – between 75% and 100% of the ensemble – while the agreement is lower (30%–50%) in West Africa and in some basins in China.

Figure A.5 presents river discharge anomalies for 2025 ranked against the historical period 1991–2020, using all gauges for which data were received from NMHSs and GRDC. Coloured basins show the anomaly for the selected station with the largest upstream catchment area within a basin, while dots mark the locations of the observational gauges, with their colour indicating the observed anomaly for 2025. Grey areas denote regions without available discharge data from NMHSs or GRDC in 2025.

Figure A.6 shows the validation of simulated discharge trends against observations for 2025 for selected gauges. While five classes were used to categorize the simulated anomalies, for validation purposes results were compared using only three aggregated labels: normal, above-normal and below-normal conditions (much above and much below normal are included within above normal and below normal, respectively). Areas where the simulated and observed classifications disagreed as to the direction of change (for example, one indicating above-normal and the other below-normal discharge) are highlighted with left slanting hatching.

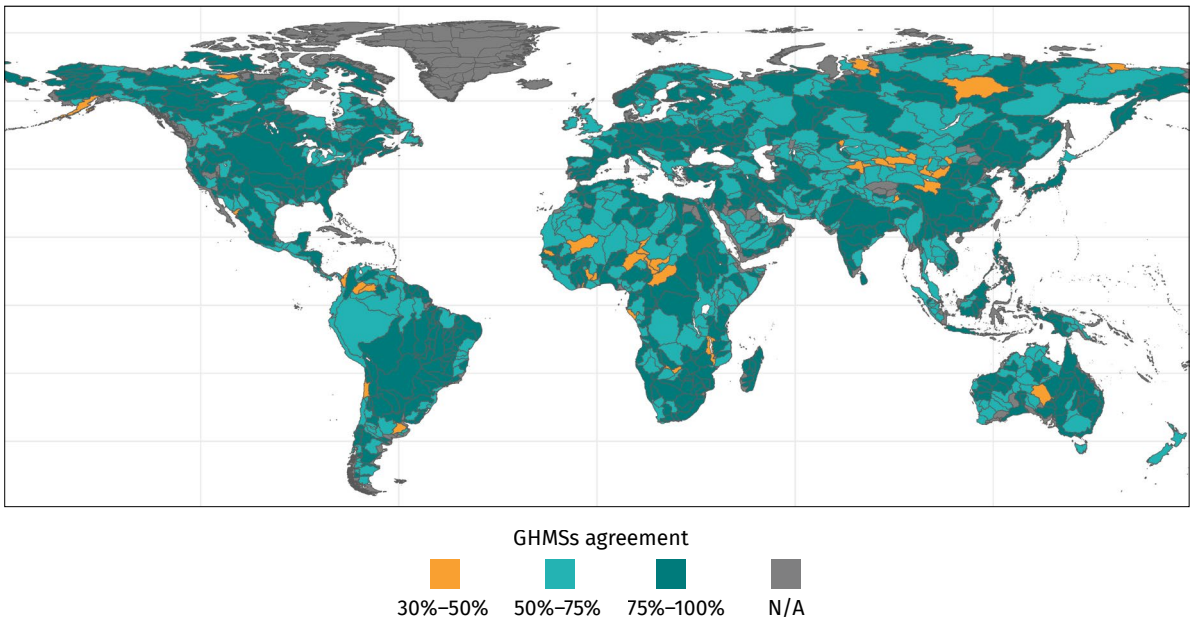


Figure A.4. Percentage of GHMSs agreeing on the annual river discharge with respect to mean (above, below, normal) for each basin

Note: The boundaries and names shown and the designations used do not imply official endorsement or acceptance by WMO or the United Nations.

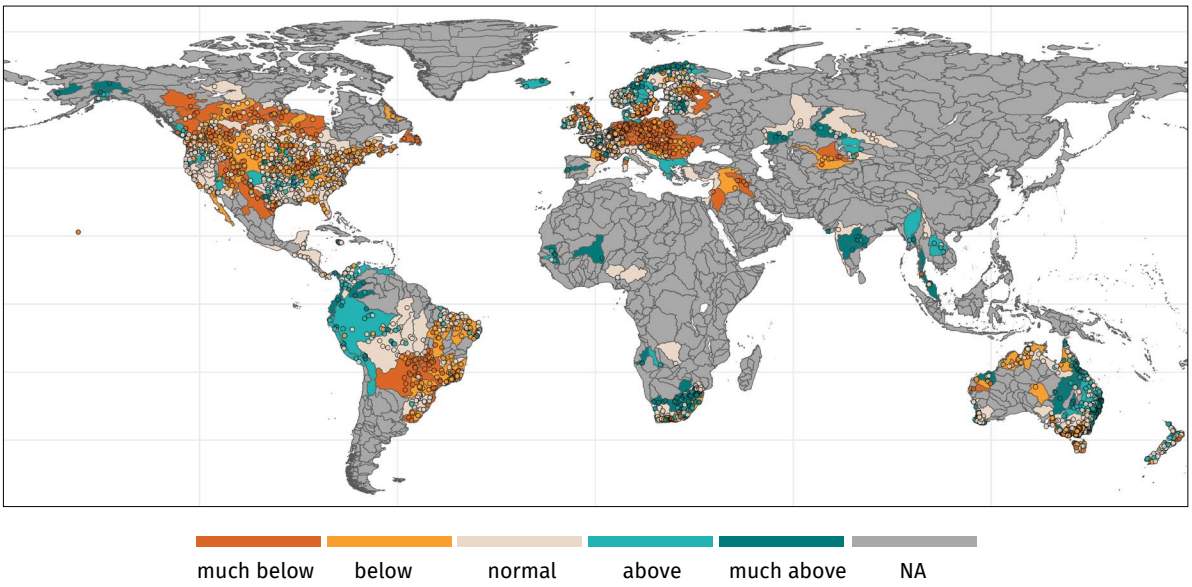


Figure A.5. River discharge in 2025 as ranked with respect to the historic period 1991–2020. The results presented here were derived from the observed discharge data, which were obtained from NMHSs and the GRDC database (basins are coloured according to the key). Dots represent the location of observed gauges for which data were received. Grey areas indicate areas where discharge data were not available from NMHSs or GRDC for 2025.

Note: The boundaries and names shown and the designations used do not imply official endorsement or acceptance by WMO or the United Nations.

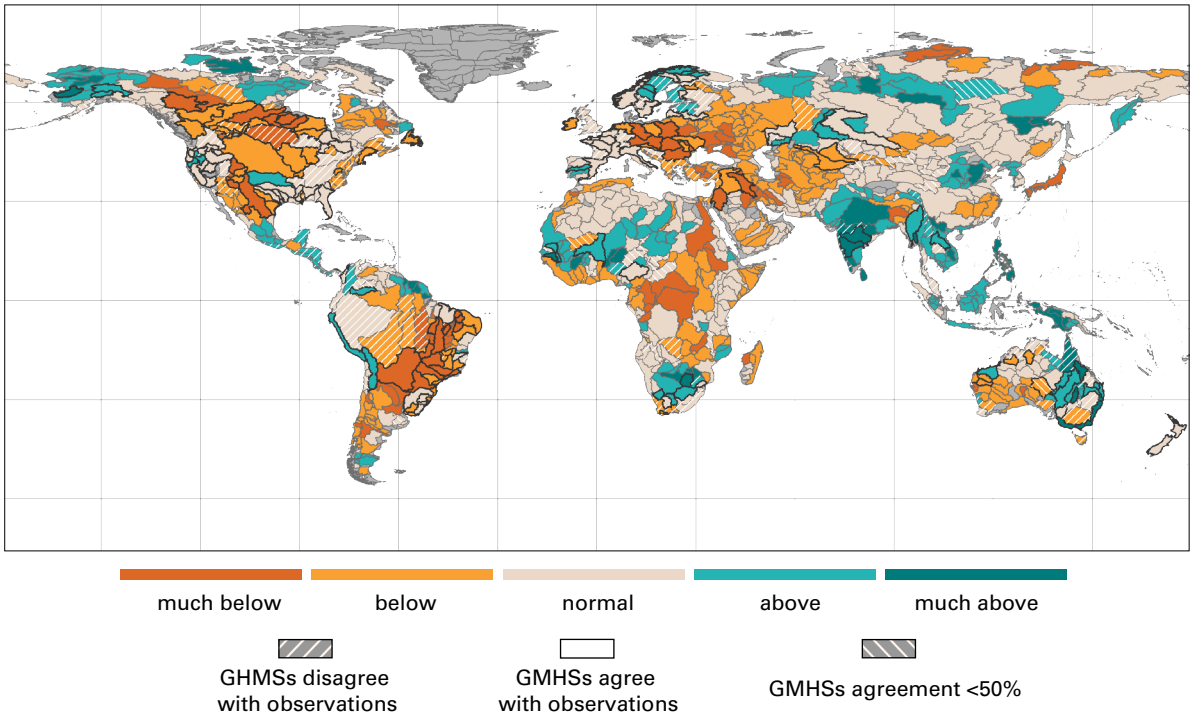


Figure A.6. Validation of modelled discharge from GHMSs for the year 2025. Basins where simulated and observed data agree on the hydrological condition are indicated by a black bold outline. Areas where GHMSs disagree with each other are marked with left slanting hatching, and areas where GHMSs disagree with observations are marked with right slanting hatching. Basins where GHMS agreement is below 50% and the multi-model mean disagrees with observations are indicated by both patterns overlapping (cross-hatching).

Note: The boundaries and names shown and the designations used do not imply official endorsement or acceptance by WMO or the United Nations.

The validation of modelled results showed agreement between observed and simulated anomalies for the year 2025 in Australia, in the eastern parts of South America (La Plata Basin), North America, parts of India (Godavari River) the Middle East, Kazakhstan, Myanmar, southern Africa and across Europe. At the same time, modelled anomalies disagreed with observations in parts of the eastern part of North America and northern part of South America (Amazon Basin), and in Queensland in Australia. In general, GHMS simulations align with observations in >63% of the basins where validation was carried out.

In some areas (for example, the UK and Ireland), there was a mismatch between the resolution of the models (catchments above 10 000 km^2 were selected for the analysis) and the observed datasets. The provision of a "national outflow" data series for the UK allowed for a simple validation of these model results, though this case underlines the importance of scale in small countries, and the need for better spatial representation of relevant catchments.

RESERVOIRS

Inflow into selected reservoirs

The modelled results for the inflow into 926 reservoirs globally were obtained from four main sources: (a) Wflow_sbm (Verseveld et al., 2024, Imhoff et al., 2024); (b) CaMa-Flood with Dam (Hanazaki et al., 2022; Yamazaki et al., 2011); (c) the WWH model (Arheimer et al., 2020); and (d) CSSPv3 (Yuan et al., 2026). The reservoirs were selected based on overlap between those four sources, based on their Global Reservoir and Dam Database (GRanD) ID (Lehner et al. 2011). Daily inflow into selected GRanD reservoirs was provided from 1991 to 2023.

(a) **Wflow_sbm:** Daily inflow and reservoir volumes were derived for the period 1991–2025 for the selected GRanD reservoirs. Simulations were conducted at 1/120° (~1 km) and were forced with downscaled MSWEPv3.16 for total precipitation, and downscaled ERA5 reanalysis for 2 m temperature and potential evaporation using de Bruin et al. (2016) formulation. The set-up of the Wflow_sbm models (using hydromt_1.3.0 and hydromt_wflow 1.0.1) was similar to that used by van der Laan et al. (2024), who validated reservoir simulations against Earth observed surface water area and in situ measured reservoir volume. For the anisotropy factor for lateral hydraulic conductivity, we used the random forest global results from Ali et al. (2025). The simulations (using wflow.jl 1.0.2) were carried out on an onsite linux cluster.

(b) **CaMa-Flood with Dam:** CaMa-Flood model (Yamazaki et al., 2011) along with the Dam operational scheme by Hanazaki et al. (2022) was implemented to conduct global simulations. The model can simulate river flows encompassing 2 169 global dams and reservoirs with a drainage area of at least 1 000 km^2. The information for each reservoir (such as the dam's name, coordinates, storage capacity and drainage area) in the model is based on GRanD (Lehner et al., 2011). The model configuration enables global simulations at a spatial resolution of 0.25° using MERIT Hydro (Yamazaki et al., 2019) as a baseline topography. The same model configuration settings, utilizing ERA5-Land reanalysis data (Muñoz Sabater, 2019) from 1991 to 2024 as a runoff forcing, have been used for the current global simulations. The temporal resolution of the model is 1 hour. However, given the reporting requirements, the outputs have been prepared at 24-hour intervals. Calibration of the model with the Dam operational scheme is unavailable. However, Hanazaki et al. (2022) conducted model validation based on simulations spanning 2001 to 2019. Validation for the model is accessible for the daily streamflow discharge of 687 gauges (located downstream of dams)

from GRDC and other institutions worldwide. The accuracy of discharge hydrographs compared to observations was evaluated by calculating Nash–Sutcliffe efficiency (NSE) (Nash and Sutcliffe, 1970) and peak discharge error (PDE). In addition to the 687 global gauges, validation is also available for inflow, outflow and storage of the Seminoe and Trinity reservoirs using in situ observation data.

(c) **World-Wide HYPE v1.3.9:** Daily inflow to GRanD reservoirs and daily reservoir volume have been delivered for the period 1991–2023. The World-Wide HYPE model was calibrated in a stepwise manner using 2 475 discharge gauges and evaluated against an additional 2 863 independent discharge gauges (Arheimer et al., 2020). The model includes around 13 000 lakes and 2 500 reservoirs. These are described in a general fashion based on information from the GRanD database. Except for a handful of places, the operating routines of the reservoirs have not yet been calibrated in WWH.

(d) **Conjunctive Surface–Subsurface Process version 3 (CSSPv3):** In CSSPv3, reservoir outflow is calculated based on current inflow, long-term average inflow and storage. The model further considers multiple beneficial functions such as hydropower, flood control and irrigation water supply.

Reservoir fullness

Recent storage estimates were derived from monthly reservoir surface areas estimated using the OPERA Level 3 Dynamic Surface Water Extent from Harmonized Landsat Sentinel-2 classified product (OPERA_L3_DSWX-HLS_V1; OPERA, 2023), after applying a cloud-correction algorithm adapted from Yadav et al. (2025). These surface-area estimates were then converted to storage using reservoir-specific area–volume–elevation relationships from Li et al. (2023), and the resulting storage estimates were compared against a historical reservoir storage climatology for 1999–2018.

For each reservoir, the 2025 annual storage estimate was calculated as the mean of valid monthly storage values. Months with more than 15% cloud-affected or ice-affected area were excluded. To avoid seasonal bias, the 2025 estimate was compared with historical annual values calculated using the same calendar months available in 2025. At least six valid months were required to assign an annual State of Water Resources status; reservoirs with fewer valid months were retained in the file but flagged as having insufficient observations.

The fullness metric indicates whether recent reservoir storage was above, below or near historical conditions. It is calculated as the difference between recent mean storage and historical mean storage, normalized by the reservoir's typical historical seasonal storage range, with safeguards to avoid instability for reservoirs with very small variability or storage. Positive values indicate storage above the historical mean, while negative values indicate storage below the historical mean. Values greater than 0.1 are classified as above historical climatology, values below –0.1 as below historical climatology, and values between –0.1 and 0.1 as near historical climatology. Figure A.7 presents reservoirs' fullness anomaly for the year 2025.

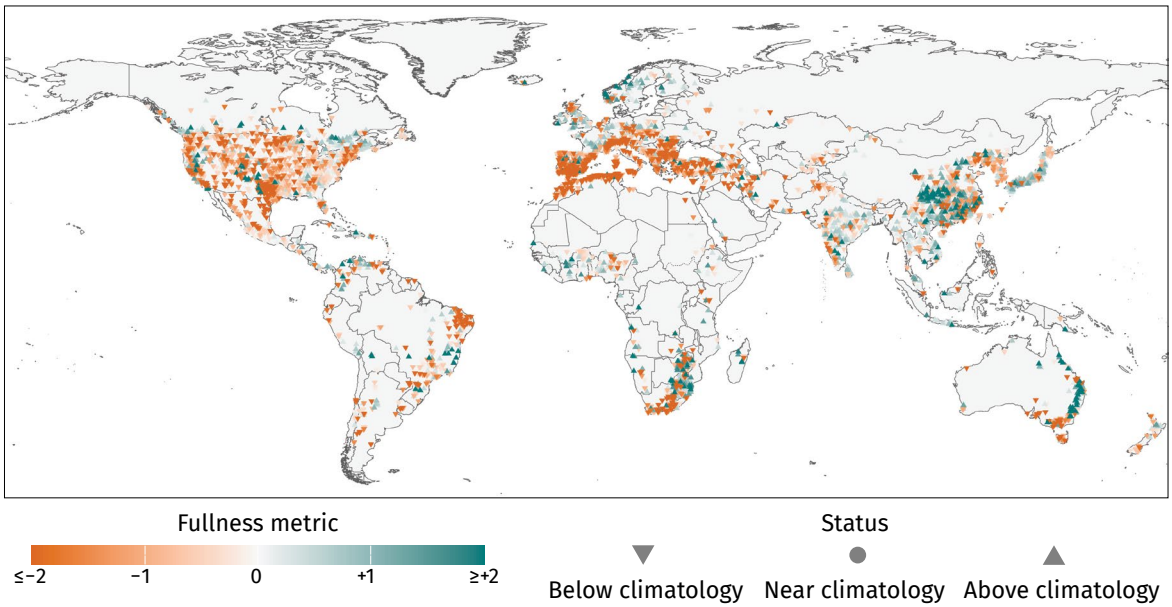


Figure A.7. Reservoirs' fullness anomaly in 2025 with respect to the historical period of 1999–2018

Note: The boundaries and names shown and the designations used do not imply official endorsement or acceptance by WMO or the United Nations.

GROUNDWATER

The methodology used to report on groundwater levels was developed and consolidated in 2023. It is described in a methodology report published in February 2024, which is available in the IGRAC GitHub repository.

Data collection and selection

Groundwater level monitoring data were collected from 51 countries. The data were downloaded from the websites of the institutions in charge of groundwater monitoring, where available. Data were otherwise requested. Table A.4 indicates how the data were collected for each country. Where data are open or permission has been given to share the raw data, it is made available for downloading on the Global Groundwater Monitoring Network (GGMN) platform.

Groundwater level data were resampled to monthly resolution. Each time series was divided into 12 monthly sub-series, which were ranked by data availability and processed sequentially. Monthly sub-series meeting the predefined gap threshold (80%) were retained for analysis, which means that the time series that are selected have data for at least 16 years out of 20. Only in the case of Lesotho, Senegal and the Gambia, the threshold was lowered to 60% to accommodate for the data gaps. This approach allowed time series with as few as one measurement per year to be included, provided measurements were taken in the same month(s) each year, to avoid inconsistent time series with measurements taken during different seasons.

The maps in Figure A.8 show point (station wise) data for groundwater collected from 51 countries.

Table A.4. Groundwater data sources

#	Country		Data source	Link
1	Australia		Requested	Bureau of Meteorology (BOM)
2	Austria*		Downloaded	https://ehyd.gv.at/#
3	Belgium	Brussels	Downloaded	https://geodata.environnement.brussels/client/bruwater/index
		Wallonia	Downloaded	https://piezometrie.wallonie.be/home.html
		Flanders	Downloaded	https://www.dov.vlaanderen.be/portaal/
4	Benin		Requested	Directorate General of Water (DGEau)/Benin
5	Brazil		Requested	Geological Survey of Brazil (SGB)
6	Canada		Requested	Natural Resources Canada (NRCan)
7	Chile		Requested	General Directorate of Water (DGA)
8	Colombia		Requested	Sub-Directorate of Water and Soil Resources, District Secretariat of the Environment
9	Costa Rica		Requested	Ministry of Environment and Energy, Department of Water Development
10	Croatia		Requested	Hrvatske vode (Croatian Water)
11	Cuba		Requested	National Institute of Hydraulic Resources (INRH)
12	Czechia		Requested	Czech Hydrometeorological Institute
13	Denmark		Downloaded	https://data.geus.dk/JupiterWWW/
14	El Salvador		Requested	Ministry of Environment
15	Estonia*		Requested	Geological Survey of Estonia
16	Finland		Requested	Finnish Environment Institute (SYKE)
17	France*		Downloaded	https://ades.eaufrance.fr/Spip?p=
18	Gambia (the)		Requested	Department of Water Resources
19	Georgia		Requested	Department of Geology, National Environmental Agency (NEA)
20	Germany†		Downloaded	https://gruvo.bgr.de/website/fss
21	Greece		Requested	Hydrogeology Department, Hellenic Survey of Geology and Mineral Exploration (HSGME)
22	Hungary		Requested	Hungarian Hydrological Forecasting Service
23	India		Requested	India Water Resources Information System (WRIS)
24	Ireland*		Downloaded	https://www.epa.ie/
25	Israel		Requested	Hydrological Service
26	Jamaica		Requested	Water Resources Authority
27	Jordan		Requested	Ministry of Water and Irrigation
28	Kenya		Requested	Water Resources Authority (WRA)
29	Latvia		Downloaded	https://videscentrs.lvgmc.lv/noverojumu-arhivs/pazemes/

#	Country	Data source	Link
30	Lesotho	Requested	Department of Water Affairs, Ministry of Natural Resources
31	Lithuania	Requested	Lithuanian Geological Survey
32	Luxembourg	Requested	Water Management Administration
33	Mexico	Downloaded	National Water Commission (CONAGUA)
34	Namibia	Requested	Ministry of Agriculture, Fisheries, Water and Land Reform, Department of Water Affairs, Geohydrology Division
35	Netherlands (Kingdom of the)*	Downloaded	https://service.pdok.nl/bzk/bro-gminsamenhang-karakteristieken/atom/bro_grondwatermonitoring_gm_in_samenhang_karakteristieken.xml
36	New Zealand	Requested	Earth Sciences New Zealand
37	Norway*	Downloaded	https://www.nve.no/english/
38	Poland	Downloaded	https://www.pgi.gov.pl/psh/materialy-informacyjne-psh/
39	Portugal	Downloaded	https://snirh.apambiente.pt/
40	Qatar	Requested	Water Operation & Control Department
41	Senegal	Requested	Directorate of Water Resources Management and Planning (DGPRE), Ministry of Water and Sanitation (MEA)
42	Serbia	Requested	Republic Hydrometeorological Service of Serbia
43	Slovakia	Requested	Slovak Hydrometeorological Institute
44	Slovenia	Requested	Slovenian Environment Agency (ARSO), Ministry of the Environment and Spatial Planning
45	South Africa	Requested	Department of Water and Sanitation (DWS)
46	Republic of Korea	Requested	Ministry of Environment, K-water
47	Sweden*	Downloaded	https://www.sgu.se/grundvatten/grundvattennivaer/matstationer/
48	Switzerland	Requested	Swiss Federal Office for the Environment (FOEN)
49	Thailand	Requested	Department of Groundwater Resources (DGR)
50	United Kingdom	Requested	British Geological Survey (BGS)
51	United States of America*	Downloaded	https://www.usgs.gov/apps/ngwmn/index.jsp

* Groundwater level database is connected to Global Groundwater Monitoring Network (GGMN) - IGRAC through an API.

† The website identifies reference monitoring stations in the country and provides the links to the States' websites where the data can be downloaded.

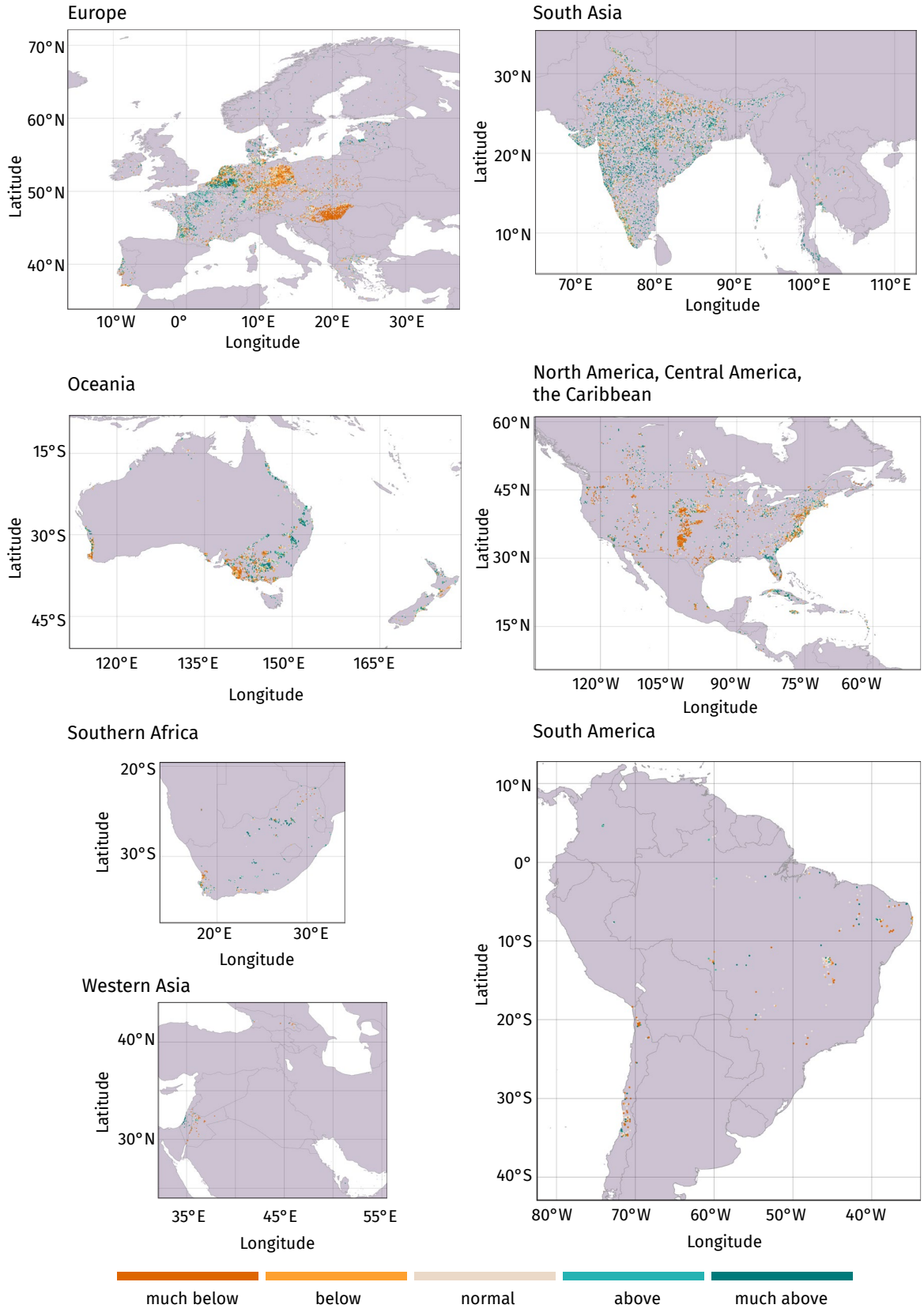


Figure A.8. Mean groundwater levels per station in 2025 as compared with the historical 2001–2020 reference period (2015–2024 for Benin, Brazil, Colombia, Costa Rica, El Salvador, Georgia, Greece, Ireland, Kenya, Luxembourg, Qatar, Senegal, Thailand, and the Gambia)

Note: The boundaries and names shown and the designations used do not imply official endorsement or acceptance by WMO or the United Nations.

Results visualization

The analysis results for groundwater levels are mapped at both monitoring station and grid levels (0.5° grid cells). For the grid-level visualization, the rankings of groundwater levels in individual wells were averaged within each corresponding grid cell, after which each grid was categorized based on the same classification scheme. While the grid-level maps are included in the main content of the report, the station-level maps are presented in Figure A.8 to provide additional details.

Regarding the station-level mapping, several boreholes are located at the same site, to monitor different aquifers at various depths. To provide a clear representation of overlapping boreholes, a GIS tool called “displacement tool” was used. This tool slightly offsets overlapping points, positioning them next to each other, as shown in Figure A.9. In the first example, on the left-hand side of Figure A.9, three different boreholes are at the same location: the average groundwater level in 2025 is normal in two of them, and above normal in the third one. In the second example, on the right-hand side of Figure A.9, two boreholes are at the same location: the average groundwater level in 2025 is below normal in both of them.



Figure A.9. Representation of overlapping boreholes

SOIL MOISTURE MODELLED

The anomaly in surface soil moisture in 2025, presented in Figure A.10 for December–February and June–August, was obtained from three GHMSs: Conjunctive Surface–Subsurface Process version 3 (CSSPv3) (Yuan et al., 2026); mesoscale Hydrologic Model (mHM) (Kumar et al., 2013; Samaniego et al., 2010, 2019); and Wflow-sbm (Eilander et al., 2021; Imhoff et al., 2020; Verseveld et al., 2024). It was then compared with the modelled historical period 1991–2020 on a monthly basis to understand root zone soil moisture patterns (at 1 m depth). The anomaly calculation used was the same as for river discharge and reservoir inflow (as per Box 2 in the Anomaly calculation section of the main report).

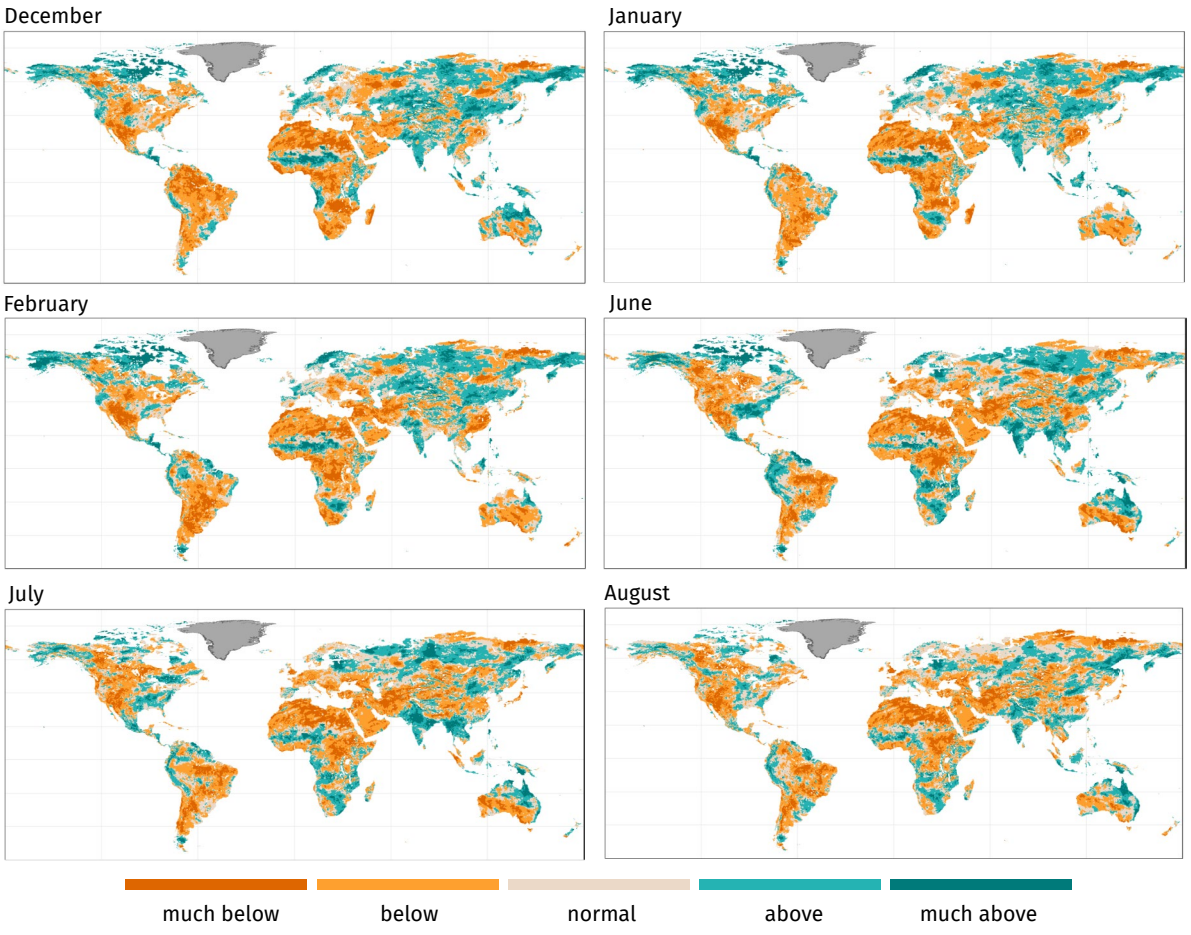


Figure A.10. Monthly root zone soil moisture conditions in 2025 (December 2024–February 2025 and June–August 2025) expressed as anomalies compared with the 1991–2020 reference period obtained from GHMSs. Greenland is masked in accordance with Global Land Ice Measurements from Space (GLIMS).

Note: The boundaries and names shown and the designations used do not imply official endorsement or acceptance by WMO or the United Nations.

SNOW WATER EQUIVALENT

To produce daily snow mass time series, daily SWE output from the Crocus-ERA5 snow model (Decharme and Barbu, 2024) and ERA5-Land model output (Muñoz Sabater, 2019) were aggregated over a given land region to produce a daily snow mass time series. For each of the two products, peak snow mass values were calculated for each hydrological year, and the resulting series of values were used to calculate 2025 percentiles relative to the 1991–2020 reference period. The two sets of percentiles were averaged together in presented results.

Ensemble mean March SWE fields over the 1991–2020 period were calculated using data from four individual gridded products:

- The European Space Agency Snow Climate Change Initiative (CCI) SWE version 2 product, derived through a combination of satellite passive microwave brightness temperatures and climate station snow depth observations (Luojus et al., 2022);
- The Modern-Era Retrospective Analysis for Research and Applications version 2 (MERRA-2) (GMAO, 2015) daily SWE fields;
- SWE output from the ERA5-Land analysis (Muñoz Sabater, 2019);
- The physical snowpack model Crocus (Decharme and Barbu, 2024) driven by ERA5 meteorological forcing.

March mean fields from each product were regridded to a common 0.5° × 0.5° regular grid and averaged together. This is the same suite of products used to produce annually updated SWE data for the *Arctic Report Card* (see, for example, Mudryk et al., 2025) and the Bulletin of the American Meteorological Society (BAMS) *State of the Climate Report* (see, for example, Mudryk et al., 2026). March 2025 SWE values were converted to percentiles using the 1991–2020 reference period on a pixel-wise basis.

TERRESTRIAL WATER STORAGE

Satellite gravimetry is the only space-based observation method capable of observing the whole water column, including surface water, soil moisture, groundwater, and snow and ice. The *State of Global Water Resources 2025* report presents an analysis of the terrestrial water storage (TWS) anomaly between the years 2002 and 2025, observed with the Gravity Recovery and Climate Experiment (GRACE) mission (2002–2017) and its successor, GRACE-Follow-On (GRACE-FO) (since 2018) (Landerer et al., 2020; Tapley et al., 2019). GRACE and GRACE-FO provide the TWS anomaly compared with the baseline of 2002–2020.

The TWS anomaly in equivalent water heights in centimetres was calculated according to Equation 1:

$$TWS_{\text{anomaly}} = TWS_t - \bar{X} \quad (1)$$

where TWS_t (cm) is the TWS value at month t of the current year and $\bar{X}$ is the long-term average TWS (cm), as calculated for 2002–2020. Equivalent water height is the theoretical mean height of the water column over the whole area being considered.

TWS for the year 2025 was ranked using similar methods as for discharge. However, the time series of TWS is too short (19 years) to perform ranking on the yearly values; therefore, the index for each month was computed and then aggregated to the yearly mean values.

For each grid point and month, the TWS value was ranked in relation to the baseline values (2002–2020). Next, these monthly percentile values were aggregated to yearly mean values. The yearly percentile rank was then used to assign the anomaly class following the classification scheme described in the Variable ranking (anomaly calculation) section.

GLACIERS

The present assessment of global glacier mass loss is based on a combination of glaciological field measurements (~500 glaciers or 1% of global glaciers) and geodetic satellite measurements (>200 000 glaciers or 96% of global glaciers) derived from the Fluctuations of Glaciers (FoG) database compiled by the World Glacier Monitoring Service (Dussaillant et al., 2025; WGMS, 2026). Winter and summer regional balances are calculated by downscaling the annual values using seasonal observations from FoG and the sine function analytical model proposed by Zemp and Welty (2023). Seasonal and annual balances follow the hydrological year, which is not the same for the northern hemisphere (NH), the southern hemisphere (SH) and the tropical (low-latitude) regions. A hydrological year cycle starts at the beginning of winter, finishes at the end of summer and is given the name of the year at the end of the cycle. For the NH, we assumed that winter lasts from October to March and summer from April to September. For the SH, we assumed that winter lasts from April to September and summer from October to March. For the low latitudes, we assumed no seasonality and, hence, plotted the annual values only. Regional winter and summer seasonal estimates are representative of the regional hydrological cycles. Therefore, seasonal balance bars are plotted with respect to their time of occurrence. On the other hand, because winter and summer occur at a different time globally, the global winter and summer seasonal estimates correspond to global hydrological years, with winter and summer global balance bars corresponding to the sum of winter and summer balances in the NH and SH regions, respectively.

We estimate the seasonal mass change for each region and year with at least one available measurement of seasonal mass change. Globally and in most regions, glaciers were near equilibrium during the 1970s and 1980s. The extraordinary rates of mass loss since the 1990s result from the compound effect of greater summer mass loss and reduced winter accumulation (Figure 24 in the main report). However, the presented seasonal mass changes are prone to high uncertainty, as they assume that the seasonal mass change amplitude measured at one or a few glaciers is representative of the entire region. This is particularly problematic in understudied regions that span multiple climate regimes (such as the southern Andes, Alaska, North Asia). Future assessments could more robustly scale limited local observations to whole regions by using glacier evolution models to account for the meteorology, topography and flow dynamics of every glacier in a region.

Glaciers exhibit large seasonal signals, such that substantial contributions to runoff exist even in net zero or positive annual mass balance years. The relative size of the seasonal signal depends on the overall climate regime: maritime or coastal glaciers exist in generally warmer and wetter climates, and are characterized by high seasonal mass turnover (large winter accumulation and large summer melt). Glaciers in these regions, such as much of Alaska or New Zealand, contribute hugely to runoff in all years. Conversely, glaciers located in continental climates – such

as Arctic Canada North – are characterized by low winter accumulation and modest summer melt. In turn, the contributions to runoff in these regions are smaller relative to the annual mass balance.

On a year-to-year basis, annual mass balance varies due to the combined impacts of anomalous winter accumulation and summer melt. For example, large inter-annual variability of seasonal mass balances in Central Europe, Scandinavia and Arctic Canada North result in extreme summer melt or anomalously low or high winter accumulation, which affects the annual mass balance in these regions for particular years. Still, we observe that long-term changes in glacier mass balance are mainly dictated by summer mass balance (Zemp et al., 2015). As such, the long-term trends of increased annual mass loss correspond with increasing summer melt, which is clearest to see in larger regions such as Alaska, western Canada and USA, or regions in the Arctic. For smaller regions, like Central Europe or New Zealand, this pattern similarly exists but is less clear to see, as absolute mass losses decrease over time due to the large fractional reduction in glaciated area. In general, the presence and extent of glaciers in each region across the world have outstanding implications on local and downstream natural hazards and water resource availability, as well as global sea-level budgets.

Global glacier mass loss is a good indicator of annual glacier contribution to global sea-level rise. However, because winters and summers occur at different times of the calendar year in the two hemispheres, global winter and summer estimates are not a good proxy to understand the impact of glacier annual loss on the hydrological cycle. Regional winter and summer mass balances provide a better understanding of the evolution and impact of glacier contribution to runoff.

Glacier contribution to seasonal river runoff

The annual mass balance of a glacier is calculated as the difference between the snow accumulation in winter (mass gain) and the melt of ice and snow during summer (mass loss) over a hydrological year, reflecting the prevalent atmospheric conditions. When measured over a long period, trends in glaciers' mass change are an indicator of climate change. The global net loss of glacier mass contributes to sea-level rise. Seasonal melting of ice and snow contributes to runoff. Therefore, glaciers contribute to seasonal runoff even in years with balanced conditions, or positive annual mass balance. This can be seen in Figure 24 in the main report, where seasonal mass balances are shown. Negative summer mass balance values (that is, ice mass loss) contribute to river flow even in years where regions experience a net positive annual mass balance (blue bars).

In general, depending on the region, precipitation and snowmelt play a larger role in modulating seasonal streamflow than glacier mass balance. However, glaciers do matter in some regions and during warm and dry months of the year. In arid and semiarid regions there is a delay between the moment when water is stored in a glacier (winter), and the moment when the meltwater is produced and released to the rivers (summer). For these regions, this seasonally delayed runoff plays a crucial role in sustaining river flows during the driest months of the year and during periods of extreme drought, compensating for otherwise reduced flows due to lack of rain and snowmelt (Dussaillant et al., 2019; Huss and Hock, 2018; Kaser et al., 2010; Pritchard et al., 2019; Radić and Hock, 2014).

When a glacier is balanced with its climate, its annual contribution to streamflow will only depend on the yearly summer balance. Contrarily, when a glacier is exposed to a climatic warming, its volume will decrease in time as water is released from its long-term storage.

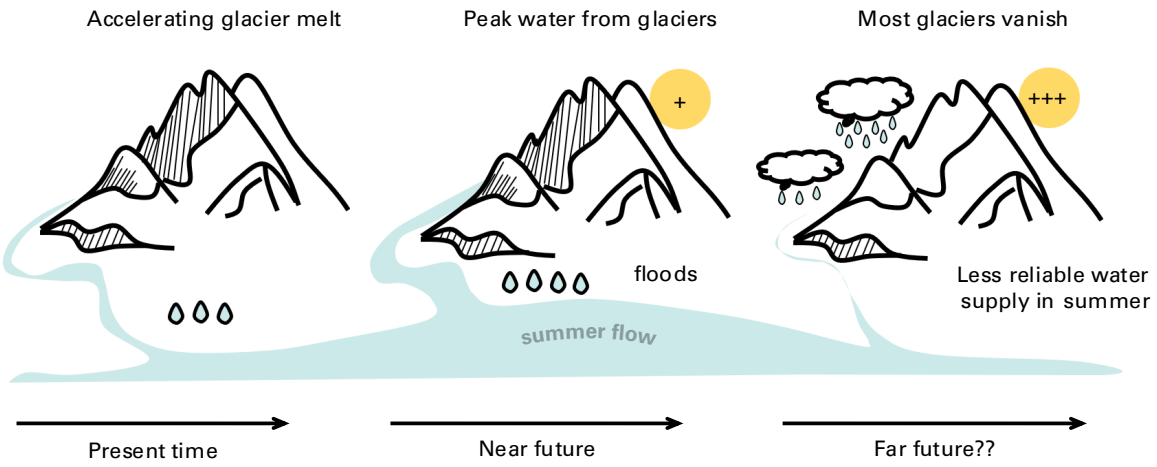


Figure A.11. Schematic view of expected runoff changes under ongoing climate change affecting total glacier meltwater contribution as well as the seasonality in water availability

Source: Adapted from Barandun et al. (2020).

As a consequence, glacier runoff is expected to increase with climate change until reaching a maximum "peak water" contribution beyond which runoff starts to gradually decrease, as the reduced glacier volume cannot support high melt rates anymore (Huss and Hock, 2018; Wimberly et al., 2025). If temperatures continue to increase, the glacier will disappear, and with it, its hydrological contribution (Figure A.11).

Concerning the future of glacier availability, Huss and Hock (2018) assessed the hydrological consequences of glacier decline around the world. The largest summer month reductions in glacier runoff by the end of the century are expected in Central Asia and the tropical and central Andes. Notably, these are the only regions where more than 50% of the total basin runoff comes from snow and ice. The net contribution of water melt depends on the glacier area, with larger regions (such as Alaska) releasing larger water volumes. However, if observed in relation to the glacier surface, the impact of glacial meltwater is independent of glacier volume and is also recognizable in regions with lower glaciation. In the European Alps, for example, glaciers also significantly contribute to runoff during summer months and help mitigate the negative hydrological effects of drought years (Huss, 2011; Huss et al., 2017).

WATER QUALITY

Observed river water quality

The quality of inland freshwater bodies depends on the physical, chemical and biological characteristics of their water and sediment, usually assessed in relation to the bodies' suitability for a particular purpose, such as drinking, swimming, agriculture and industrial use, or capacity to sustain aquatic ecosystems. Water quality is measured using a combination of field tests, laboratory analysis and, more recently, sensor-based monitoring. While laboratory analyses allow for the evaluation of hundreds of different characteristics, the complexity of sampling and laboratory analyses and their related costs prevent high spatial and temporal resolutions for these measurements in many parts of the world. In situ sensor-based methods are limited to a few physical and chemical characteristics but can measure at high temporal frequencies, enabling the analysis of short-term variations in water quality. In order to align the assessment of water quality with other observed variables in this report, only daily time series data from automatic monitoring networks for water temperature, dissolved oxygen, pH and electrical conductivity were considered. Due to the fact that automatic sensor networks only became more widely used in the 2010s, a reference period of 10 years was selected. The data were either downloaded from online sources or requested from the data providers. Time series data with temporal resolutions higher than one day (for example, recordings every 10 minutes) were aggregated to daily mean values.

The data were filtered for data completeness using the following criteria:

- Only time series for which at least 80% of daily values were valid in a 10-year reference period and the 2025 reporting year were included;

- During the reference period, one calendar month of consecutive missing daily values per year was permitted as long as the other reference years contained valid data for that calendar month.

For each country, a suitable 10-year reference period was selected based on the maximum number of stations with time series complying with the above criteria. This resulted in different reference periods for the countries included. Due to time constraints, no further quality assurance of the data could be carried out. Out of 816 stations in six countries for which data were initially collected, 442 stations in six countries satisfied the completeness criteria. The spatial distribution of the stations is presented in Figure A.12, with the countries, their respective reference periods and number of stations listed in Table A.5.

Table A.5. Reference periods and number of monitoring stations used for the six countries

Country	*Reference period*	*Number of stations*				
		Water temperature	*Dissolved oxygen*	*pH*	*Electrical conductivity*	*Total*
Australia	2011–2020	-	-	-	9	9
France	2011–2020	4	-	-	-	4
Republic of Korea	2014–2023	7	4	7	7	7
United Kingdom	2014–2023	4	4	4	4	4
United States of America	2014–2023	378	103	71	177	399
Switzerland	2012–2021	9	-	-	-	9

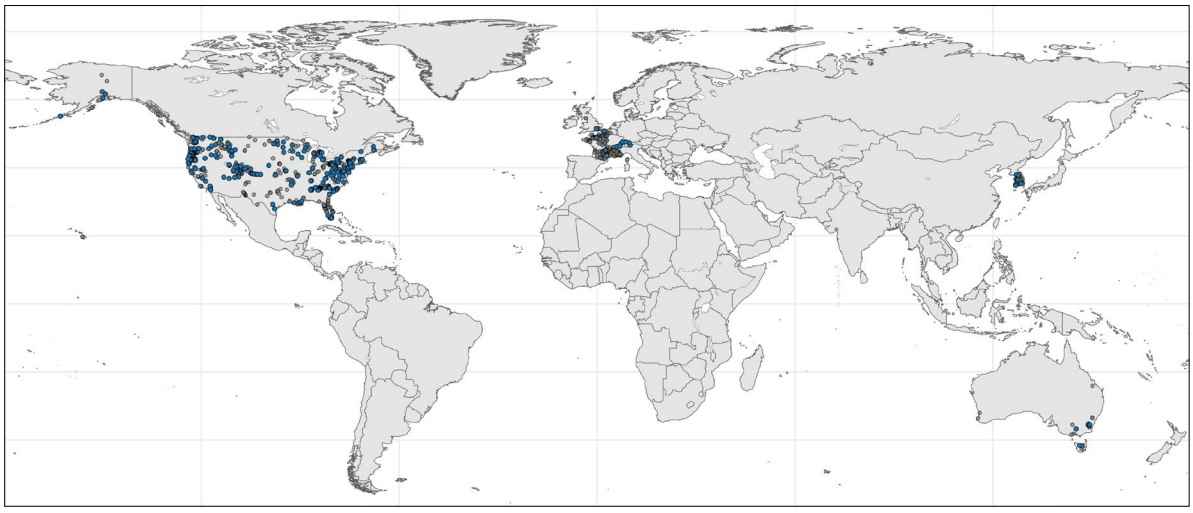


Figure A.12. Locations of the monitoring stations for which data were used (in blue) and excluded (in grey) from the report

Note: The boundaries and names shown and the designations used do not imply official endorsement or acceptance by WMO or the United Nations.

Dissolved oxygen

Similar to water temperature, dissolved oxygen is a key water quality characteristic because it directly affects the health of aquatic ecosystems. Aquatic organisms such as fish and invertebrates need oxygen to survive. Low levels of dissolved oxygen can cause hypoxia, stressing or killing these organisms. Bacteria consume oxygen when decomposing organic matter, reducing dissolved oxygen and increasing nutrient levels. This can lead to eutrophication, which can cause algal blooms that further deplete oxygen.

In 2025, above- and much-above-normal dissolved oxygen levels were observed at 45% of monitoring stations, with 32% of stations showing normal and 23% below- and much-below-normal levels (Figure A.13).

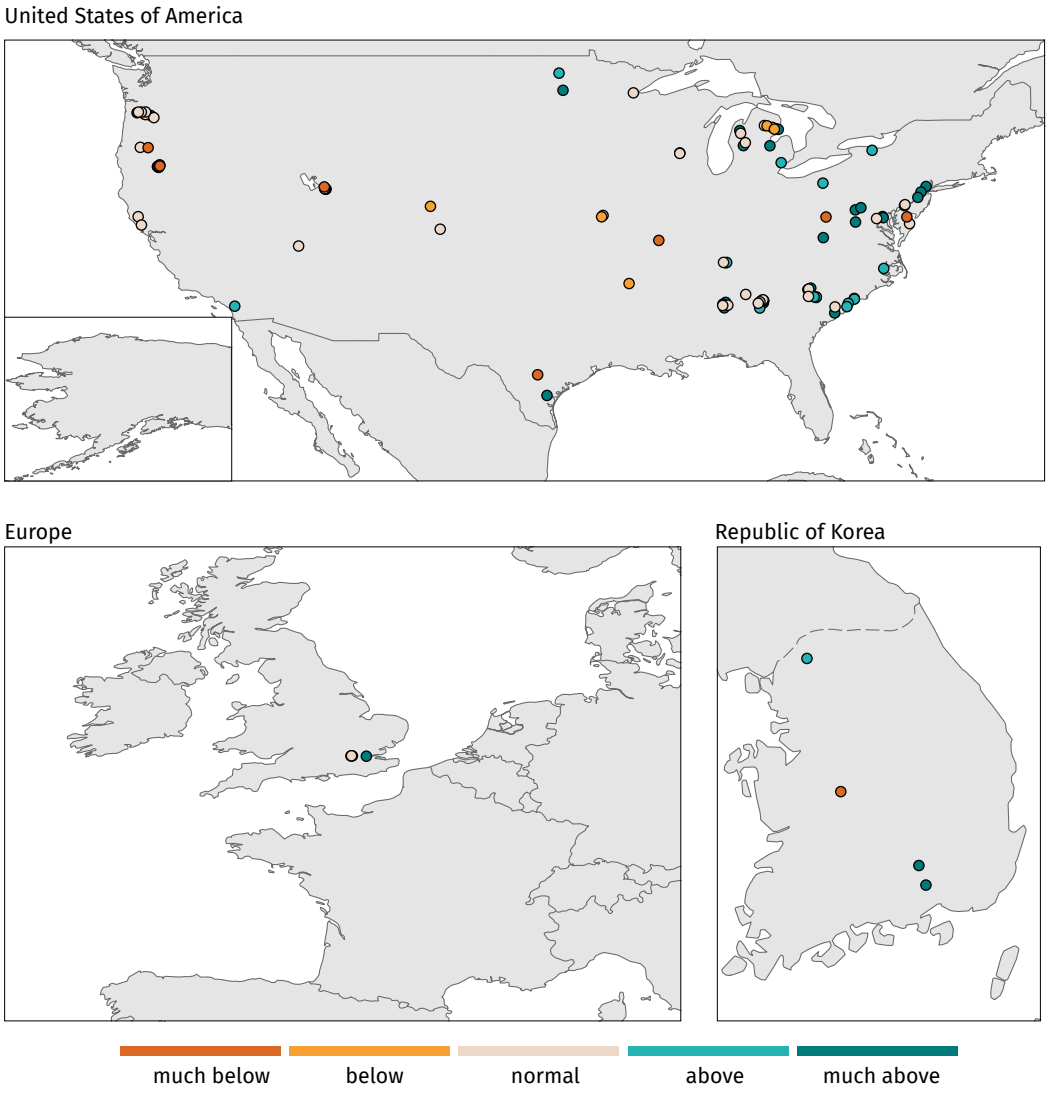


Figure A.13. Dissolved oxygen anomalies in rivers in 2025 compared to a 10-year reference period between 2011 and 2023 (note: varying reference periods were applied depending on the data availability, see Table A.5)

Note: The boundaries and names shown and the designations used do not imply official endorsement or acceptance by WMO or the United Nations.

pH

The hydrogen potential (pH), a measure of the acidity or basicity of water, affects chemical and biological processes in water such as the solubility and availability of nutrients and metals. In acidic water (low pH), toxic metals become more soluble and harmful, whereas in alkaline water (high pH) the availability of certain nutrients is reduced. The level of pH also affects aquatic organisms, which often require a pH range between 6.5 and 8.5 to flourish. River water pH is shaped by geology, biological activity, and climate and hydrological conditions, and can be further influenced by human activities such as agriculture, wastewater discharge and atmospheric deposition.

The majority (62%) of the 88 stations analysed in 2025 showed above- and much-above-normal pH levels, 28% normal and 10% below- and much-below-normal levels (Figure A.14). Across the USA the pH was mostly above to much above normal in 2025, except for some stations on the west coast and northern east coast. In the UK, pH was below normal.

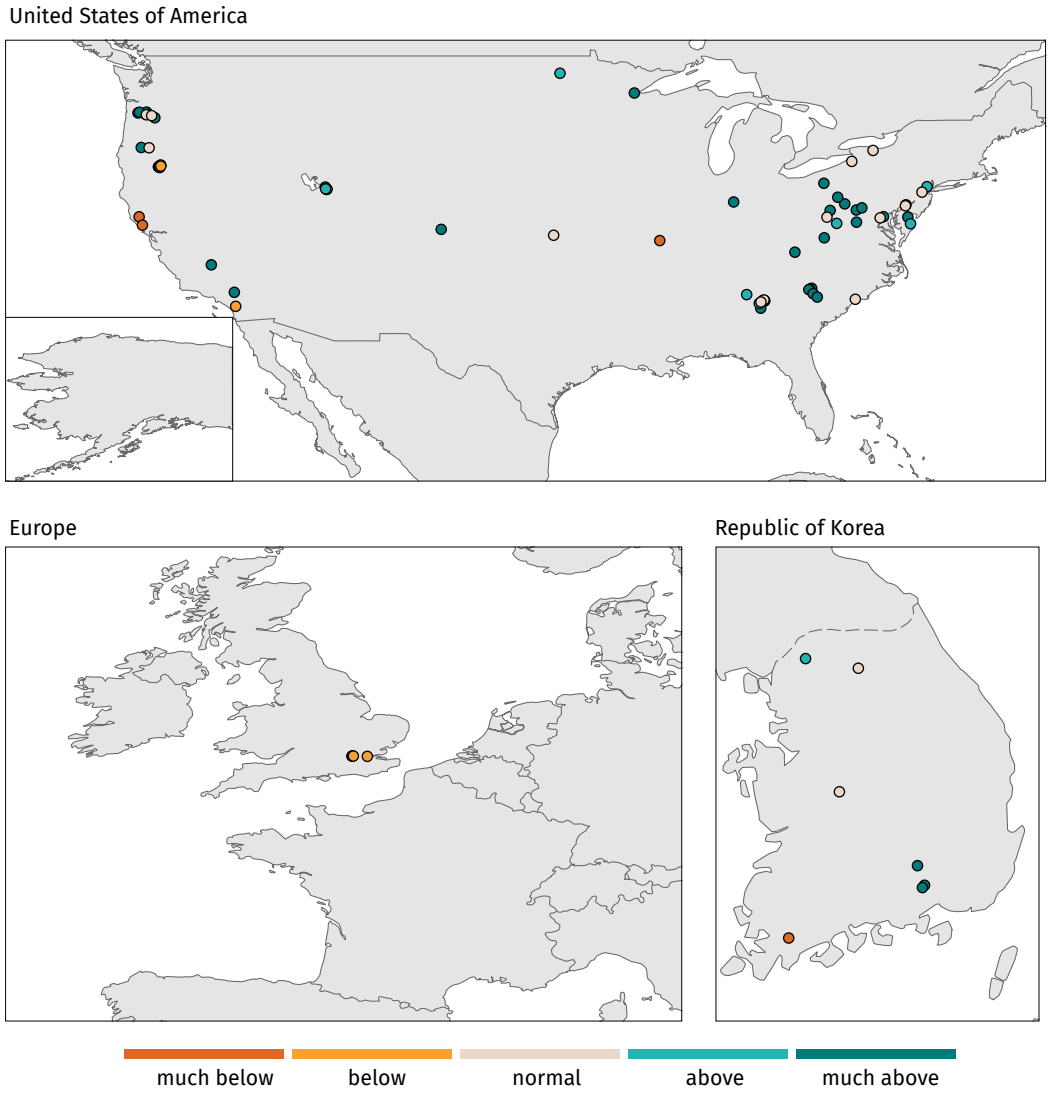


Figure A.14. pH anomalies in rivers in 2025 compared to a 10-year reference period between 2011 and 2023 (note: varying reference periods were applied depending on the data availability, see Table A.5)

Note: The boundaries and names shown and the designations used do not imply official endorsement or acceptance by WMO or the United Nations.

Electrical conductivity

Electrical conductivity reflects the amount of dissolved salts and ions in water, which can affect ecosystem health and water usability. Many aquatic organisms are sensitive to changes in salinity, especially if they occur suddenly. High levels of electrical conductivity can limit the suitability of water for drinking, irrigation or industrial uses. River water conductivity generally increases with higher concentrations of dissolved salts and nutrients from geology, evaporation or human inputs, and decreases when waters are diluted by rainfall, snowmelt or low mineral runoff.

Electrical conductivity above- and much-above-normal levels occurred at 53% of the monitoring stations analysed in 2025, whereas 34% of the stations showed normal levels and 13% below- or much-below-normal levels (see Figure A.15).

Electrical conductivity was normal and above normal across considered stations in the Republic of Korea and the UK. In the USA the picture was somewhat contrasted, with stations located across the west coast and central-south USA seeing below-normal and normal electrical conductivity, while stations in the central-east and east coast of the USA above- to much-above normal electrical conductivity.

WATER SURFACE ELEVATION DATA

The Surface Water and Ocean Topography (SWOT) mission, launched in December 2022, provides a new global capability for observing inland water dynamics from space. Using a wide-swath Ka-band radar interferometer, SWOT measures water surface elevation and extent over rivers, lakes, reservoirs, wetlands and floodplains, overcoming many of the spatial limitations of conventional nadir altimetry. These observations are especially valuable in remote and transboundary basins, where ground-based monitoring is often sparse, inconsistent or constrained by data-sharing limitations. By providing spatially consistent information on surface water elevation changes across political boundaries, SWOT enables improved monitoring of floods, droughts, reservoir dynamics and basin-scale water availability, and offers a foundation for more integrated hydrological monitoring and modelling systems (Getirana et al., 2024), including efforts to reduce uncertainty in global flood monitoring and interpretation of hydrological extremes (Getirana et al., 2026).

To compare surface water conditions in 2025 to 2024, we leveraged satellite observations from SWOT. Specifically, we obtained water surface elevation (WSE) observation time series from the SWOT_L2_HR_RiverSP_D reach-level data product for each river reach defined in the SWOT prior river database (SWORD), which represents global rivers that are ≥50–100 m wide (Altenau et al., 2021). The quality of the WSE observations collected by SWOT can be impacted by various factors including the crossover calibration quality, dark water, ice and specular ringing, altogether leading to reach-level errors on the order of ~11–13 cm (Stuurman, 2024). Therefore, to remove erroneous WSEs, we filtered the time series for each reach by removing observations that (1) were within 10 km of the nadir track and (2) had a reach bitwise quality flag decimal value ≥262144

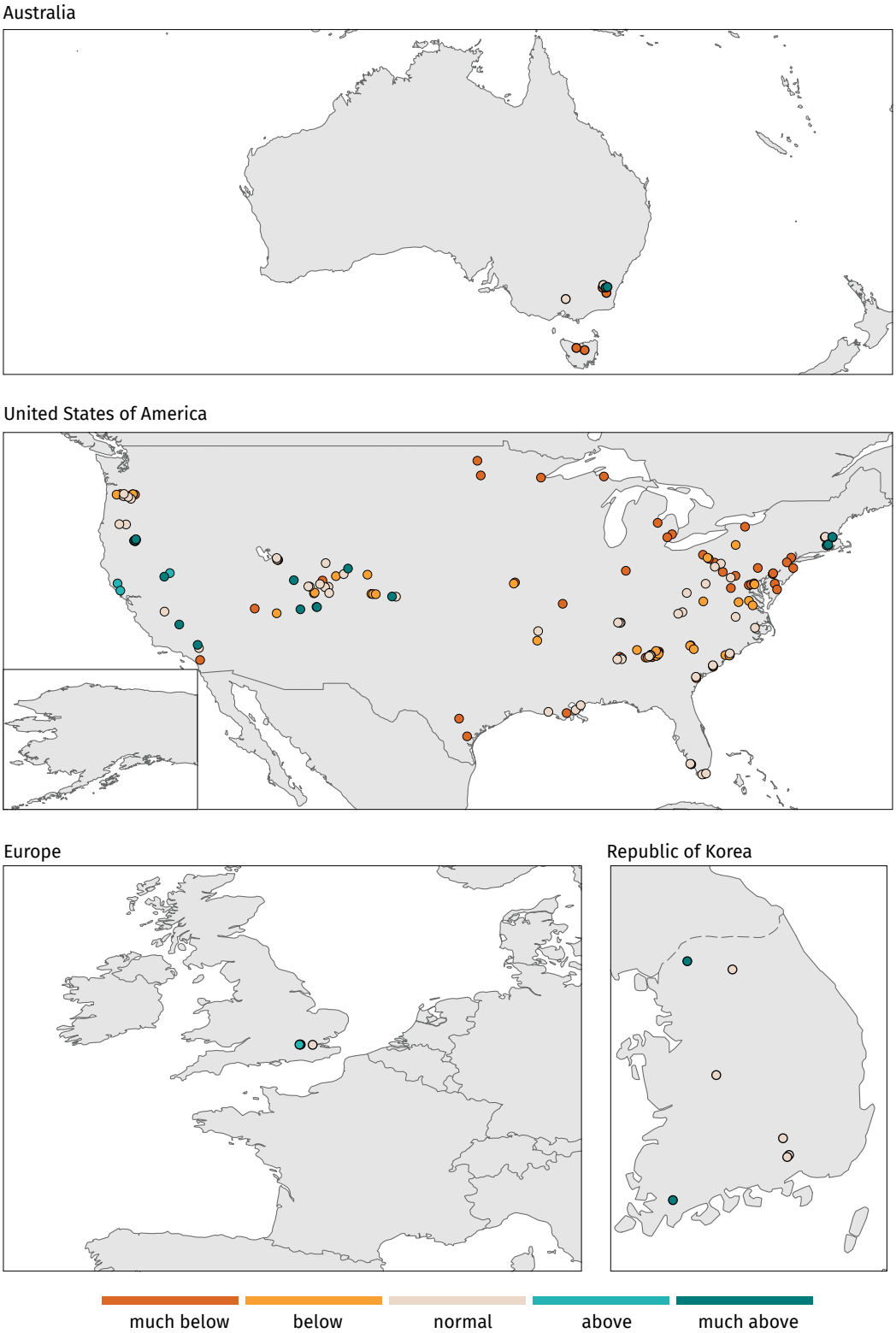


Figure A.15. Electrical conductivity anomalies in rivers in 2025 compared to a 10-year reference period between 2011 and 2023 (note: varying reference periods were applied depending on the data availability, see Table A.5)

Note: The boundaries and names shown and the designations used do not imply official endorsement or acceptance by WMO or the United Nations.

(SWOT, 2025).[1] Using the filtered time series for each river reach, we compared the annual maximum WSE in 2025 to 2024 and normalized the result using Equation 2:

$$WSE_{diff} = \frac{\max(WSE_{2025}) - \max(WSE_{2024})}{\sigma_{WSE}} \quad (2)$$

where σ_{WSE} is computed across 2024 and 2025 together. Note that WSE_{diff} was unable to be calculated for a river reach if all observations were removed in the filtering process. Next, we aggregated WSE_{diff} results to each level 4 basin in the HydroBASINS dataset (Lehner and Grill, 2013) by computing the percentage of total valid reach length within each basin that had (1) a higher annual maximum WSE in 2025 compared to 2024 $(WSE_{diff}>0)$ and (2) a lower annual maximum WSE in 2025 compared to 2024 $(WSE_{diff}<0)$. If less than 10% of the SWORD reaches in a level 4 basin had a valid WSE_{diff}, then the basin was removed from the aggregation analysis.

[1] A bitwise decimal value of 262144 corresponds to bit 18 (2^{18} = 262144). SWOT stores quality information as a bitwise flag: a single whole number that records the outcome of many separate quality checks at once, each check switching on one binary digit ("bit"). The number is therefore a code rather than a value on a continuous scale, which is why the thresholds are not round decimals. Because each bit represents a power of two, the value 262144 (i.e. 2^{18}) marks the point at which an observation is classified as erroneous.

REFERENCES

Alfieri, L.; Burek, P.; Dutra, E. et al. GloFAS – Global Ensemble Streamflow Forecasting and Flood Early Warning. *Hydrology and Earth System Sciences* **2013**, *17* (3), 1161–1175. https://doi.org/10.5194/hess-17-1161-2013.

Ali, A. N. A. M.; Imhoff, R. O.; Weerts, A. H. Machine Learning for Predicting Spatially Variable Lateral Hydraulic Conductivity: A Step towards Efficient Hydrological Model Calibration and Global Applicability. *ESS Open Archive* **2025**. https://essopenarchive.org/doi/full/10.22541/essoar.174016989.99005964.

Arheimer, B.; Pimentel, R.; Isberg, K. et al. Global Catchment Modelling Using World-Wide HYPE (WWH), Open Data, and Stepwise Parameter Estimation. *Hydrology and Earth System Sciences* **2020**, *24* (2), 535–559. https://doi.org/10.5194/hess-24-535-2020.

Barandun, M.; Fiddes, J.; Scherler, M. et al. The State and Future of the Cryosphere in Central Asia. *Water Security* **2020**, *11*, 100072. https://doi.org/10.1016/j.wasec.2020.100072.

Beck, H. E.; Wood, E. F.; Pan, M. et al. MSWEP V2 Global 3-Hourly 0.1° Precipitation: Methodology and Quantitative Assessment. *Bulletin of the American Meteorological Society* **2019,** *100* (3), 473–500. https://doi.org/10.1175/BAMS-D-17-0138.1.

Berg, P.; Almén, F.; Bozhinova, D. HydroGFD3.0 (Hydrological Global Forcing Data): A 25 Km Global Precipitation and Temperature Data Set Updated in near-Real Time. *Earth System Science Data* **2021**, *13* (4), 1531–1545. https://doi.org/10.5194/essd-13-1531-2021.

Biswas, N. K.; Hossain, F.; Bonnema, M. et al. Towards a Global Reservoir Assessment Tool for Predicting Hydrologic Impacts and Operating Patterns of Existing and Planned Reservoirs. *Environmental Modelling & Software* **2021**, *140*, 105043. https://doi.org/10.1016/j.envsoft.2021.105043.

Boergens, E.; Güntner, A.; Dobslaw, H. et al. Quantifying the Central European Droughts in 2018 and 2019 With GRACE Follow-On. *Geophysical Research Letters* **2020**, *47* (14), e2020GL087285. https://doi.org/10.1029/2020GL087285.

Boussetta, S.; Balsamo, G.; Arduini, G. et al. ECLand: The ECMWF Land Surface Modelling System. *Atmosphere* **2021**, *12* (6), 723. https://doi.org/10.3390/atmos12060723.

Centre for Research on the Epidemiology of Disasters (CRED). *EM-DAT*; CRED/UCLouvain: Brussels, Belgium. http://www.emdat.be.

Collischonn, W.; Fan, F. M.; Possantti, I. et al. The Exceptional Hydrological Disaster of April-May 2024 in Southern Brazil. *Brazilian Journal of Water Resources* **2025**, *30*, e1. https://doi.org/10.1590/2318-0331.302520240119.

Decharme, B.; Barbu, A. Crocus-ERA5 Daily Snow Product over the Northern Hemisphere at 0.25° Resolution; Version 2023; *Zenodo* **2024**. https://doi.org/10.5281/zenodo.10943718.

Donchyts, G.; Winsemius, H.; Baart, F. et al. High-Resolution Surface Water Dynamics in Earth's Small and Medium-Sized Reservoirs. *Scientific Reports* **2022**, *12* (1), 13776. https://doi.org/10.1038/s41598-022-17074-6.

Dussaillant, I.; Berthier, E.; Brun, F. et al. Two Decades of Glacier Mass Loss along the Andes. *Nature Geoscience* **2019**, *12* (10), 802–808. https://doi.org/10.1038/s41561-019-0432-5.

Dussaillant, I.; Hugonnet, R.; Huss, M. et al. Annual Mass Change of the World's Glaciers from 1976 to 2024 by Temporal Downscaling of Satellite Data with in Situ Observations. *Earth System Science Data* **2025**, *17* (5), 1977–2006. https://doi.org/10.5194/essd-17-1977-2025.

Egas, H. M.; Stabile, R. A.; de Andrade, M. R. M. et al. Comprehensive Inventory and Initial Assessment of Landslides Triggered by Autumn 2024 Rainfall in Rio Grande Do Sul, Brazil. *Landslides* **2025**, *22*, 579–589. https://doi.org/10.1007/s10346-024-02410-w.

Eilander, D.; van Verseveld, W.; Yamazaki, D. et al. A Hydrography Upscaling Method for Scale-Invariant Parametrization of Distributed Hydrological Models. *Hydrology and Earth System Sciences* **2021**, *25* (9), 5287–5313. https://doi.org/10.5194/hess-25-5287-2021.

Elmi, O.; Tourian, M. J. Retrieving Time Series of River Water Extent from Global Inland Water Data Sets. *Journal of Hydrology* **2023**, *617*, 128880. https://doi.org/10.1016/j.jhydrol.2022.128880.

Elmi, O.; Tourian, M. J.; Saemian, P. et al. Remote Sensing-Based Extension of GRDC Discharge Time Series - A Monthly Product with Uncertainty Estimates. *Scientific Data* **2024**, *11* (1), 240. https://doi.org/10.1038/s41597-024-03078-6.

Global Modeling and Assimilation Office (GMAO). *inst3_3d_asm_Cp: MERRA-2 3D IAU State, Meteorology Instantaneous 3-hourly (p-coord, 0.625x0.5L42)*, version 5.12.4; Goddard Space Flight Center Distributed Active Archive Center (GSFC DAAC): Greenbelt, USA, 2015. https://doi.org/10.5067/VJAFPLI1CSIV.

Grimaldi, S.; Salamon, P.; Russo, C. et al. GloFAS v4.0: Towards Hyper-resolution Hydrological Modelling at Global Scale. In *European Geosciences Union (EGU) Abstracts EGU General Assembly 2023*, Vienna, Austria, 23–28 April 2023. https://doi.org/10.5194/egusphere-egu23-3410.

Hales, R. C.; Nelson, E. J.; Souffront, M. et al. Advancing Global Hydrologic Modeling with the GEOGloWS ECMWF Streamflow Service. *Journal of Flood Risk Management* **2022**, *18* (1), e12859. https://doi.org/10.1111/jfr3.12859.

Hanazaki, R.; Yamazaki, D.; Yoshimura, K. Development of a Reservoir Flood Control Scheme for Global Flood Models. *Journal of Advances in Modeling Earth Systems* **2022**, *14* (3), e2021MS002944. https://doi.org/10.1029/2021MS002944.

Hersbach, H.; Bell, B.; Berrisford, P. et al. The ERA5 Global Reanalysis. *Quarterly Journal of the Royal Meteorological Society* **2020**, *146* (730), 1999–2049. https://doi.org/10.1002/qj.3803.

Huang, Q.; Zhang, Y.; Ma, N. et al. Estimating Vegetation Greening Influences on Runoff Signatures Using a Log-Based Weighted Ensemble Method. *Water Resources Research* **2022**, *58* (12), e2022WR032492. https://doi.org/10.1029/2022WR032492.

Huss, M. Present and Future Contribution of Glacier Storage Change to Runoff from Macroscale Drainage Basins in Europe. *Water Resources Research* **2011**, *47* (7). https://doi.org/10.1029/2010WR010299.

Huss, M.; Hock, R. Global-Scale Hydrological Response to Future Glacier Mass Loss. *Nature Climate Change* **2018**, *8* (2), 135–140. https://doi.org/10.1038/s41558-017-0049-x.

Huss, M.; Bookhagen, B.; Huggel, C. et al. Toward Mountains without Permanent Snow and Ice. *Earth's Future* **2017**, *5* (5), 418–435. https://doi.org/10.1002/2016EF000514.

Imhoff, R. O.; van Verseveld, W. J.; van Osnabrugge, B. et al. Scaling Point-Scale (Pedo)Transfer Functions to Seamless Large-Domain Parameter Estimates for High-Resolution Distributed Hydrologic Modeling: An Example for the Rhine River. *Water Resources Research* **2020**, *56* (4), e2019WR026807. https://doi.org/10.1029/2019WR026807.

Kaser, G.; Großhauser, M.; Marzeion, B. Contribution Potential of Glaciers to Water Availability in Different Climate Regimes. *Proceedings of the National Academy of Sciences* **2010**, *107* (47), 20223–20227. https://doi.org/10.1073/pnas.1008162107.

Kobayashi, S.; Ota, Y.; Harada, Y. et al. The JRA-55 Reanalysis: General Specifications and Basic Characteristics. *Journal of the Meteorological Society of Japan. Ser. II* **2015**, *93* (1), 5–48. https://doi.org/10.2151/jmsj.2015-001.

Kumar, R.; Samaniego, L.; Attinger, S. Implications of Distributed Hydrologic Model Parameterization on Water Fluxes at Multiple Scales and Locations. *Water Resources Research* **2013**, *49* (1), 360–379. https://doi.org/10.1029/2012WR012195.

Landerer, F. W.; Flechtner, F. M.; Save, H. et al. Extending the Global Mass Change Data Record: GRACE Follow-On Instrument and Science Data Performance. *Geophysical Research Letters* **2020**, *47* (12), e2020GL088306. https://doi.org/10.1029/2020GL088306.

Lehner, B.; Döll, P. Development and Validation of a Global Database of Lakes, Reservoirs and Wetlands. *Journal of Hydrology* **2004**, *296* (1), 1–22. https://doi.org/10.1016/j.jhydrol.2004.03.028.

Lehner, B.; Liermann, C. R.; Revenga, C. et al. High-Resolution Mapping of the World's Reservoirs and Dams for Sustainable River-Flow Management. *Frontiers in Ecology and the Environment* **2011**, *9* (9), 494–502. https://doi.org/10.1890/100125.

Lehner, B.; Reidy Liermann, C.; Revenga, C. et al. *Global Reservoir and Dam Database, Version 1 (GRanDv1): Dams, Revision 01*; NASA Socioeconomic Data and Applications Center (SEDAC), 2011. https://doi.org/10.7927/H4N877QK.

Lehner, B.; Grill, G. Global River Hydrography and Network Routing: Baseline Data and New Approaches to Study the World's Large River Systems. *Hydrological Processes* **2013**, *27* (15), 2171–2186. https://doi.org/10.1002/hyp.9740.

Luojus, K.; Moisander, M.; Pulliainen, J. et al. *ESA Snow Climate Change Initiative (Snow_cci): Snow Water Equivalent (SWE) Level 3C Daily Global Climate Research Data Package (CRDP) (1979–2020), version 2.0*; NERC EDS Centre for Environmental Data Analysis, 2022. https://doi.org/10.5285/4647cc9ad3c044439d6c643208d3c494.

Ma, W.; Ishitsuka, Y.; Takeshima, A. et al. Applicability of a Nationwide Flood Forecasting System for Typhoon Hagibis 2019. *Scientific Reports* **2021**, *11* (1), 10213. https://doi.org/10.1038/s41598-021-89522-8.

Marsh, T.; Sanderson, F.; Swain, O. *Derivation of the UK National and Regional Runoff Series*; National Environment Research Council (NERC): Wallingford, UK, 2015. https://nora.nerc.ac.uk/id/eprint/510580/.

Messager, M. L.; Lehner, B.; Grill, G. et al. Estimating the Volume and Age of Water Stored in Global Lakes Using a Geo-Statistical Approach. *Nature Communications* **2016**, *7* (1), 13603. https://doi.org/10.1038/ncomms13603.

Mudryk, L. R.; Chereque, A. E.; Derksen, C. et al. Terrestrial Snow Cover: Arctic Report Card 2024; Moon, T. A.; Druckenmiller, M. L.; Thoman, R. L., Eds.; NOAA Technical Report OAR ARC; 24-04; National Oceanic and Atmospheric Administration, 2024. https://doi.org/10.25923/4bb3-3f87.

Mudryk, L. R.; Elias Chereque, A.; Derksen, C. et al. Terrestrial Snow Cover [in "State of the Climate in 2024"]. *Bulletin of the American Meteorological Society* **2025**, *106* (8), S335–S338. https://doi.org/10.1175/BAMS-D-25-0104.1.

Müller Schmied, H.; Cáceres, D.; Eisner, S. et al. The Global Water Resources and Use Model WaterGAP v2.2d: Model Description and Evaluation. *Geoscientific Model Development* **2021**, *14* (2), 1037–1079. https://doi.org/10.5194/gmd-14-1037-2021.

Müller Schmied, H.; Trautmann, T.; Ackermann, S. et al. The Global Water Resources and Use Model WaterGAP v2.2e: Description and Evaluation of Modifications and New Features. *Geoscientific Model Development* **2024**, *17* (23), 8817–8852. https://doi.org/10.5194/gmd-17-8817-2024.

Muñoz Sabater, J. *ERA5-Land Hourly Data from 1950 to Present; Copernicus Climate Change Service (C3S) Climate Data Store (CDS)*, 2019. https://doi.org/10.24381/cds.e2161bac.

Murray, A. M.; Jørgensen, G. H.; Godiksen, P. N. et al. DHI-GHM: Real-Time and Forecasted Hydrology for the Entire Planet. *Journal of Hydrology* **2023**, *620*, 129431. https://doi.org/10.1016/j.jhydrol.2023.129431.

Nash, J. E., & Sutcliffe, J. V. River flow forecasting through conceptual models Part I—A discussion of principles. *Journal of Hydrology* **1970**, *10* (3), 282–290. https://doi.org/10.1016/0022-1694(70)90255-6.

de Oliveira Andrades-Filho, C.; Mexias, L. F. S.; Quevedo, R. P. et al. The Biggest Landslide Event in Brazil: Preliminary Analysis of the Rio Grande Do Sul Mega Disaster in May 2024. *Landslides* **2025**, *22* (11), 3615–3624. https://doi.org/10.1007/s10346-025-02587-8.

Pritchard, H. D. Asia's Shrinking Glaciers Protect Large Populations from Drought Stress. *Nature* **2019**, *569* (7758), 649–654. https://doi.org/10.1038/s41586-019-1240-1.

Radić, V.; Hock, R. Glaciers in the Earth's Hydrological Cycle: Assessments of Glacier Mass and Runoff Changes on Global and Regional Scales. *Surveys in Geophysics* **2014**, *35* (3), 813–837. https://doi.org/10.1007/s10712-013-9262-y.

Reinecke, R.; Stein, L.; Gnann, S. et al. Uncertainties as a Guide for Global Water Model Advancement. *WIREs Water* **2025**, *12* (3), e70025. https://doi.org/10.1002/wat2.70025.

Saemian, P.; Elmi, O.; Stroud, M. et al. Satellite Altimetry-Based Extension of Global-Scale in Situ River Discharge Measurements (SAEM). *Earth System Science Data* **2025**, *17* (5), 2063–2085. https://doi.org/10.5194/essd-17-2063-2025.

Samaniego, L.; Kaluza, M.; Kumar, R. et al. Mesoscale Hydrologic Model; *Zenodo*, **2019**. https://doi.org/10.5281/zenodo.3239055.

Samaniego, L.; Kumar, R.; Attinger, S. Multiscale Parameter Regionalization of a Grid-Based Hydrologic Model at the Mesoscale. *Water Resources Research* **2010**, *46* (5). https://doi.org/10.1029/2008WR007327.

Sutanudjaja, E. H.; van Beek, R.; Wanders, N. et al. PCR-GLOBWB 2: A 5 Arcmin Global Hydrological and Water Resources Model. *Geoscientific Model Development* **2018**, *11* (6), 2429–2453. https://doi.org/10.5194/gmd-11-2429-2018.

Tapley, B. D.; Watkins, M. M.; Flechtner, F. et al. Contributions of GRACE to Understanding Climate Change. *Nature Climate Change* **2019**, *9* (5), 358–369. https://doi.org/10.1038/s41558-019-0456-2.

Tourian, M. J.; Elmi, O.; Shafaghi, Y. et al. HydroSat: Geometric Quantities of the Global Water Cycle from Geodetic Satellites. *Earth System Science Data* **2022**, *14* (5), 2463–2486. https://doi.org/10.5194/essd-14-2463-2022.

van der Laan, E.; Hazenberg, P.; Weerts, A. H. Simulation of Long-Term Storage Dynamics of Headwater Reservoirs across the Globe Using Public Cloud Computing Infrastructure. *Science of The Total Environment* **2024**, *931*, 172678. https://doi.org/10.1016/j.scitotenv.2024.172678.

van Verseveld, W. J.; Weerts, A. H.; Visser, M. et al. Wflow_sbm v0.7.3, a Spatially Distributed Hydrological Model: From Global Data to Local Applications. *Geoscientific Model Development* **2024**, *17* (8), 3199–3234. https://doi.org/10.5194/gmd-17-3199-2024.

Wang, J.; Walter, B. A.; Yao, F. et al. GeoDAR: Georeferenced Global Dams and Reservoirs Dataset for Bridging Attributes and Geolocations. *Earth System Science Data* **2022**, *14* (4), 1869–1899. https://doi.org/10.5194/essd-14-1869-2022.

Wimberly, F.; Ultee, L.; Schuster, L. et al. Inter-Model Differences in 21st Century Glacier Runoff for the World's Major River Basins. *The Cryosphere* **2025**, *19* (4), 1491–1511. https://doi.org/10.5194/tc-19-1491-2025.

World Glacier Monitoring Service (WGMS). *Global Glacier Change Bulletin No. 5 (2020–2021)*. Zemp, M.; Gärtner-Roer, I.; Nussbaumer, S. U. et al., Eds.; WGMS: Zurich, Switzerland, 2023, 134 pp. [publication based on database version: doi:10.5904/wgms-fog-2023-09]. https://wgms.ch/downloads/WGMS_GGCB_05.pdf.

Yamazaki, D.; Kanae, S.; Kim, H. et al. A Physically Based Description of Floodplain Inundation Dynamics in a Global River Routing Model. *Water Resources Research* **2011**, *47* (4). https://doi.org/10.1029/2010WR009726.

Yamazaki, D.; Ikeshima, D.; Sosa, J. et al. MERIT Hydro: A High-Resolution Global Hydrography Map Based on Latest Topography Dataset. *Water Resources Research* **2019**, *55* (6), 5053–5073. https://doi.org/10.1029/2019WR024873.

Yoshimura, K.; Sakimura, T.; Oki, T. et al. Toward Flood Risk Prediction: A Statistical Approach Using a 29-Year River Discharge Simulation over Japan. *Hydrological Research Letters* **2008**, *2*, 22–26. https://doi.org/10.3178/hrl.2.22.

Yuan, X.; Ji, P.; Wang, L. et al. High-Resolution Land Surface Modeling of Hydrological Changes Over the Sanjiangyuan Region in the Eastern Tibetan Plateau: 1. Model Development and Evaluation. *Journal of Advances in Modeling Earth Systems* **2018**, *10* (11), 2806–2828. https://doi.org/10.1029/2018MS001412.

Zemp, M.; Welty, E. Temporal Downscaling of Glaciological Mass Balance Using Seasonal Observations. *Journal of Glaciology* **2023**, 69 (278), 1–6. https://doi.org/10.1017/jog.2023.66.

Zhang, Y.; Kong, D.; Gan, R. et al. Coupled Estimation of 500 m and 8-Day Resolution Global Evapotranspiration and Gross Primary Production in 2002–2017. *Remote Sensing of Environment* **2019**, *222*, 165–182. https://doi.org/10.1016/j.rse.2018.12.031.

Ziese, M.; Schneider, U.; Meyer-Christoffer, A. et al. The GPCC Drought Index – a New, Combined and Gridded Global Drought Index. *Earth System Science Data* **2014**, *6* (2), 285–295. https://doi.org/10.5194/essd-6-285-2014.

For more information, please contact:

World Meteorological Organization

7 bis, avenue de la Paix – P.O. Box 2300 – CH 1211 Geneva 2 – Switzerland

Global Communications and Engagement Office

Email: communication@wmo.int

wmo.int

JN 26534